University of Nevada, Reno

Spectra Aerosol Light Scattering and Absorption for Laboratory and Urban Aerosol

A dissertation submitted in partial fulfillment of
the requirement for the degree of Doctor of
Philosophy in Physics

By

Madhu S. Gyawali

William P. Arnott, Ph.D./Dissertation Advisor

May, 2012

THE GRADUATE SCHOOL

We recommend that the dissertation
prepared under our supervision by

MADHU S GYAWALI

Entitled

Spectral Aerosol Light Scattering and Absorption for Laboratory and Urban Aerosol

be accepted in partial fulfillment of the
requirements for the degree of

DOCTOR OF PHILOSOPHY

William P. Arnott, Ph. D., Advisor

Hans Moosmüller, Ph. D., Committee Member

Ronald A. Phaneuf, Ph. D., Committee Member

Henry Fu, Ph. D., Committee Member

Mae S. Gustin, Ph. D., Graduate School Representative

Marsha H. Read, Ph. D., Dean, Graduate School

May, 2012

Abstract

Atmospheric aerosols considerably influence the climate, reduce visibility, and cause problems in human health. Aerosol light absorption and scattering are the important factors in the radiation transfer models. However, these properties are associated with large uncertainties in climate modeling. In addition, atmospheric aerosols widely vary in composition and size; their optical properties are highly wavelength dependent. This work presents the spectral dependence of aerosol light absorption and scattering throughout the ultraviolet to near-infrared regions. Data were collected in Reno, NV from 2008 to 2010. Also presented in this study are the aerosol optical and physical properties during carbonaceous aerosols and radiative effects study (CARES) conducted in Sacramento area during 2010.

Measurements were made using photoacoustic instruments (PA), including a novel UV 355 nm PA of our design and manufacture. Comparative analyses are presented for three main categories: (1) aerosols produced by wildfires and traffic emissions, (2) laboratory-generated and wintertime ambient urban aerosols, and (3) urban plume and biogenic emissions. In these categories, key questions regarding the light absorption by secondary organic aerosols (SOA), so -called brown carbon (BrC), and black carbon (BC) will be discussed. An effort is made to model the emission and aging of urban and biomass burning aerosol by applying shell-core calculations.

Multispectral PA measurements of aerosols light absorption and scattering coefficients were used to calculate the Ångström exponent of absorption (AEA) and single scattering albedo (SSA). The AEA and SSA values were analyzed to differentiate the aerosol sources. The California wildfire aerosols exhibited strong wavelength dependence of

aerosol light absorption with AEA as $\lambda^{-2.1}$ for 405 and 870 nm, in contrast to the relatively weak wavelength dependence of traffic emissions aerosols for which AEA varied approximately as λ^{-1}. By using a shell-core model, we verified, for the first time, that AEA can be as high as 1.6 even for non-absorbing coating on BC, suggesting that the organic coating need not be intrinsically brown to observe effects commonly attributed to BrC absorption. Additionally, for laboratory generated incense burning aerosols, AEA varied as $\lambda^{-4.5}$ for wavelengths ranging from 355 to 1047 nm. In contrast, the wood smoke aerosols during winter had a much weaker wavelength dependence ($\lambda^{-1.1}$), comparable to that of traffic emission aerosols. During these observations, the multispectral SSA decreased with the wavelength for traffic-related emissions, yet it increased for biomass and incense burning aerosol. The strong spectral dependence was due to the enhanced light absorption by BrC at UV and blue wavelengths. In all cases, results of this analysis suggested that inefficient smoldering combustion processes can emit predominantly BrC, in comparison to high-temperature and flaming burning processes.

During the CARES field campaign, aerosols were dominated by biogenic emissions. Aerosol light absorption was modestly enhanced ($\lambda^{-1.6}$) at shorter wavelengths (355, 375, 405, and 532 nm) compared to 870 and 1047 nm, likely due to the spectral dependence of coating on BC. The secondary organic aerosol (SOA) mass concentration steadily increased in the latter half of the campaign, with strong 355 nm aerosol light scattering. Overall, results of this field campaign showed that the biogenic SOA was not BrC, i.e. it didn't have intrinsic characteristics near UV absorption. These results should be further tested and analyzed to assess the full implications of BrC aerosol light absorption.

Acknowledgements

I would like to express my sincere gratitude to my principal supervisor, Dr. W. P. Arnott, for allowing me the opportunity to study at a world-class research facility for my Ph.D. Thank you for providing quality scientific advice in publishing papers and writing this dissertation. I am greatly indebted to him for his support, excellent guidance and for introducing me to the aerosol and atmospheric physics community.

I would also like to express my gratitude to my committee members for the time and guidance they have provided in my final step toward graduation. Thank you, Dr. W. P. Arnott, Dr. Hans Moosmüller, Dr. Ronald A. Phaneuf, Dr. Henry Fu, and Dr. Mae S. Gustin.

Thanks to everyone in Dr. William P. Arnott's and Dr. Hans Moosmüller's group. Thanks to Dr. Hans Moosmüller for his professional advice and valuable scientific contributions to my research papers. My special thanks go to Ben Sumlin, for his assistance in relation to writing my research papers and dissertation.

My particular thanks to Dr. Rahul A. Zaveri, Pacific Northwest National Laboratory (PNNL), for the opportunity to work on the Carbonaceous Aerosol and Radiative Effects Study (CARES), and also for involving me in the chamber study at the PNNL. Many thanks to Dr. Manvendra K. Dubey and Dr. Bradley A. Flowers from Los Alamos National Laboratory (LANL) for sharing photoacoustic data, and Dr. Qi Zhang, Dr. Ari Setyan from the University of California, Davis, and Dr. Chen Song from PNNL for sharing AMS and SMPS data from the CARES campaign.

I would like to extend thanks to all of my friends at the Department of Physics and Chemistry and the Atmospheric Science Department of UNR/DRI for their memorable help and support. I am also grateful to my friend Tulsi Paudel for his help on the statistical analysis of the data.

Financial support to this work was provided by various agencies: the National Science Foundation, the U.S. Department of Energy Atmospheric System Research, the NASA EPSCoR program, the Pacific Northwest National Laboratory, and the University of Nevada, Reno. I greatly acknowledge their support.

Finally, many thanks go to my family here and back home. I want to acknowledge my mom, brother and other family members for their constant encouragement and love. I appreciate sincerely my wonderful wife, Gita, and our two daughters Neha and Mallika. Thank you for your love, patience and support.

Table of Contents

List of Figures:

Glossary of Acronyms (in order of appearance)

PA-Photoacoustic instrument

SOA-Secondary organic aerosol

BrC-Brown carbon

BC-Black carbon

AEA-Angström exponent of absorption

SSA-Single scattering albedo

OA-Organic aerosol

POA-Primary organic aerosol

CARES-Carbonaceous aerosol and radiative effects study

SMPS-Scanning mobility particle sizer

HR-AMS-High resolution aerosol mass spectrometer

ASL-Above sea level

UV-Ultraviolet

VIS-Visible

IR-Infrared

LAOC-Light absorbing organic carbon

ALAOC-Apparent light absorbing organic carbon

NSF-National Science Foundation

DOE-Department of energy

ASP-Atmospheric science program

$PM_{2.5}$- Particulate matter with aerodynamic diameters less than 2.5 µm

PM_{10}- Particulate matter with aerodynamic diameters less than 10 µm

SOA-Secondary organic aerosol

RI-Refractive index

Nd:YAG- Neodymium-doped yttrium aluminum garnet

PMT- Photomultiplier tube

AES- Angström exponent of scattering

AESSA- Angström exponent of single scattering albedo

BAM- Beta attenuation monitor

FRM- Federal reference method

CE- Combustion efficiency

LT-Local time

BL-Boundary layer

AEE- Angström exponent of extinction

CRD-Cavity ring down

PM_1- Particulate matter with aerodynamic diameters less than 1 µm

Site T0-American River College campus

Site T1-Northside School campus in Cool

NW-Northwest

DMA-Differential mobility analyzer

CPC-Condensation particle counter

SW-Southwest

VOC-Volatile organic carbon

OOA-Oxygenated organic aerosol

HOA- Hydrogenated organic aerosol

APS-Aerosol particle sizer

1 Introduction

1.1 Description of Atmospheric Aerosol

The term "aerosol" refers to the collections of small particles of solids or liquids suspended in a gas. These nano-, micro- and millimeter size particles are primarily produced in three different ways: through combustion processes, through windblown dust, and through chemical reactions in the atmosphere. These aerosols are classified as primary and secondary depending upon their formation process in the atmosphere and might be composed of organic and inorganic species (Seinfeld and Pandis, 2006; Kokhanovsky, 2008). The aerosols that are directly emitted into the atmosphere are termed primary aerosols such as sea salt, dust, biomass-burning aerosols, and volcanic aerosols. These also include anthropogenic aerosols such as black carbon (BC) and aerosols produced during agricultural activities (Perlwitz et al., 2001). The secondary aerosols are often produced in the atmosphere by gas-to-particle conversion. The other component, organic aerosols (OA), can be either primary or secondary and are similarly classified as primary organic aerosols (POA), and secondary organic aerosols (SOA).

The concentrations, size and chemical compositions of atmospheric aerosols vary greatly in space and time, and consequently in their effects on radiative properties. The size distribution of the atmospheric aerosols is crucial for the Earth's radiation balance as well as for the human's health. For example, aerosol particles ranging in diameter from 0.1 to 1.0 μm are the most influential in modifying the incoming solar radiation due to the similarity of particle size and the solar spectral range. Furthermore, the chemical composition of the aerosol determines how it interacts with solar radiation, i.e. how much solar radiation will be absorbed and scattered. Sulfate, nitrate, and certain OA efficiently scatter solar radiation back into space and can cool Earth's surface (Dickerson et al., 1997), while BC and some OA, also called brown carbon (BrC), absorb radiation readily and can warm the atmosphere (Andreae and Gelencser, 2006). Depending upon their chemical compositions, dust impacts solar radiation to varying degrees. Mineral dust absorbs UV and visible radiation, mostly due to the presence of iron compounds such as hematite (Sokolik et al., 1993).

1.2 Motivation for this Study

Aerosols are a major uncertainty in understanding the global climate change (Schwartz and Andreae, 1996) via their direct (scattering and absorption of solar radiation) and indirect (influence of aerosols on cloud droplet) effects. Uncertainty from the direct effect of aerosols is in part due to the varied nature of OA (Kanakidou et al., 2005), while no estimate is given for the indirect effect of aerosol, only an uncertainty range is presented (Schwartz and Andreae, 1996). Precise knowledge of the spectral dependent of aerosol light absorption and scattering is crucial to better understand the aerosol effect on the global climate (Clarke et al., 2007).

Aerosols can adversely affect human health (Dockery et al., 1996), degrade visibility (Watson, 2002), and potentially modify the Earth's radiative balance (Charlson et al., 1992; Sokolik and Toon, 1996). Arrhenius was the first scientist to study the link between fossil fuel combustion and the increased atmospheric concentration of carbon dioxide (CO_2), which might change the Earth's heat balance and cause a warming of the atmosphere (Arrhenius, 1896). Through absorption and scattering of sunlight, aerosols have a radiative effect on the climate comparable in magnitude to that of CO_2. The aerosol impact is much more transient since their atmospheric life time is one week to one month before they are deposited on the surface through dry or wet deposition processes involving precipitation.

Increasingly strong evidence provided by the Intergovernmental Panel on Climate Change (IPCC, 2001) suggests that the Earth is responding to perturbations in its composition, which is known as global climate change. The strongest absorber of solar radiation per unit mass is BC, the sooty emission often seen spewing from the tailpipe of poorly managed diesel engines.

Previous research has clearly indicated that the Asian Brown Cloud (ABC) (the thick haze of mostly BC, BrC, and dust caused primarily by traffic emissions, biomass burning and agricultural activities) is rapidly melting Himalayan glaciers (Ramanathan and Carmichael, 2008). It is reported that the ABC is as much to blame as greenhouse gases for the warming observed in the Himalayas over the past half century.

The findings presented in this dissertation and subsequent analysis will address the major issues in reducing the uncertainties of anthropogenic influences on air quality and climate, as well as provide new insights on the nature of light absorbing OA or BrC.

1.3 Description of the Study

This study involves in-situ measurements and analysis of multispectral aerosol light absorption and scattering by using the photoacoustic (PA) instruments. From 2008 to 2010, ambient data were collected in Reno, NV from various light absorbing and non-absorbing aerosols. For example, during July 2008, the measurements were largely affected by California wildfires, while the month of August 2008 was mostly affected by traffic emissions. The California wildfires produced significant amounts of short wavelength absorbing species such as OA or BrC, while the temperature inversions during the winter of 2009 and 2010 resulted in high concentration of BC and non-absorbing OA. Laboratory-generated aerosols, such as incense burning, salt, and kerosene flame soot served to calibrate and evaluate the PA. Furthermore, incense burning aerosols were used to study the enhanced absorption of BrC, towards the ultraviolet (UV) regions. Also included in this investigation is the data collected during the Carbonaceous Aerosols and Radiative Effects Study (CARES), held in the Sacramento, CA area in June 2010. Scanning mobility particle sizer (SMPS) and high resolution aerosol mass spectrometer (HR-AMS) measurements for particle size distribution and size-resolved chemical composition were concurrently used to characterize the aerosol optical properties during the campaign. Mie theory calculations and shell-core model were used for aerosol light absorption and scattering analysis.

1.3.1 Photoacoustic instrument (PA)

Figure 1.1 presents the schematic of photoacoustic instrument (PA). PA can directly measure aerosol light absorption coefficients for suspended particles. In operation of the photoacoustic instrument, the sample air flow is continuously drawn through an acoustical resonator. The sample air is illuminated by a power modulated laser radiation at the acoustic resonance frequency of the resonator (~ 1500 HZ). The radiation is absorbed by particles within the sample air, and is immediately transferred to the surrounding air as heat. The associated pressure change contributes to a standing wave in the resonator that is detected by a microphone located at a pressure anti-node. The simultaneous light scattering measurement is carried out with a cosine-weighted sensor positioned at the centre of the cavity to act as a reciprocal nephelometer. Chapter 3 presents the detailed working principle of PA.

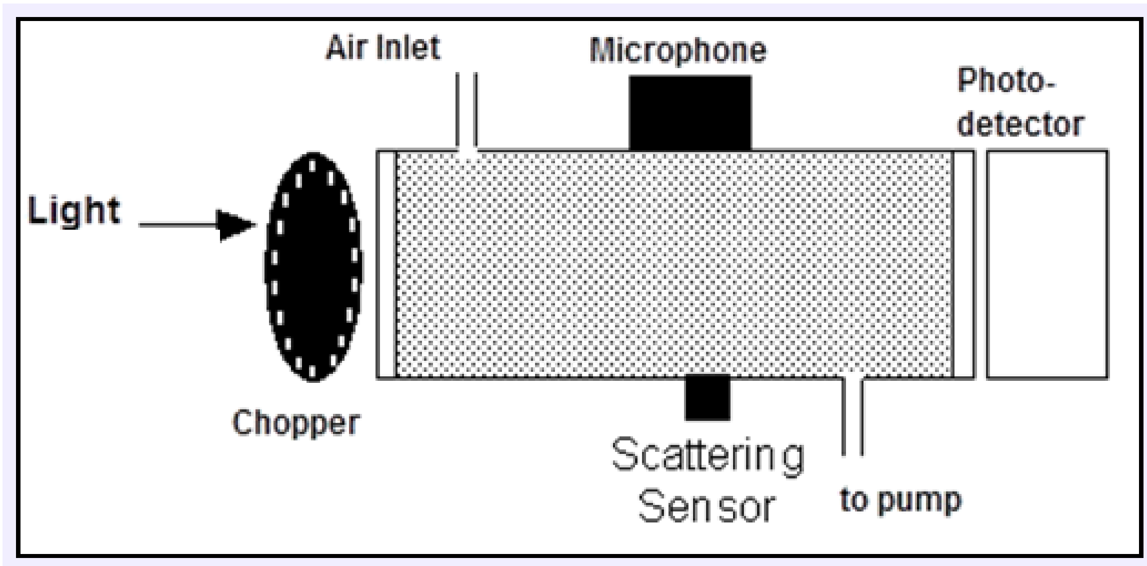

Figure 1.1 Schematic of Photoacoustic (PA) instrument

In addition to aerosol light absorption and scattering measurements at 355 nm (a diode pumped Nd:YAG laser with frequency tripling to produce 355 nm), absorption and scattering measurements in this study were also made simultaneously with a dual-wavelength PA operating at 405 and 870 nm (a laser diode), and two single-wavelength PAs operating at 532 and 1047 nm (Nd:YAG). Operation of PA is carried out in a narrow wavelength range at which a power modulated laser source is available and motivation for measurements, such as whether absorption and scattering measurements of ultraviolet (UV), visible, or infrared (IR) radiation are desired.

It has been shown that absorption at UV wavelengths is strong for some organic carbon components (Kirchstetter, Novakov, and Hobbs, 2004), and absorption at near-IR wavelengths responds overwhelmingly to black carbon (BC). Figure 1.2 shows the absorption coefficients in Mm^{-1} for wavelengths from near UV to near IR vs. time for laboratory generated incense aerosols. This shows that there is an enhanced absorption near UV wavelengths by organic aerosols, while the absorption coefficients towards near IR wavelengths are almost negligible. This highlights the fact that the UV wavelengths are required to study the optical properties of the organic aerosol (OA).

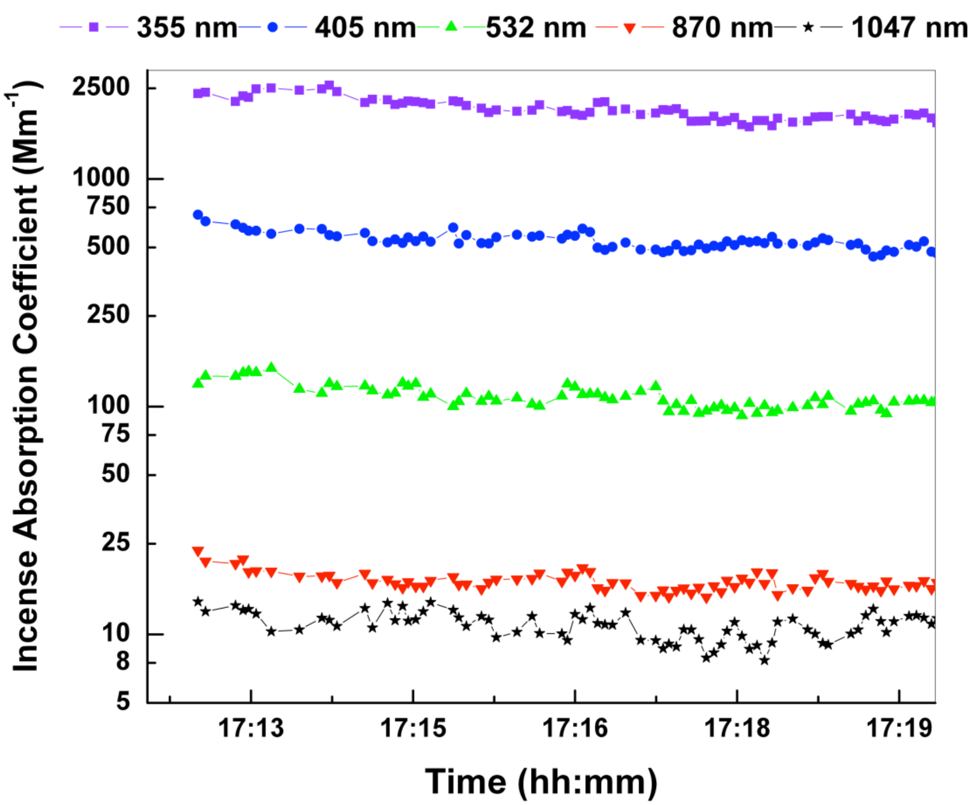

Figure 1.2 Absorption coefficients of incense aerosols for wavelengths from 355 to 1047 nm

1.3.2 Sites included in this Study

1.3.2.1 Reno, NV, USA

Reno is situated just east of the Sierra Nevada on the western edge of the Great Basin (~1,300 m ASL). Reno is naturally an excellent location for aerosol research. It is a basin city where cold air from the surrounding mountain ranges pools in the valley floor almost every night, unless there is strong wind. The cold, sluggish air promotes accumulation of air pollution in the inversion. Under meteorological conditions of high pressure, strong multi-day inversions can develop hazardous levels of air pollutions, including aerosols, oxides of carbon and nitrogen, and organic gases. Strong windstorms associated with meteorological low pressure come through to clear out the pollutants. Inversions happen in all seasons in Reno because of the city's topography, and the air above Reno is so dry and cold at night that the surface cools quickly by emission of infrared radiation. In addition, the episodic effects of biomass burning as part of the ecosystem contributed to the significant amount of light absorbing OA in the Reno area.

1.3.2.2 Sacramento, CA, USA

Sacramento (altitude ~ 30 m ASL) lies at the center of California's Sacramento Valley, which covers the northern third of the broad and agriculturally rich Central Valley. Two ground sites were strategically chosen to study the evolution and transport of urban emissions and their interaction with biogenic emissions in the relatively clean forested area. The urban site, T0 (altitude ~ 30 m ASL), was located on the American

River College campus, ~14 km northeast of the downtown Sacramento area. The other site included in this study was in Cool, CA, (altitude ~450 m ASL), located ~40 km northeast of downtown Sacramento, CA on the Northside School campus.

1.3.3 Dissertation Structure

This dissertation consists of two published and one to be submitted peer reviewed articles:

1) Chapter 2 is a paper comparing and contrasting the multispectral aerosol light scattering and absorption in Reno between the smoky month of July, 2008, (resulting from ~1000 lightning-triggered fires in Northern California) and the relatively clean month of August 2008. The citation is as follows:

Gyawali, M., Arnott, W. P., Lewis, K., and Moosmüller, H.: In situ aerosol optics in Reno, NV, USA during and after the summer 2008 California wildfires and the influence of absorbing and non-absorbing organic coatings on spectral light absorption, Atmos. Chem. Phys., 9, 8007-8015, doi:10.5194/acp-9-8007-2009.

2) Chapter 3 is a paper on the analysis of aerosol optical properties, using a novel UV 355 nm instrument of our design and manufacture, along with existing photoacoustic instruments operating at 405, 532, 870, and 1047 nm. The citation is as follows:

Gyawali, M., Arnott, W. P., Zaveri, R. A., Song, C., Moosmüller, H., Liu, L., Mishchenko, M. I., Chen, L.-W. A., Green, M. C., Watson, J. G., and Chow, J. C.: Photoacoustic optical properties at UV, VIS, and near IR wavelengths for laboratory generated and winter time ambient urban aerosols, Atmos. Chem. Phys., 12, 2587-2601, doi:10.5194/acp-12-2587-2012.

3) Chapter 4 is a soon to be submitted paper to the CARES special issue in the Journal, “Atmospheric Chemistry and Physics”. This paper is about the Carbonaceous Aerosol and Radiative Effects Study (CARES), a multi-institutional project for characterizing the transformation and transport of aerosols from the San Francisco Bay Area through the biogenic foothills to Cool, California. The following will be the author names and title of the article:

Gyawali, M., Arnott, W. P., Zaveri, R. A., Flowers, B., Dubey, M. K., Setyan, A., Zhang, Q., Song, C., Radney, J. G., Atkinson, D. B., Gorkowski, K., Mazzoleni, C., Moosmüller, H., Influence of Chemical Transformation and Meteorological Transport on Multispectral Aerosol Light Scattering, Absorption, and Extinction during the 2010 CARES campaign.

1.4 References:

Andreae, M. O. and Gelencser, A.: Black carbon or brown carbon? The nature of light-absorbing carbonaceous aerosols RID B-1068-2008, Atmos. Chem. Phys., 6, 3131–3148, 2006.

Arrhenius, S.: XXXI. On the influence of carbonic acid in the air upon the temperature of the ground, Philosophical Magazine Series 5, 41(251), 237–276, doi:10.1080/14786449608620846, 1896.

Charlson, R., Schwartz, Hales, J., Cess, R., Coakley, J.,Hansen, J., and Hofman, D.: Climate forcing by anthropogenic aerosols, Science, 255(5043), 423–430, doi:10.1126/science.255.5043.423, 1992.

Clarke, A., McNaughton, C., Kapustin, V., Shinozuka, Y., Howell, S., Dibb, J., Zhou, J., Anderson, B., Brekhovskikh, V., Turner, H. and Pinkerton, M.: Biomass burning and pollution aerosol over North America: Organic components and their influence on spectral optical properties and humidification response, J. Geophys. Res., 112, doi:200710.1029/2006JD007777, 2007.

Dickerson, R. R., Kondragunta, S., Stenchikov, G., Civerolo, K. L., Doddridge, B. G. and Holben, B. N.: The Impact of Aerosols on Solar Ultraviolet Radiation and Photochemical Smog, Science, 278(5339), 827–830, doi:10.1126/science.278.5339.827, 1997.

Dockery, D. W., Cunningham, J., Damokosh, A. I., Neas, L. M., Spengler, J. D., Koutrakis, P., Ware, J. H., Raizenne, M. and Speizer, F. E.: Health effects of acid aerosols on North American children: respiratory symptoms., Environ Health Perspect, 104(5), 500–505, 1996.

Kanakidou, M., Seinfeld, J. H., Pandis, S. N., Barnes, I., Dentener, F. J., Facchini, M. C., Van Dingenen, R., Ervens, B., Nenes, A., Nielsen, C. J., Swietlicki, E., et al.: Organic aerosol and global climate modelling: a review, Atmos. Chem. Phys., 5(4), 1053–1123, doi:10.5194/acp-5-1053-2005, 2005.

Kirchstetter, T. W., Novakov, T., and Hobbs, P. V. (2004). Evidence that the spectral dependence of light absorption by aerosols is affected by organic carbon. Journal of Geophysical Research 109(D21209), doi:10.1029/2004JD00499.

Kokhanovsky, A. A.: Aerosol Optics: Light Absorption And Scattering by Particles in the Atmosphere, Praxis publishing Ltd, Chichester, UK, 2008.

Perlwitz, J., Tegen, I. and Miller, R. L.: Interactive soil dust aerosol model in the GISS GCM 1. Sensitivity of the soil dust cycle to radiative properties of soil dust aerosols, J. Geophys. Res., 106(D16), PP. 18,167–18,192, doi:200110.1029/2000JD900668, 2001.

Ramanathan, V. and Carmichael, G.: Global and regional climate changes due to black carbon, Nature Geoscience, 1(4), 221–227, doi:10.1038/ngeo156, 2008.

Schwartz, S. E. and Andreae, M. O.: Uncertainty in Climate Change Caused by Aerosols, Science, 272(5265), 1121–1121, doi:10.1126/science.272.5265.1121, 1996.

Seinfeld, J. H. and Pandis, S. N.: Atmospheric chemistry and physics: from air pollution to climate change, Wiley., 2006.

Sokolik, I., Andronova, A. and Johnson, T. C.: Complex refractive index of atmospheric dust aerosols, Atmospheric Environment. Part A. General Topics, 27(16), 2495–2502, doi:10.1016/0960-1686(93)90021-P, 1993.

Sokolik, I. N. and Toon, O. B.: Direct radiative forcing by anthropogenic airborne mineral aerosols, doi:10.1038/381681a0, 381(6584), 681–683, doi:10.1038/381681a0, 1996.

Watson, J. G.: Visibility: science and regulation, J Air Waste Manag Assoc, 52(6), 628–713, 2002.

2 In situ aerosol optics in Reno, NV, USA during and after the summer 2008 California wildfires and the influence of absorbing and non absorbing organic coatings on spectral light absorption

2.1 Abstract

Hundreds of wildfires in Northern California were sparked by lightning during the summer of 2008, resulting in downwind smoke for the months of June and July. Comparisons are reported for aerosol optics measurements in Reno Nevada made during the very smoky summer month of July and the relatively clean month of August. Photoacoustic instruments equipped with integrating nephelometers were used to measure aerosol light scattering and absorption at wavelengths of 405 nm and 870 nm, revealing a strong variation of the aerosol light absorption with wavelength. Insight on fuels burned is gleaned from comparison of Ångström exponents of absorption (AEA) versus single scattering albedo (SSA) of the ambient measurements with laboratory biomass smoke measurements for many fuels. Measurements during the month of August, which were largely unaffected by fire smoke, exhibit surprisingly low AEA for aerosol light absorption when the SSA is highest, again likely as a consequence of the underappreciated wavelength dependence of aerosol light absorption by particles coated with non absorbing organic and inorganic matter. Coated sphere calculations were used to show that AEA as large as 1.6 are possible for wood smoke even with non-absorbing

organic coatings on black carbon cores, suggesting care be exercised when diagnosing AEA.

2.2 Introduction

Biomass burning is a significant global source of trace gases and particles in the atmosphere. Optical properties of aerosols emitted from biomass burning are highly uncertain due to the uncertainty in combustion factors, burned areas, and the types of fuels (Ito and Penner, 2004), the flaming and smoldering phase of burning, as well as rapidly changing atmospheric conditions (Chen et al., 2007; Hudson et al., 2004). Biomass burning aerosols grow upon aging due to coagulation and condensation and exhibit increased scattering coefficients (Johnson et al., 2008). Biomass burning aerosol significantly alter the Earth's radiation by scattering and absorbing solar radiation (Chen et al., 2006; Lewis et al., 2008). Biomass burning has short and long term consequences on the radiation budget (Naik et al., 2007), as the increased light scattering by particles cools the Earth's surface but the increased CO_2 warms the surface in the long term. Accelerating death rates of old forest trees may soon strongly impact short and long term atmospheric composition.

The wildfire activity in the western US has increased in recent decades mainly due to severe droughts and abundant fuels (Westerling et al., 2006). California is among the states that have the highest wildfire activity, generally starting mid-May and ending in October (Pfister et al., 2008). In summer 2008, Northern California lightning triggered most of 2780 individual fires observed, burning 4,686 km^2 [http://en.wikipedia.org/wiki/Summer_2008_California_wildfires]. At times, smoke from

California wildfires can be observed moving from the west to east coast (Hoff et al., 2005).

In this study, in situ optical characteristics of summer 2008 California wildfire aerosols are reported and compared with those from urban pollution. A dual wavelength photoacoustic instrument operating simultaneously at 405 nm and 870 nm was used for the measurement of aerosol light absorption and scattering (Lewis et al., 2008). The simultaneous measurement at these two wavelengths provides insight into the optical characteristics of black carbon (BC) or “soot”, potentially modified by non-absorbing organic carbon (OC) coatings and light absorbing organic carbon (LAOC) or “brown carbon” (BrC), the two main light absorbing carbonaceous substances in the atmosphere (Moosmüller et al., 2009). The photoacoustic instrument draws sample air continuously through its acoustical resonator and illuminates it with power modulated laser radiation at the acoustic resonance frequency of the resonator. The heating of the particles takes place due to the absorption of laser radiation and the heat rapidly transfers to the surrounding air. The resulting periodic pressure fluctuations are measured by a microphone (Arnott et al., 1999). Scattering measurements are carried out in the photoacoustic instrument with the technique of reciprocal nephelometry (Lewis et al., 2008; Mulholland and Bryner, 1994; Rahmah et al., 2006). The instrument is calibrated by using a high concentration of absorbing gas or kerosene-flame soot or laboratory generated aerosol with extinction dominated by scattering (Arnott et al., 2000; Lewis et al., 2008). Generally, the absorption by BC in the region from 370 nm to 950 nm is inversely proportional to the wavelength, whereas absorption due to BrC is stronger towards UV regions (Moosmüller et al., 2009). Hence multi wavelength measurements are needed to adequately address the absorption characteristics of carbonaceous aerosols in the atmosphere (Andreae and Gelencsér, 2006). Photoacoustic absorption measurements are not affected by filter matrix artifacts that can be complicated by organic coatings (Lack et al., 2008; Subramanian et al., 2007).

In addition to truly light absorbing organic carbon (LAOC), the light absorption of BC can be enhanced by non-absorbing OC that will be referred to as apparently light absorbing carbon (ALAOC), independent of whether the coating absorbs light or not. It is the total effect of the coating on the fractal soot core. Part of the affect the ALAOC may be to collapse the core, thereby changing its absorption. It is easy to confuse LAOC and ALAOC. In LAOC black carbon cores are coated with organic matter that typically absorbs more strongly at shorter wavelengths than at longer wavelengths. However, for ALAOC, it is acknowledged in this definition that there may be strong wavelength dependence in the light absorption amplification of a black carbon core by organic coatings that do not absorb light at all. Later work will refine the definition of the Ångström exponent of absorption to clearly distinguish between ALAOC and LAOC, and it will be clearly shown that filter based methods do not diagnose ALAOC well because particle bound OC can surround the filter media. Here, an investigation is performed to elucidate the likely error involved in naively interpreting Ångström exponent of absorption measurements solely in terms of LAOC without considering ALAOC.

2.3 Measurements and analysis

Fig. 2.1 shows a satellite image of the smoke extending from the northern California east, beyond Reno, NV on July 10, which was the smokiest day of the summer 2008 in Reno, NV. The image shows that Reno is about 100 miles away from the center of the major wild fire sources of July 2008. This smoke source and wind trajectory were similar for much of month of July. The dual wavelength photoacoustic instrument was operated continuously from the starting of July to the end of August, 2008, where the measurements were carried out for 22 days in July and 27 days in August (interrupted for instrument calibration). The measurements were obtained at the Physics building of University of Nevada, Reno, USA. Besides having a couple of minor roads circling the University, two freeways are nearly one mile away from the University. The University is located in the center of the city.

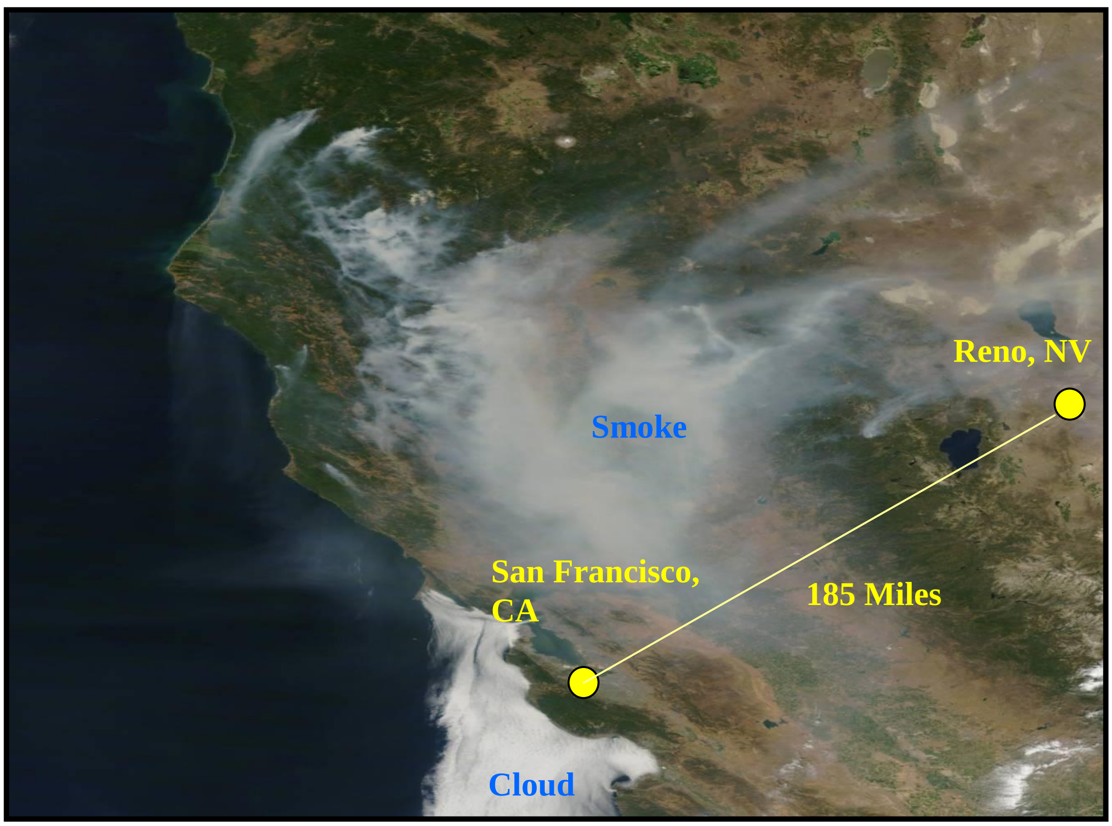

Figure 2.1 Satellite image of smoke extending from northern California to Reno, Nevada on July 10, 2008. The smoke sources and wind trajectory were similar for much of month of July

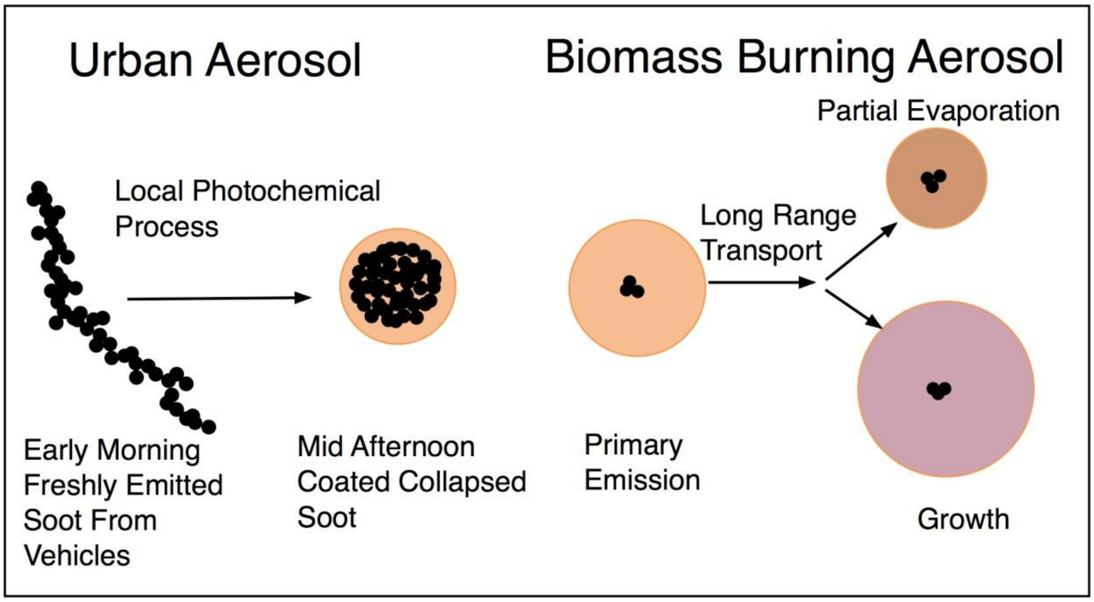

Figure 2.2 Conceptual model of emission and aging of urban and biomass burning aerosol.

Detailed examinations of BC particles show that they consist of agglomerations of small spherical spherules (Liu et al., 2008). The spherules bind together due to the electrostatic force (Bruce et al., 1991). The mixing state of BC particles changes in the aging process due to condensation, coagulation and photochemical oxidation (Oshima et al., 2009). In this process the coating with water soluble compounds like ammonium sulfate makes them hydrophilic.

Fig. 2.2 shows the conceptual model of the aging of the urban aerosol and biomass burning aerosol (especially for primary emission of ponderosa pine-like burning aerosol) in which small BC cores are heavily coated with organics (Lewis et al., 2009). Open chain BC particles from biomass burning becomes closely packed spheres due to water uptake and condensation of inorganic and organic compounds (Hallett et al., 1989). Immediately after emission from the source the BC particles might have internal and external mixing states but with the aging process in the atmosphere the simple shell-core model (described later) is plausible for biomass burning aerosols (Martins et al., 1998) and mid day urban aerosol coated with generated particulate matter.

2.3.1 Aerosol extinction variation

The extinction (sum of absorption and scattering) variation presented here was the daily average of half hour measurements for the period of July and August 2009 respectively. The photoacoustic measurements of absorption and scattering coefficients have 5% and 15% relative uncertainty respectively (Lewis et al., 2008). The time series of scattering and absorption (half hour average) measurements reached maximum values of 1230 Mm^{-1} and 106 Mm^{-1} at 405 nm and 476 Mm^{-1} and 30 Mm^{-1} at 870 nm on July 10, 2008 and of 154 Mm^{-1} and 18 Mm^{-1} at 405 nm and 52 Mm^{-1} and 7 Mm^{-1} at 870 nm on July 30, 2008 respectively. The daily maximum scattering and absorption were decreasing between these days. Between July 5 to July 10 the scattering and absorption coefficients were higher for both wavelengths but less than the maximum values mentioned above. Similarly, the time series of scattering and absorption coefficients were maximum at 129 Mm^{-1} and 28 Mm^{-1} at 405 nm and 64 $Mm^{-1}$and 11 Mm^{-1} at 870 nm on August 05, 2008. These higher values in early August might be due to some sporadic smoke in the local area, but of much lower magnitude than in July. Slightly lower values of scattering and absorption were found from August 11 to 15. For the rest of days these values were significantly less. In Mexico City, due to the diurnal change in the primary aerosol sources and photochemically-generated secondary aerosol, the scattering was maximum several hours later in the day than absorption (Paredes-Miranda et al., 2009). In our study scattering contributed most of the extinction at both 405 nm and 870 nm for both months. The evidence of vehicular emission dominance for the extinction in August was apparent in the aerosol extinction variation (Fig. 2.3) with the maximum in the extinction around the morning rush hour (from 6 AM to 11 AM), and nearly symmetrical low values on either side of the maximum for both 405 nm and 870 nm in August. In contrast, morning rush hour made only a small contribution to extinction in July. The extinction starts to decrease from 8 AM and becomes minimum around 1 PM and starts to increase continuously. These variations of extinction at both 405 nm and 870 nm in July exhibited the delaying effect of smoke on the daytime boundary layer development (Rissler et al., 2006).

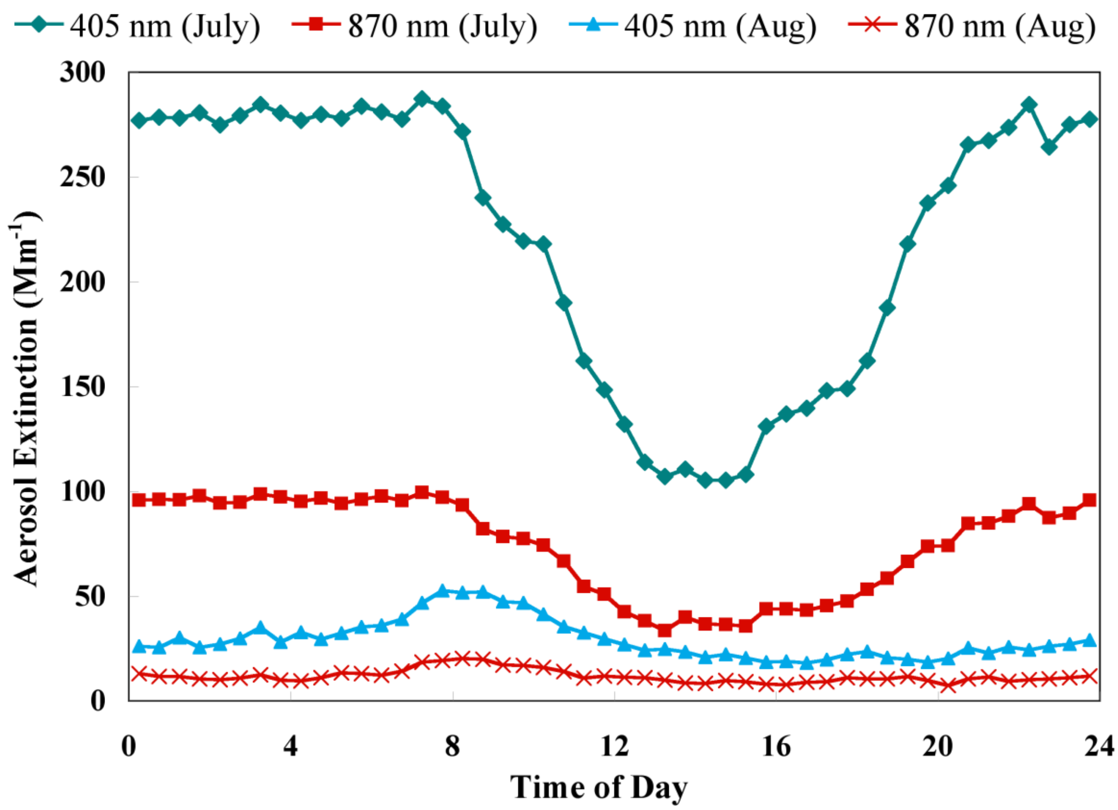

Figure 2.3 The monthly averaged, diurnal apparently light absorbing organic carbon (ALAOC) for July and August 2008.

The monthly averaged diurnal aerosol extinction as function of time of day (Fig. (2.4)) indicates strong impacts of biomass aerosol in July compared to August at both 405 nm and 870 nm.The extinction for July shows a clear diurnal pattern, with aerosol extinction decreasing gradually after 8 AM due to the expansion of the boundary layer and increased wind speed diluting the plume. For August, a morning rush hour peak was observed from 6 AM to 11 AM coinciding with increased traffic volume at a time when boundary layer dilution is near its minimum and wind speeds are still low.

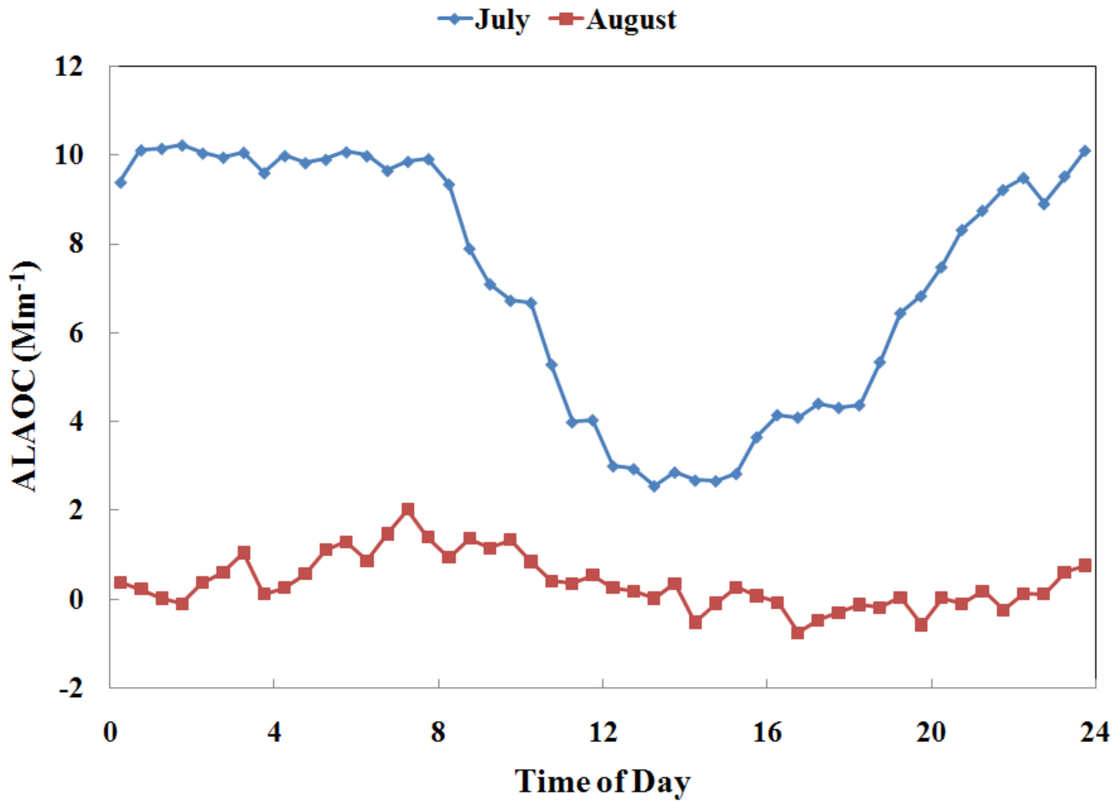

Figure 2.4 The monthly averaged, diurnal apparently light absorbing organic carbon (ALAOC) for July and August 2008.

2.3.2 Naive estimate of LAOC: ALAOC

The apparent light absorption coefficient β_{ALAOC} due to organic carbon aerosol at 405 nm is written as

$$\beta_{ALAOC} = \beta_{abs}(405\,nm) - \beta_{abs}(870\,nm) * 870/405 \quad , \qquad (1)$$

where β_{abs}(405 nm) and β_{abs}(870 nm) are the aerosol absorption coefficients at 405 and 870 nm, respectively. Here, the assumption is that BC absorbs both at 405 nm and 870 nm whereas LAOC absorbs strongly at 405 nm and negligibly at 870 nm. The second term is the equivalent BC absorption at 405 nm assuming inverse wavelength dependence. Equation (1) acknowledges that some of the relative enhancement of absorption at 405 nm may be due to wavelength selective amplification by a non-absorbing organic coating, in addition to any contribution by organic carbon that may absorb strongly at 405 nm and not at 870 nm. Figure 2.4 shows the calculated monthly averaged ALAOC for the months of July and August. ALAOC was higher for July and almost nonexistent for August, which is consistent with the notion that organic matter emission from motor vehicles does not contain strong chromophores nor is abundant enough to cause strong coating effects. In addition, the BC core size for wood smoke is much smaller than for vehicular emissions. In July note as much as 10 Mm^{-1} absorption due to ALAOC, suggesting that biomass burning was the main source of ALAOC during our measurements.

2.3.3 Single Scattering Albedo (SSA)

Single scattering albedo (SSA) is defined as the ratio of scattering coefficient to extinction coefficient. Figure 2.5 illustrates the monthly averaged SSA for 405 nm and 870 nm. It depicts the contrasts between SSA for the months of July and August where aerosol absorption was dominated by wildfire aerosols and vehicular emissions, respectively, and highlights the different optical properties of the aerosols measured during this time period. It is noteworthy that the calculated SSA was consistently higher

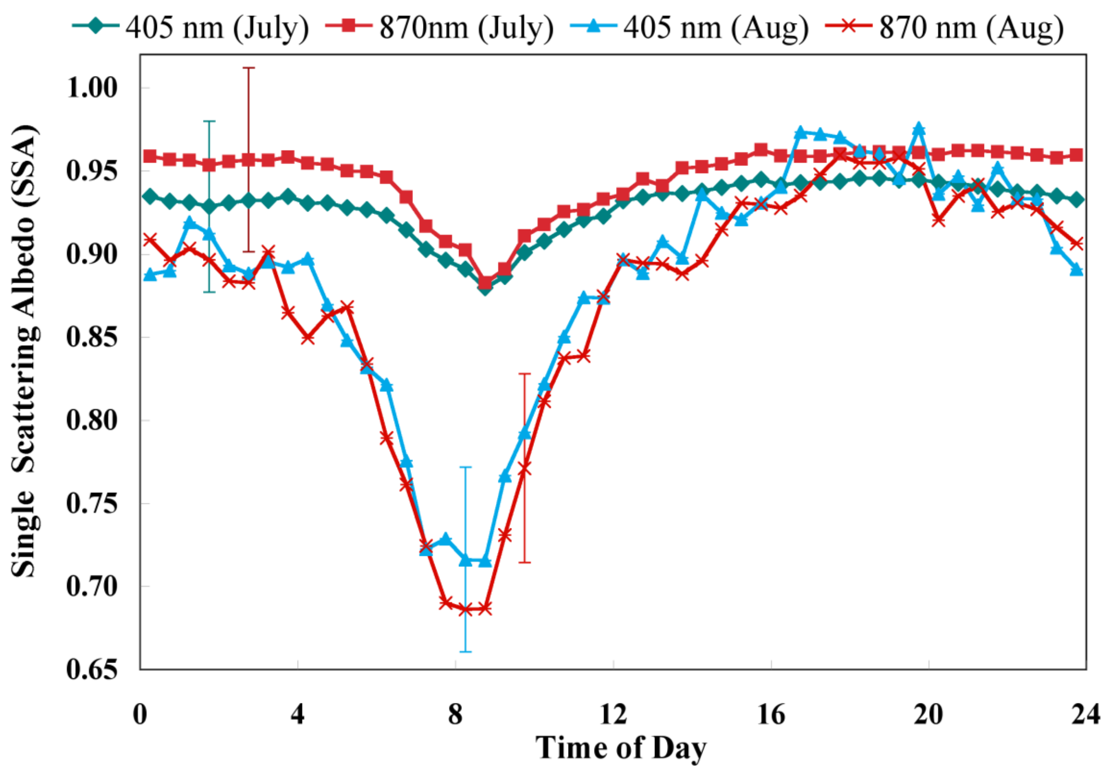

Figure 2.5 The monthly averaged, diurnal aerosol SSA for 405 nm and 870 nm for the months of July and August 2008. SSA is higher for the smoky month of July. Note the minimum around the morning rush hour due to the higher vehicular emission. LAOC causes the SSA at 405 nm to be lower than at 870 nm in July. Uncertainty on SSA was determined by assuming 5% relative uncertainty in photoacoustic absorption coefficient measurements and 15% relative uncertainty in scattering coefficient measurements.

at 870 nm than at 405 nm during July where SSA at 870 nm varies from 0.88 to 0.96 and SSA at 405 nm varies from 0.88 to 0.93. This can be attributed to the large proportion of ALAOC in wildfire aerosol transport from California that preferentially absorbs radiation in the UV region (Andreae and Gelencsér, 2006) thereby lowering the SSA at 405 nm. Contrary to this observation, during August SSA at 405 nm (0.71 - 0.97) was in general higher than SSA at 870 nm (0.68- 0.95) suggesting the dominance of the BC emission from vehicles with absorption coefficients inversely proportional to the wavelength. Also apparent from Fig. 2.5 is the strong diurnal cycle on SSA, with minima in the morning rush hour (6:00 – 10:00 AM) and maxima on either side. This can be explained in terms of local conditions associated with the rush hour vehicular emissions and mixing of the aerosol with the development of the boundary layer. The photochemical activity during day time and the growth of particle size might have increased the scattering activity of the aerosol that causes the higher value of SSA at both wavelengths in the later part of day.

2.3.4 Ångström Exponent of Absorption (AEA)

The wavelength dependence of absorption is conventionally quantified using the AEA (α_{abs}), which for the wavelengths of 405 and 870 nm can be written as

$$\alpha_{abs} = -\ln[\beta_{abs}(405nm)/\beta_{abs}(870nm)]/\ln[405/870], \tag{2}$$

where $\beta_{abs}(405)$ and $\beta_{abs}(870)$ are the absorption coefficients at 405 and 870 nm, respectively.

A plot of the monthly averaged, diurnal Ångström exponent of absorption (AEA) for 405-870 nm is shown in Fig. 2.6. Strong diurnal cycles of AEA during July and August are apparent in these observations. This clearly distinguishes the dependence of AEA for the months of July and August. During July AEA varies from 1.42 to 2.07, and is consistent with the measurements reported elsewhere for biomass burning aerosols (Bergstrom et al., 2007; Clarke et al., 2007; Kirchstetter et al., 2004). The diurnal pattern of AEA for July shows it's minimum around morning rush hour which can be attributed to the local dominance of vehicular emission of the black carbon. During the "normal" month of August AEA varies from 0.88 to 1.28. Most of the AEA values are closer to 1.0 during the morning rush hour and until afternoon as observed by the same authors and are described as the characteristics of the black carbon or “soot” (Moosmüller et al., 2009). AEA starts to decrease afternoon and is minimum in the later part of the day at 0.88. At this time of day, the concentration of BC decreases with the expansion of boundary layer. But mixing, coating, and coagulation of BC with organic and inorganic aerosols affect its absorption in the diluted state. The enhancement might be slightly greater for 870 nm than for 405 nm at this time, consistent with low AEA values. Further, our simulations of AEA shows the possibility of getting AEA values less than one for uncoated as well as coated carbon spheres.

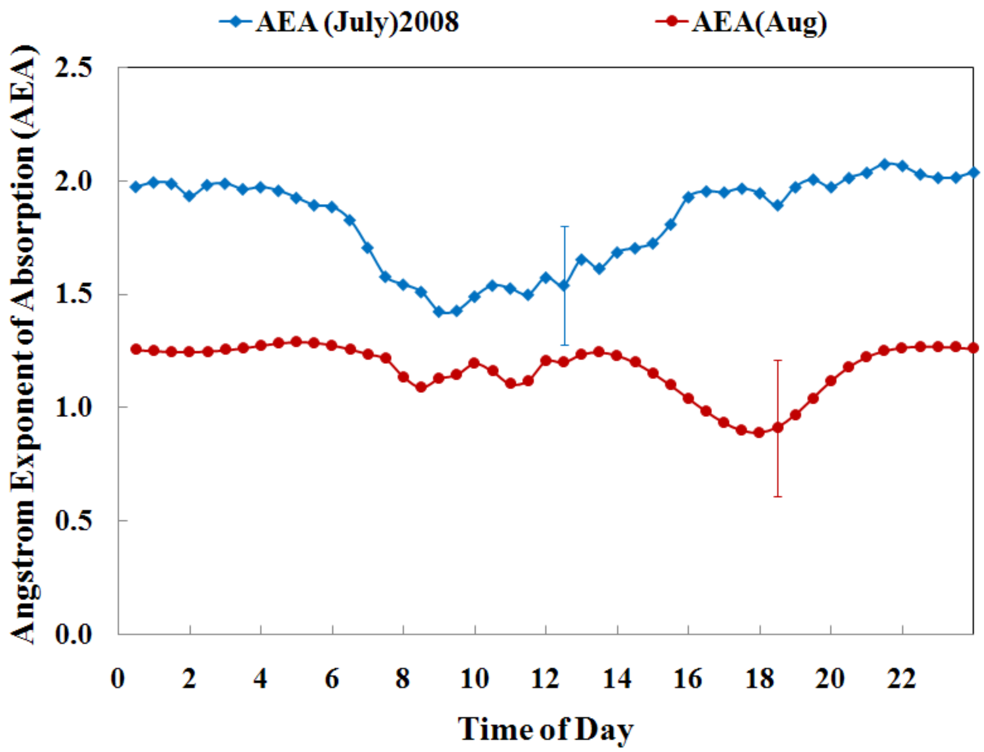

Figure 2.6 The monthly averaged, diurnal aerosol AEA (405-870 nm) for the months of July and August vs. time of a day. Uncertainty on AEA was determined by assuming 5% relative uncertainty in photoacoustic absorption coefficient measurements.

Bergstrom, et al. (2007) pointed out that the observation of AEA less than one is interesting and might be due to measurement uncertainties or due to slightly larger values of the imaginary part of the refractive index at longer wavelengths for certain particles. Very low values of AEA have been reported without explanation for different situations (Bergstrom et al., 2007; Clarke et al., 2007; Roden et al., 2006; Subramanian et al., 2007; Yang et al., 2009). Clark, et al. (AGU poster, 2005) has mentioned an AEA from 0.3 to 1.3 for urban air.

2.3.5 Comparison with Laboratory Observations

A comparison of optical properties of California wildfire smoke aerosol of summer 2008 was made with the optical properties of emissions from the laboratory combustion of wildland and agricultural fuels in the Fire Science Laboratory of the USFS in Missoula, MT (Lewis et al., 2008) as shown in Fig. 2.7. This comparison reveals that the optical properties of the California wildfire smoke aerosol of summer 2008 are closest to those of emissions from the combustion of different pine fuels. The observed SSA at Reno, NV of the California wildfire of summer 2008 was slightly greater than observed at the laboratory, possibly due to the increase of SSA during about six hours of aging since emission (Abel et al., 2003) and also possibly influenced by differences in fuel moisture and combustion conditions.

2.3.6 Simulations and Discussion

The optical model of a highly absorbing BC core surrounded by a nonabsorbing shell is suggested for biomass burning aerosols (Martins et al., 1998) and for aged atmospheric soot (Bond and Bergstrom, 2006). However, this model may be unreliable for freshly emitted aerosols and long chain aggregates of BC particles near the source in

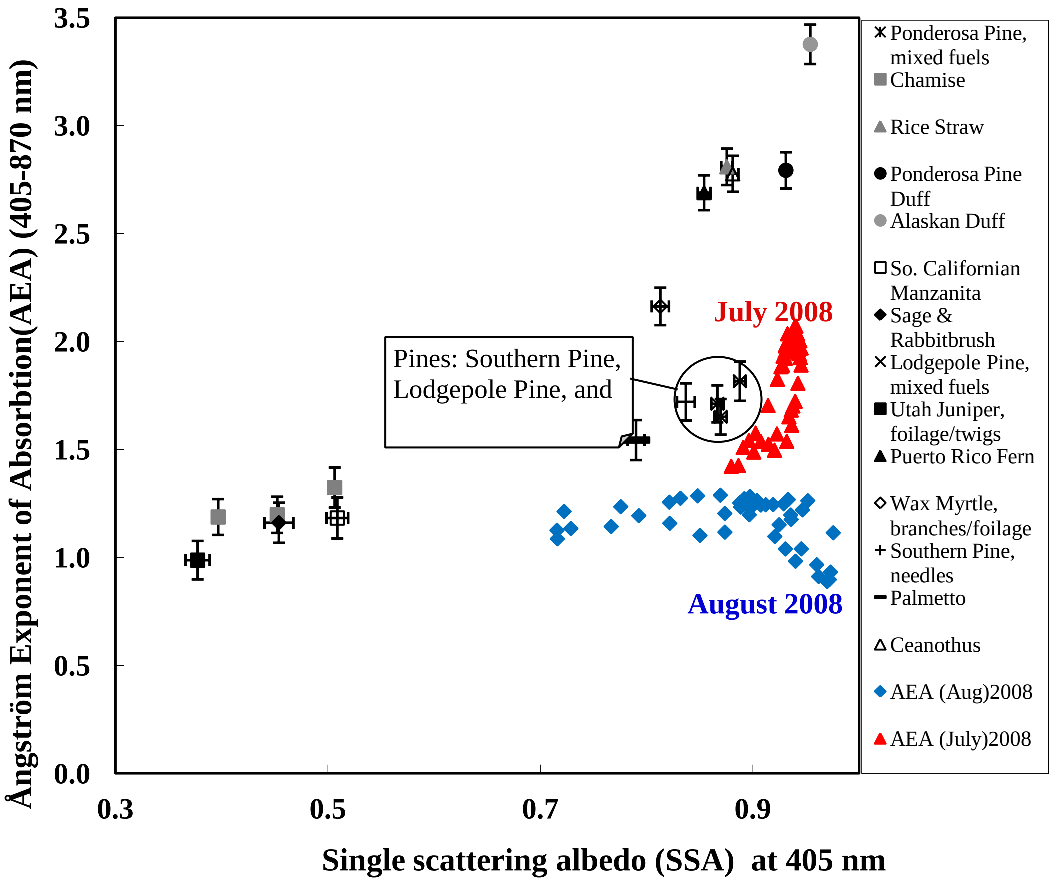

Figure 2.7 A comparison of monthly averaged, diurnal Ångström exponent of absorption (AEA) versus single scattering albedo (SSA) at 405 nm for the months of July and August 2008 with the AEA and SSA of the laboratory burned fuels. The comparison illustrates that the optical properties of California wildfires aerosols of 2008 are similar to pine smoke aerosols.

urban locations. Shell-core model may overestimate aerosol light absorption by less than 15 % in comparison to the random location of soot agglomerates (Fuller et al., 1999). This overestimate is due to the focusing of electromagnetic energy at the BC core due to lensing (Redemann et al., 2001). Laboratory investigations have been conducted to confirm the atmospheric BC aerosol coating effect on absorption (Schnaiter et al., 2005) in which soot particles were coated with secondary organic matter. Schwarz et al. (2008) discussed the use of the shell-core approach for in situ measurements of light absorption in the tropical atmosphere. The coating on BC particles increases with altitude to the lower stratosphere (Schwarz et al., 2008).

Ponderosa pine and other pine species were the typical fuels for the Northern California wild fires in 2008. In primary emissions of smoke from burning ponderosa pine, a mass fraction of less than 1% black carbon and around 99% organic matter was observed, and the black carbon core diameter was typically 50 nm (Lewis et al., 2009). The fractal structure of biomass burning aerosols becomes compacted during atmospheric aging (Chakrabarty et al., 2007) and increasingly spherical due to a coating of secondary species like organic matter, and nitrate or sulfate species from gas to particle conversion (Martins et al., 1998).

In August 2008, local traffic related emissions were the dominant black carbon source. Aerosol absorption measurements in the early morning are dominated by freshly emitted soot particles having low fractal dimension whereas within three hours after sunrise, absorption is due to photochemically-aged soot that is typically more hygroscopic than the fresh soot (Moffet and Prather, 2009). The soot core size after coating is typically around 200 nm (Moffet and Prather, 2009).

The shell-core model for aerosol light absorption and scattering was used to explore the parameter space of AEA relevant to observations. The aim of the simulations presented here was to investigate the theoretically possible variations on AEA for uncoated and coated carbonaceous spheres. The core refractive index was taken to be wavelength independent. For uncoated BC spheres with a complex refractive index of

(1.55, 0.8i), AEA for 405 and 870 nm varies from 1.0 to 1.1 and to -0.24, as function of the core diameter as shown in Fig. 2.8. AEA increases to about 1.11 for a core diameter of about 0.07 µm and then decreases continuously, reaching a minimum of about -0.24 around 0.72 µm and increases towards its geometrical limit of zero for large spheres.

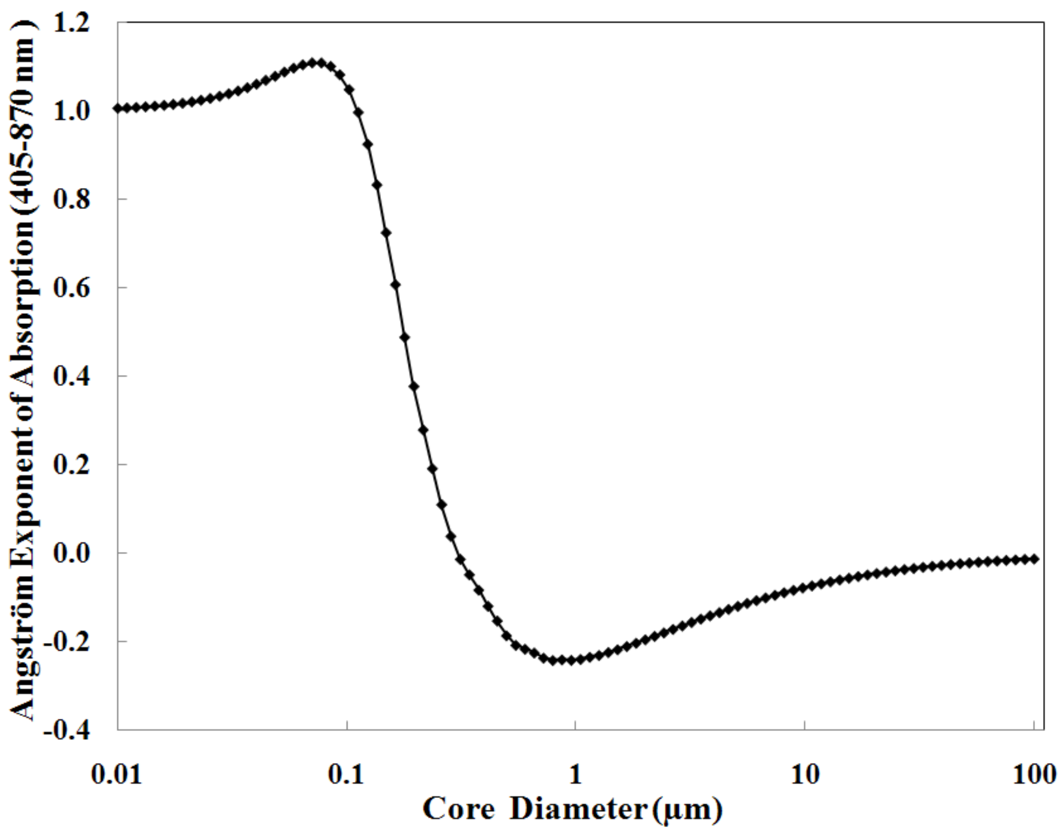

Figure 2.8 . Ångström exponent of absorption (AEA) as function of core diameter from Mie theory for the uncoated sphere model for monodisperse black carbon having a refractive index (1.55, 0.8 i).

The effects of non absorbing coatings (refractive index 1.5, 0.0i), and absorbing coatings (refractive index 1.5, 0.012i at 405 nm and 1.5, 0.0i at 870 nm) on AEA are shown in Figs. 2.9 and 2.10 respectively. The regions denoted by 'C' in these figures represent the aerosol conditions in Reno, and likely other cities, in the afternoon when secondary aerosol mass has condensed on soot cores and compacted them by collapse to a more spherical shape. ‘F’ in these figures represents the core sizes and coatings typical of ponderosa pine fire aerosol. ‘F’ and 'C’ are representative of the afternoon aerosol conditions in the months of July (smoky) and August (urban aerosol only), respectively. For an identical core surrounded by a spherical coating with refractive index of (1.5, 0.0i), AEA becomes as large as 1.6, even though the coating is non absorbing, for example, in the parameter space near point ‘F’ in Fig. (2.9). It is noteworthy that point ‘F’ in Fig. (2.9) coincides with typical BC core and coating diameters observed in ponderosa pine smoke (Lewis et al., 2009). To reiterate, the coating need not be absorbing to give an AEA between 405 nm and 870 nm significantly larger than unity. By contrast, point ‘C’ in Figs. (2.9) and (2.10), representative of the parameter space commonly observed for urban soot when coated and collapsed at mid day due to secondary aerosol formation on the soot (Schnaiter et al., 2003), corresponds to AEA significantly less than unity for both absorbing and non absorbing coatings. However, freshly emitted soot in the predawn hours before collapse to a more compact shape is likely to have an AEA greater than or equal to unity (Bergstrom et al., 2007) as observed in Fig. (2.6). These calculations were performed with monodisperse particles. The features such as the black islands (Figure 2.9) and the spiky structures (Figure 2.10), are caused by the "Mie wiggles" and will disappear for polydisperse model calculations. The power law enhancement caused by nonabsorbing coatings is also clearly seen with calculations using polydisperse aerosols.

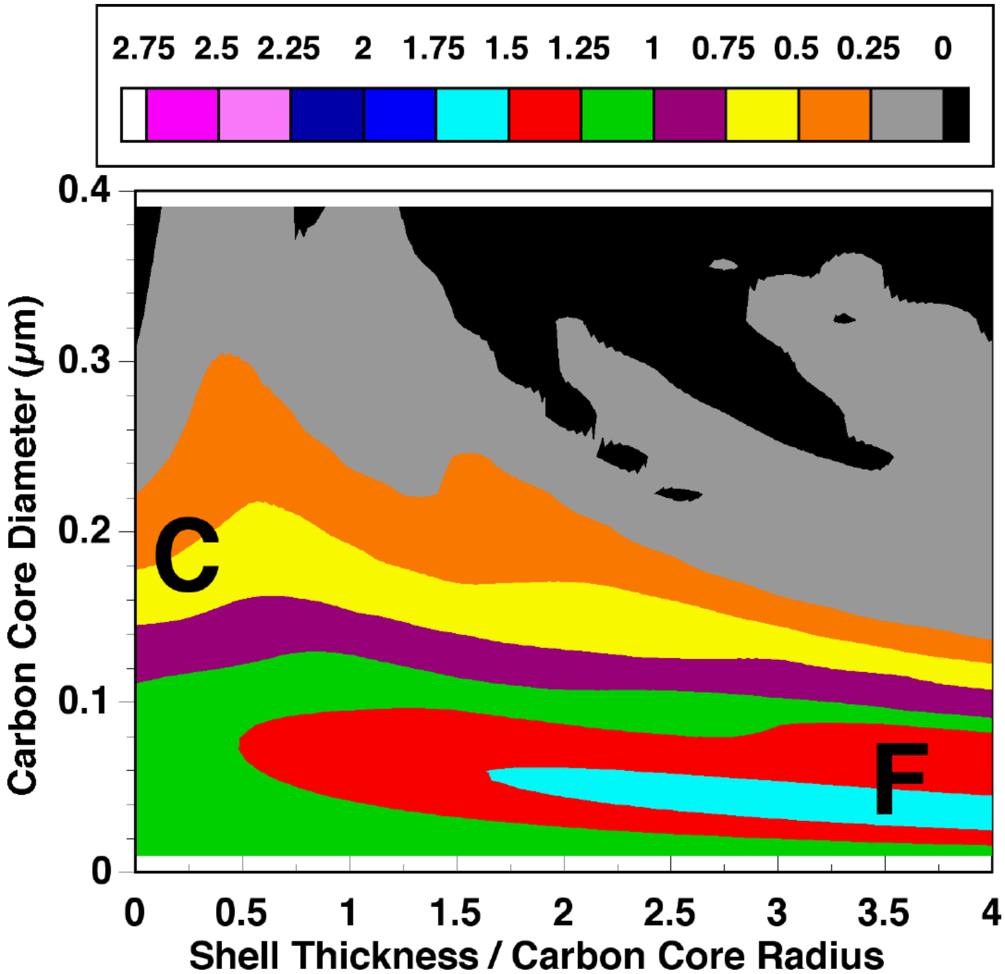

Figure 2.9 Simulation of the Ångström exponent of absorption from values at 405 nm and 870 nm as a function of coating thickness and core diameter for a core with refractive index (1.55, 0.8 i) and a coating with refractive index (1.5, 0.0i). In this case, the coating does not absorb light. The regions denoted by 'C' represent aerosol conditions likely on cities in the afternoon when secondary aerosol has condensed on soot cores and compacted them to a more spherical shape. The regions denoted by 'F' represent the core size and coatings typical of ponderosa pine smoke aerosol.

The relative minimum in the AEA for the typical urban conditions in the afternoon as shown in Fig. 2.6 is associated with point 'C' in either Figs. 2.9 or 2.10. In other words, relatively large carbon cores typical of collapsed primary emissions of soot from motor vehicles in cities when coated with either absorbing or non absorbing shells have AEA significantly less than unity for wavelengths 405 nm and 870 nm. By contrast, the smoky month of July, as shown in Fig. (2.5), has AEA as large as 2, suggesting that the model point ‘F’ in Fig. (2.9) for the core with an absorbing coating is the correct interpretation for the cause of these observed values of AEA.

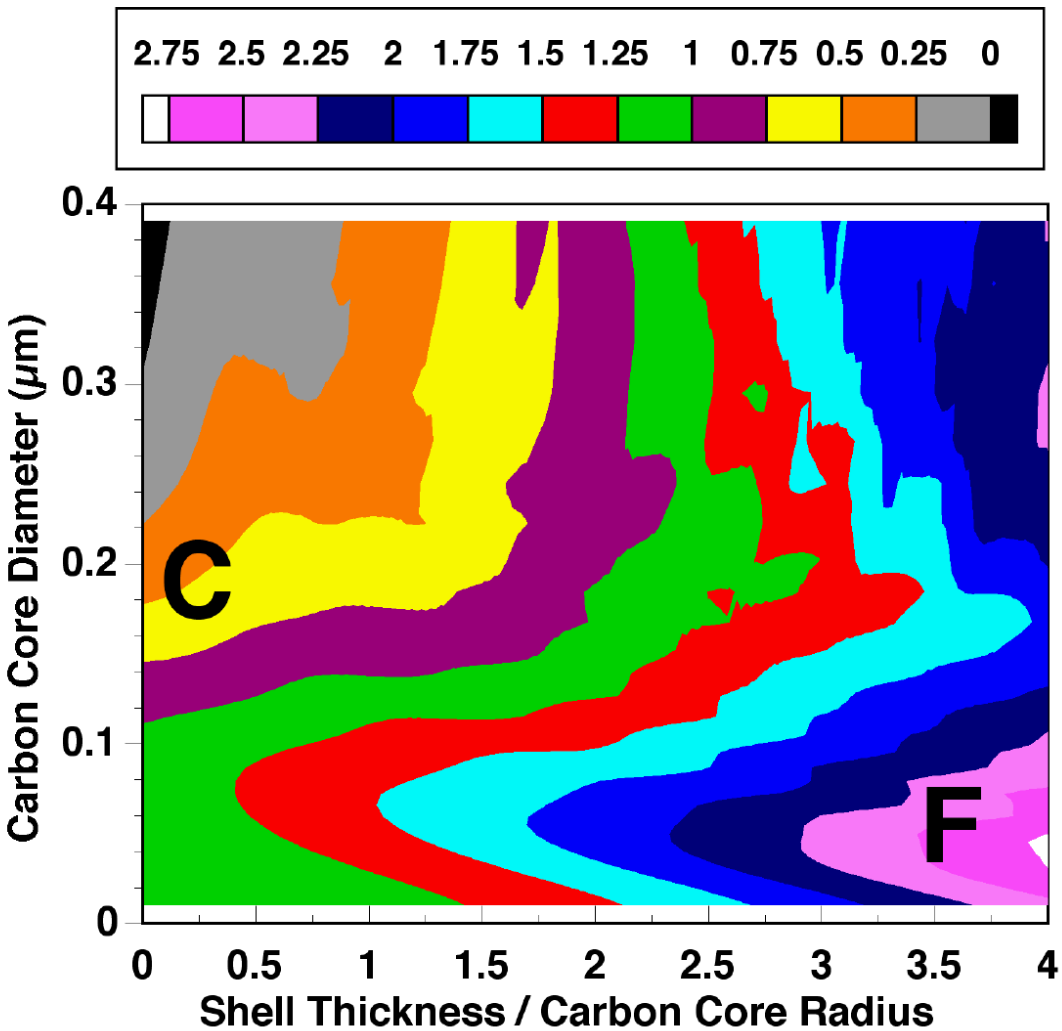

Figure 2.10 Same as Figure 2.9, though for a core with refractive index (1.55, 0.8i) and a coating with a refractive index of (1.5, 0.012i) at 405 nm and (1.5, 0.0i) at 870 nm. This coating selectively absorbs light at 405 nm. The regions denoted by ‘C’ represent aerosol conditions for cities in the afternoon when secondary aerosol has condensed on soot cores and compacted them to a more spherical shape. The regions denoted by ‘F’ represent the core size and coatings typical of ponderosa pine smoke aerosol.

2.4 Conclusions

The simulations confirm that large AEA values are possible even when coatings do not absorb light, especially when the BC core is much smaller than the wavelength of the laser used for aerosol optics measurements. The organic coating need not be intrinsically brown to observe effects commonly referred to as those caused by brown carbon light absorption. For relatively small cores, increasing coating thickness increases the AEA while for large cores, AEA does not change dramatically as function of coating thickness.

On average, during the smoky month of July 2008 aerosol light extinction coefficients observed in Reno, NV were about an order of magnitude larger than those observed during the comparably smoke free month of August 2008. The diurnal variation of aerosol extinction suggests that vertical development of the boundary layer is delayed under smoky conditions, likely due to reduction of the solar forcing at the surface. Comparison with laboratory generated wood smoke suggests that the aerosol optics in July is consistent with a predominant fuel source of pine needles and litter.

Measurements in August were typical of urban plumes. Midday values of the AEA were found to be significantly less than unity, as has been noted before. A likely explanation for this effect is that the wavelength range 405 nm to 870 nm was large, and absorbing particle size is likely larger coincident with low AEA values. Particle absorption could be in the surface area regime at 405 nm, whereas it could be in the volume or resonance regime for 870 nm for sufficiently large particles. This work illustrates that aerosol optics can be quite different for vehicular-related and biomass burning-aerosol.

2.5 Acknowledgements;

We acknowledge support by NSF, DOE ASP, JFSP through NPS, and the University of Nevada Reno. We are grateful to the crew of the FLAME1 experiment in Missoula Montana that resulted in the laboratory data on biomass burning aerosol optics. We acknowledge NASA and Jeffery Reid for providing a satellite image and discussions.

2.6 References

Abel, S. J., Haywood, J. M., Highwood, E. J., Li, J., and Buseck, P. R.: Evolution of biomass burning aerosol properties from an agricultural fire in southern Africa, Geophys. Res. Lett., 30, 1783, doi:10.1029/2003GL017342, 2003.

Andreae, M. O., and Gelencsér, A.: Black carbon or brown carbon? The nature of light-absorbing carbonaceous aerosols, Atmos. Chem. Phys., 6, 3131-3148, 2006,

http://www.atmos-chem-phys.net/6/3131/2006/.

Arnott, W. P., Moosmüller, H., Rogers, C. F., Jin, T., and Bruch, R.: Photoacoustic spectrometer for measuring light absorption by aerosols: Instrument description, Atmos. Env., 33, 2845-2852, 1999.

Arnott, W. P., Moosmüller, H., and Walker, J. W.: Nitrogen dioxide and kerosene-flame soot calibration of photoacoustic instruments for measurement of light absorption by aerosols, Rev. Sci. Ins., 71, 4545-4552, 2000.

Bergstrom, R. W., Pilewskie, P., Russell, P. B., Redemann, J., Bond, T. C., Quinn, P. K., and Sierau, B.: Spectral absorption properties of atmospheric aerosols, Atmos. Chem. Phys., 7, 5937-5943, 2007, http://www.atmos-chem-phys.net/7/5937/2007/.

Bond, T. C., and Bergstrom, R. W.: Light absorption by carbonaceous particles: An investigative review, Aerosol Science & Technology, 40, 27-67, 2006.

Bruce, C. W., Stromberg, T. F., Gurton, K. P., and Mozer, J. B.: Trans-spectral absorption and scattering of electromagnetic radiation by diesel soot, Appl. Opt., 30, 1537-1546, 1991.

Chakrabarty, R. K., Moosmüller, H., Arnott, W. P., Garro, M. A., Slowik, J. G., Cross, E. S., Han, J. H., Davidovits, P., Onasch, T. B., and Worsnop, D. R.: Light scattering and absorption by fractal-like carbonaceous chain aggregates: comparison of theories and experiment, Appl. Opt., 46, 6990-7006, 2007.

Chen, L.-W. A., Moosmüller, H., Arnott, W. P., Chow, J. C., Watson, J. G., Susott, R. A., Babbitt, R. E., Wold, C. E., Lincoln, E. N., and Hao, W. M.: Emissions from laboratory combustion of wildland fuels: Emission Factors and Source Profiles, Environ. Sci. Technol., 41, 4317- 4325, 2007.

Chen, L.-W. A., Moosmüller, H., Arnott, W. P., Chow, J. C., Watson, J. G., Susott, R. A., Babbitt, R. E., Wold, C. E., Lincoln, E. N., and Hao, W. M.: Particle emissions from laboratory combustion of wildland fuels: In situ optical and mass measurements, Geophys. Res. Lett., 33, L04803, doi:10.1029/2005GL024838, 2006.

Clarke, A., McNaughton, C., Kapustin, V., Shinozuka, Y., Howell, S., Dibb, J., Zhou, J., Anderson, B., Brekhovskikh, V., Turner, H., and Pinkerton, M.: Biomass burning and pollution aerosol over North America: Organic components and their influence on spectral optical properties and humidification response, J. Geophys. Res., 112, D12S18, doi: 10.1029/2006JD007777, 2007.

Fuller, K. A., Malm, W. C., and Kreidenweis, S. M.: Effects of mixing on extinction by carbonaceous particles, J. Geophys. Res., 104(D13), 15,941-915,954, 1999.

Hallett, J., Hudson, J. G., and Rogers, C. F.: Characterization of Combustion Aerosols for Haze and Cloud Formation, Aer. Sci. Tech., 10, 70-83, 1989.

Hoff, R. M., Palm, S. P., Engel-Cox, J. A., and Spinhirne, J.: GLAS long-range transport observation of the 2003 California forest fire plumes to the northeastern US Geophys. Res. Lett., 32, L22S08, doi:10.1029/2005GL023723, 2005.

Hudson, P. K., Murphy, D. M., Cziczo, D. J., Thomson, D. S., de Gouw, J. A., Warneke, C., Holloway, J., Jost, H.-J., and Hübler, G.: Biomass-burning particle measurements: Characteristic composition and chemical processing, J. Geophys. Res., 109, D23S27, doi: 10. 1029/2003JD004398, 2004.

Ito, A., and Penner, J. E.: Global estimates of biomass burning emissions based on satellite imagery for the year 2000, J. Geophys. Res., 109, D14S05, doi: 10. 1029/2003JD004423, 2004.

Johnson, B. T., Osborne, S. R., Haywood, J. M., and Harrison, M. A. J.: Aircraft measurements of biomass burning aerosol over West Africa during DABEX, J. Geophys. Res., 113, D00C06, doi: 10. 1029/2007JD009451, 2008.

Kirchstetter, T. W., Novakov, T., and Hobbs, P. V.: Evidence that the spectral dependence of light absorption by aerosols is affected by organic carbon, J. Geophys. Res., 109, D21208, doi:10.1029/2004JD004999, 2004.

Lack, D. A., Cappa, C. D., Covert, D. S., Baynard, T., Massoli, P., Sierau, B., Bates, T. S., Quinn, P. K., Lovejoy, E. R., and Ravishankara, A. R.: Bias in Filter-Based Aerosol Light Absorption Measurements Due to Organic Aerosol Loading: Evidence from Ambient Measurements, Aer. Sci. Tech., 42, 1033-1041, doi: 10. 1080/02786820802389277, 2008.

Lewis, K., Arnott, W. P., Moosmüller, H., and Wold, C. E.: Strong spectral variation of biomass smoke light absorption and single scattering albedo observed with a novel dual wavelength photoacoustic instrument, J. Geophys. Res., 113, D16203, doi:10.1029/2007JD009699, 2008.

Lewis, K. A., Arnott, W. P., Moosmüller, H., Chakrabarti, R. K., Carrico, C. M., Kreidenweis, S. M., Day, D. E., Malm, W. C., Laskin, A., Jimenez, J. L., Ulbrich, I. M., Huffman, J. A., Onasch, T. B., Trimborn, A., Liu, L., and Mishchenko, M. I.: Reduction in biomass burning aerosol light absorption upon humidification: roles of inorganically-induced hygroscopicity, particle collapse, and photoacoustic heat and mass transfer, Atmos. Chem. Phys. Diccuss., 9, 15247-15294, 2009, www.atmos-chem-phys-discuss.net/9/15247/2009/.

Liu, L., Mishchenko, M. I., and Arnott, W. P.: A study of radiative properties of fractal soot aggregates using the superposition T-matrix method, J. Quant. Spectrosc. Radiat. Transfer, 109, 2656-2663, doi:10.1016/j.jqsrt.2008.05.001, 2008.

Martins, J. V., Artaxo, P., Liousse, C., Reid, J. S., Hobbs, P. V., and Kaufman, Y. J.: Effects of black carbon content, particle size, and mixing on light absorption by aerosols from biomass burning in Brazil, J. Geophys. Res., 103(D4), 32,041-32,050, 1998.

Moffet, R. C., and Prather, K. A.: In-situ measurements of the mixing state and optical properties of soot with implications for radiative forcing estimates, PNAS, 106(29), 11872-11877, doi: 10.1073/pnas.0900040106, 2009.

Moosmüller, H., Chakrabarty, R. K., and Arnott, W. P.: Aerosol Light Absorption and its Measurement: A Review, J. Quant. Spectrosc. Radiat. Transfer, 110, 844-878, doi: 10. 1016/j.jqsrt.2009.02.035, 2009.

Mulholland, G. W., and Bryner, N. P.: Radiometric model of the transmission cell-reciprocal nephelometer, Atmos. Env., 28, 873-887, 1994.

Naik, V., Mauzerall, D. L., Horowitz, L. W., Schwarzkopf, M. D., Ramaswamy, V., and Oppenheimer, M.: On the sensitivity of radiative forcing from biomass burning aerosols and ozone to emission location, Geophys. Res. Lett., 34, L03818, doi: 10.1029/2006GL028149, 2007.

Oshima, N., Koike, M., Zhang, Y., Kondo, Y., Moteki, N., Takegawa, N., and Miyazaki, Y.: Aging of black carbon in outflow from anthropogenic sources using a mixing state resolved model: Model development and evaluation, J. Geophys. Res., 114, D06210, doi: 10.1029/2008JD010680, 2009.

Paredes-Miranda, G., Arnott, W. P., Jimenez, J. L., Aiken, A. C., Gaffney, J. S., and Marley, N. A.: Primary and secondary contributions to aerosol light scattering and absorption in Mexico City during the MILAGRO 2006 campaign, Atmos. Chem. Phys., 9, 3721–3730, 2009, www.atmos-chem-phys.net/9/3721/2009/.

Pfister, G. G., Wiedinmyer, C., and Emmons, L. K.: Impacts of the fall 2007 California wildfires on surface ozone: Integrating local observation with global model simulations, Geophys. Res. Lett., 35, L19814, doi: 10. 1029/2008GL034747, 2008.

Rahmah, A. A., Arnott, W. P., and Moosmüller, H.: Integrating nephelometer with a low truncation angle and an extended calibration scheme., Meas. Sci. Technol., 17, 1723-1732, 2006.

Redemann, J., Russell, P. B., and Hamill, P.: Dependence of aerosol light absorption and single-scattering albedo on ambient relative humidity for sulfate aerosols with black carbon cores., J. Geophys. Res., 106(D21), 27,485-27,495, 2001.

Rissler, J., Vestin, A., Swietlicki, E., Fisch, G., Zhou, J., Artaxo, P., and Andreae, M. O.: Size distribution and hygroscopic properties of aerosol particles from dry-season biomass burning in Amazonia, Atmos. Chem. Phys., 6, 471-491, 2006, www.atmos-chem-phys.org/acp/6/471/.

Roden, C. A., Bond, T. C., Conway, S., and Pinel, A. B. O.: Emission Factors and Real-Time Optical Properties of Particles from Traditional Wood Burning Cookstoves, Environmental science & technology, 40 (21), 6750-6757, 2006.

Schnaiter, M., Horvath, H., Möhler, O., Naumann, K. H., Saathoff, H., and Schöck, W.: UV-VIS-NIR spectral optical properties of soot and soot-containing aerosols, Journal of Aerosol Science, 34, 1421-1444, doi.10.1016/S0021-8502(03)00361-6, 2003.

Schnaiter, M., Linke, C., Möhler, O., Naumann, K.-H., Saathoff, H., Wagner, R., and Schurath, U.: Absorption amplification of black carbon internally mixed with secondary organic aerosol, J. Geophys. Res., 110, D19204, doi:10.1029/2005JD006046, 2005.

Schwarz, J. P., Spackman, J. R., Fahey, D. W., Gao, R. S., Lohmann, U., Stier, P., Watts, L. A., Thomson, D. S., Lack, D. A., Pfister, L., Mahoney, M. J., Baumgardner, D., Wilson, J. C., and Reeves, J. M.: Coatings and their enhancement of black carbon light absorption in the tropical atmosphere, J. Geophys. Res., 113, D03203, doi:10.1029/2007JD009042, 2008.

Subramanian, R., Roden, C. A., Boparai, P., and Bond, T. C.: Yellow beads and missing particles: Trouble ahead for filter-based absorption measurements., Aerosol Science & Technology, 41, 630-637, 2007.

Toon, O. B. and Ackerman, T. P.: Algorithms for the calculation of scattering by stratified spheres, Appl. Opt., 20, 3657-3660, 1981.

Westerling, A. L., Hidalgo, H. G., Cayan, D. R., and Swetnam, T. W.: Warming and Earlier Spring Increase Western U.S. Forest Wildfire Activity, Science, 313, 940-943, 2006.

Yang, M., Howell, S. G., Zhuang, J., and Huebert, B. J.: Attribution of aerosol light absorption to black carbon, brown carbon, and dust in China – interpretations of atmospheric measurements during EAST-AIRE, Atmos. Chem. Phys., 9, 2035–2050, 2009, http://www.atmos-chem-phys.net/9/2035/2009/.

3 Photoacoustic optical properties at UV, VIS, and near IR wavelengths for laboratory generated and winter time ambient urban aerosols

3.1 Abstract

We present the laboratory and ambient photoacoustic (PA) measurement of aerosol light absorption coefficients at ultraviolet wavelength (i.e., 355 nm) and compare with measurements at 405, 532, 870, and 1047 nm. Simultaneous measurements of aerosol light scattering coefficients were achieved by the integrating reciprocal nephelometer within the PA's acoustic resonator. Absorption and scattering measurements were carried out for various laboratory-generated aerosols, including salt, incense, and kerosene soot to evaluate the instrument calibration and gain insight on the spectral dependence of aerosol light absorption and scattering. Ambient measurements were obtained in Reno, Nevada, between 18 December 2009 and 18 January 2010. The measurement period included days with and without strong ground level temperature inversions, corresponding to highly polluted (freshly emitted aerosols) and relatively clean (aged aerosols) conditions. Particulate matter (PM) concentrations were measured and analyzed with other tracers of traffic emissions. The temperature inversion episodes caused very high concentration of $PM_{2.5}$ and PM_{10} (particulate matter with aerodynamic diameters less than 2.5 µm and 10 µm, respectively) and gaseous pollutants: carbon monoxide (CO), nitric oxide (NO), and nitrogen dioxide (NO_2). The diurnal change of absorption and scattering coefficients during the polluted (inversion) days increased approximately by a factor of two for all wavelengths compared to the clean days. The spectral variation in aerosol absorption coefficients indicated a significant amount of absorbing aerosol from traffic emissions and residential wood burning. The analysis of single scattering albedo

(SSA), Ångström exponent of absorption (AEA), and Ångström exponent of scattering (AES) for clean and polluted days provides evidences that the aerosol aging and coating process is suppressed by strong temperature inversion under cloudy conditions. In general, measured UV absorption coefficients were found to be much larger for biomass burning aerosol than for typical ambient aerosols.

3.2 Introduction

Atmospheric aerosols impact air quality and Earth's radiation balance. Aerosol light scattering redistributes electromagnetic energy in the atmosphere, whereas light absorption transforms it into thermal energy by heating absorbing aerosols and their surroundings. The absorption and scattering coefficients of aerosol are needed for modeling atmospheric radiation transfer (Clarke et al., 1987). These quantities are challenging to quantify and are associated with large uncertainties in the radiative forcing (Bergstrom et al., 2007; Bergstrom et al., 2009). Aerosol optical properties depend on particle size, morphology, refractive index (RI), and wavelength of electromagnetic radiation and must be specified over the entire solar spectrum (Levoni et al., 1997).

Carbonaceous aerosols account for much of the atmospheric particulate matter mass that affects incoming solar radiation via scattering and absorption (Sun et al., 2007). These aerosols consist of two major carbon components, elemental carbon (EC), and organic aerosol (OA) (Seinfeld and Pandis, 2006). Black carbon (BC) is operationally defined through an aerosol light absorption measurement; for near infrared wavelengths BC strongly correlates with EC due to its quasi-graphitic structure. BC is emitted as a result of incomplete combustion of carbon-rich fuels. The other component, OA, though present in much higher mass concentrations than BC for ambient samples, is more elusive as its origins as well as optical and chemical properties vary greatly with source, transformation, and sink (D'Alessio et al., 1998). OA exhibits many molecular forms that have different physical and chemical properties and often exists independently of BC (Jacobson et al., 2000). The OA that is directly emitted from combustion or biogenic processes is referred to as primary organic aerosol (POA). OA is also formed in-situ through the oxidation of gaseous organic precursors that transfer to the aerosol phase by condensation or nucleation, referred to as secondary organic aerosol (SOA). SOA formation involves two processes: gas-phase chemical transformation and change of phase. Photochemical transformation also promotes inorganic aerosol formation.

BC strongly absorbs throughout the entire solar spectrum (Horvath, 1993; Moosmuller et al., 2009). The refractive index (RI) of BC depends predominantly on fuel type, combustion phase, degree of graphitization, and atmospheric processing (Andreae and Gelencsér, 2006; Bond and Bergstrom, 2006). Pure carbon (i.e., graphitic state) has RI as large as 2 +1i, where the real and imaginary parts of RI impact both light scattering and absorption. The formation of BC through pyrolysis of hydrocarbon fuels is a complicated process. This process leads to the formation of complex substances like oils, tars, and solids, while the adsorption and continuing elimination of hydrogen at higher temperature results in an increase in crystal size and graphitization of the fuel (Grisdale, 1953). For instance, diesel soot appears as an onion-shell structure of nano crystalline graphite having domain sizes of 2-3 nm (Wentzel et al., 2003). Out of the four valence electrons of carbon atoms in graphite, three are in the hybrid sp^2 state and one is in the p state. The electrons in the hybrid state form σ bonds and those in the p state form π bonds due to the mutual overlapping above and below the graphitic plane, and become delocalized (Bond and Bergstrom, 2006). Electrons in the π bond can move rather freely and absorb electromagnetic radiation from at least the UV to the near IR. Electrons in σ bonds are effective in ultraviolet (UV) absorption.

While BC aerosols absorb strongly over the entire solar spectrum, some OA absorbs efficiently in the UV and blue regions (Barnard et al., 2008; Bergstrom et al., 2007; Bond, 2001; Chakrabarty et al., 2010; Jacobson, 1999; Kirchstetter et al., 2004; Martins et al., 2009; Roden et al., 2006). These organic materials appear yellowish/brownish and are known as "brown carbon" (Andreae and Gelencsér, 2006). Brown carbon (BrC) is commonly found in secondary and biomass burning aerosols (e.g. Andreae and Gelencsér, 2006; Chakrabarty et al., 2010; Chen et al., 2010). UV radiation encompasses only 10% of the total solar irradiance, so details of its direct radiative forcing are often ignored in climate modeling (Corr et al., 2009). There have been many investigations of aerosol optical properties in the visible spectrum, though in situ measurements of UV absorption by ambient aerosols are rare (Kikas et al., 2001; Taylor et al., 2008).

Radiative transfer in the UV with respect to photochemistry has motivated us to develop a new photoacoustic instrument and nephelometer that can measure in situ aerosol absorption and scattering coefficients at UV wavelengths. Ajtai et al., (2010) and Ajtai et al., (2011) have previously demonstrated the use of a four-wavelength (including 266 and 355 nm) photoacoustic instrument measuring aerosol light absorption coefficients for laboratory-generated and ambient aerosols. UV radiation is the dominant driver of atmospheric chemistry. The photo dissociation of gaseous species due to UV radiation is responsible for smog and ozone formation in the troposphere (Jacobson, 1999). Most photolysis is due to UV radiation between 290 to 420 nm (Hofzumahaus and

Kraus, 2002). Jacobson (1999) found that the nearly 50% decline in UV radiation within the boundary layer (BL) in Los Angles was due to substantial UV absorption by nitrated and aromatic aerosols and gaseous species. A very recent study indicated nighttime formation of particulate organic nitrate and organosulfate species in coal-fired power plant plumes (Zaveri et al., 2010) that may also absorb UV radiation the following day.

This study reports multispectral photoacoustic absorption and scattering measurements at wavelengths 355, 405, 532, 870, and 1047 nm for laboratory-generated aerosol as well as for ambient aerosol during the months of December 2009 and January 2010. The hourly concentrations of $PM_{2.5}$ and PM_{10} and gaseous pollutants (CO, NO, and NO_2) are also analyzed for the same period. The simultaneous measurement of aerosol optical properties at multiple wavelengths provides an improved coverage of the solar spectrum and offers a way to single out the spectral signature of BC and OA aerosols. Nevertheless, our previous investigation (Gyawali et al., 2009) suggests that even non-absorbing coatings on BC can be disguised as BrC or light absorbing OA, so it is not always possible to separate the effects of coatings on amplifying aerosol absorption and intrinsic absorption by the coating (Jacobson et al., 2000).

3.3 Photoacoustic instrument and laboratory generated aerosols

3.3.1 Instrument description

The photoacoustic instrument (PA) is one of the few devices that provide the fundamental in-situ measurement of light absorption coefficients for suspended particles. The detailed working mechanism, measurement accuracy, evaluation and calibration of PA have been described previously (Arnott et al., 2000; Arnott et al., 2005a; Arnott et al., 2005b; Lewis et al., 2008; Moosmüller et al., 1998). Here we describe the basic principle and calibration technique applied for the 355 nm instrument. The 355 nm instrument uses a compact crystal laser system, a diode pumped Nd:YAG laser with frequency tripling to produce 355 nm laser output. The laser is an active Q-switched operating from 1 to 20 kHz. In the operation of the PA, sample air is continuously introduced into the acoustic resonator section and is illuminated by laser radiation, power-modulated at the acoustic resonance frequency. The radiation is absorbed by particles within the sample air, and is assumed to be immediately transferred to the surrounding air as heat. The associated pressure change contributes to a standing wave in the resonator that is detected by a microphone located at a pressure anti-node (Arnott et al., 1999). The simultaneous light scattering measurement is carried out with a cosine-weighted sensor positioned at the centre of the cavity to act as a reciprocal nephelometer (Lewis et al., 2008; Abu-Rahmah et al., 2006). The sensor is fiber coupled to a photomultiplier tube (PMT) for light scattering detection. A piezoelectric transducer positioned at a pressure anti-node of the resonator cavity is used periodically to determine the resonance frequency and quality factor of the resonator. The absorption and scattering coefficients measurements have 5% and 15% uncertainty for sub-2.5-micron diameter particles (Lewis et al., 2008). The detection limit of 355 nm instrument for absorption coefficient was on the order of 0.4 Mm^{-1}.

Light absorption and scattering measurements in this study were made simultaneously with a dual-wavelength PA operating at 405 and 870 nm (Lewis et al., 2008), and two single-wavelength PAs operating at 532 and 1047 nm (Arnott et al., 2000; Arnott et al., 2005b). Prior to the ambient measurements, all PAs were calibrated and their performance was evaluated by generating a wide range of absorbing and scattering aerosol in the laboratory as described by Lewis et al. (2008).

The light absorption coefficient, β_{abs}, in dimension of inverse length is obtained from,

$$\beta_{abs} = \frac{P_m A_{res}}{P_L(\gamma - 1)} \frac{\pi^2 f_0 \cos(\phi_m - \phi_L)}{Q} \ , \qquad (1)$$

where P_m and P_L are the measured microphone pressure and laser power at the resonance frequency f_o, A_{res} is the resonator cross-sectional area, Q is the quality factor, γ is the ratio of isobaric and isochoric specific heats of air, and ϕ_m and ϕ_L are the electric phases of the microphone pressure and laser power measurements, respectively. The resonance frequency and quality factor depend on temperature, pressure, and relative humidity. For the sample air, these quantities are measured by pressure, temperature, and relative humidity sensors located in the sample line downstream of the resonator.

The scattering coefficient, β_{sca} in dimension of inverse of length, is obtained from

$$\beta_{sca} = \alpha \frac{|P_{PMT}|}{|P_L|} \ ,$$

(2)

where α is the calibration factor determined at the time of instrument calibration and $|P_{PMT}|$ and $|P_L|$ are the magnitudes of Fourier transform of the PMT and laser power at the resonance frequency, respectively.

3.3.2 Calibration

Calibration of the photoacoustic instruments, for light absorption, is accomplished in three ways. First and foremost, the instrument can be independently prepared for quantitative measurements from a fundamental perspective. We have derived and verified a 1-D model equation for the acoustical resonator taking into account the operating frequency, microphone calibration, laser power calibration, resonator quality factor measurement, resonator cross sectional area, and gas constant for air (ratio of specific heats) (Arnott, et al., 1999). This method has been evaluated by us and others using light absorption by NO_2 at 532 nm (Arnott, et al., 2000). We use a commercially available microphone-calibrator for the microphone calibration, for the 1" microphones we use in the instrument. Propagating error through this fundamental procedure for instrument calibration, we arrive at a calibration accuracy of +- 5%, with the weakest part of the calibration procedure associated with the laser power measurement. Then, as long as we can measure laser power accurately at other wavelengths, we can use the same microphone calibration for any wavelength since the microphone is a 'color blind' sensor. NO_2 photolysis at 405 nm and shorter wavelengths prevents direct measurement of path extinction = photoacoustic absorption since some of the absorbed optical power goes into bond breaking rather than to heat. O_2 has been investigated as a calibration gas in the oxygen A band spectral region near 760 nm (oxygen A band, tunable laser) but in this wavelength range, gaseous light absorption involves significant relaxation processes that are mediated by water vapor (Gilles et al., 2010; Tian et al., 2009). In this case, the molecular physics of oxygen is very interesting, but the accuracy of using gas calibration for aerosol light absorption measurement is less assured. The use of Absorption = Extinction - Scattering for aerosol is an evaluation of the calibration achieved by the fundamental method. Extinction and scattering measurements both have uncertainties in excess of that achievable by the fundamental calibration method.

For the calibration of PA operating at 355 nm, high concentrations of laboratory-produced purely scattering (table salt) and strongly absorbing (kerosene soot) aerosols were used, which resulted in a measurable attenuation of the laser beam intensity in the resonator. The salt was dissolved in water and nebulizers were used to produce airborne droplets from the salt solution. Dried salt aerosols were introduced into the resonator for scattering calibration. A fast photodiode attached to an integrating sphere is used to determine the laser power. The extinction of light passing through aerosol can be expressed using Bouger-Lambert's law,

$$I = I_0 \exp(-\beta_{ext} * L_{res}) \tag{3}$$

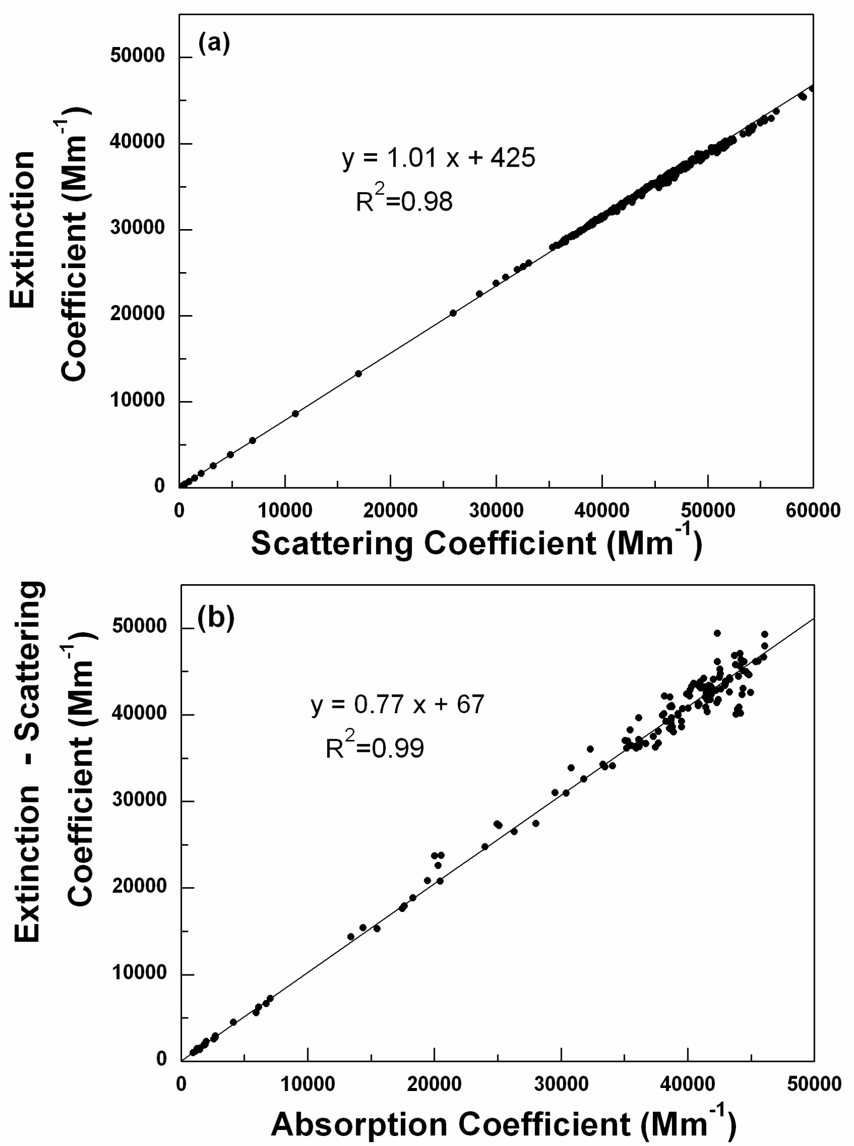

Figure 3.1 Plots of 355 nm calibration curves for (a) scattering measurements of negligibly absorbing salt aerosol, and (b) absorption measurements of kerosene soot.

where I and I_o are the laser power with and without salt aerosol in the resonator, β_{ext} is the extinction coefficient of the aerosol, and L_{res} is the length of the resonator, 24.86 cm. The aerosol extinction coefficient calculated from equation (3) is compared with the scattering measurements to obtain the scattering calibration factor of equation (2). Figure 3.1a shows the linear regression between the measured extinction and scattering in which the near unity value of R^2 depicts the excellent correlation between these quantities. Also note the slope of the regression line is near unity, which means the extinction was overwhelmingly due to scattering and no further adjustments are needed for the scattering calibration. After the scattering calibration, the process was repeated with kerosene soot for absorption calibration. Figure 3.1b shows the linear regression between the absorption measurements and extinction-scattering calculation. The slope of the regression line indicates that measured absorption coefficients at 355 nm should be increased by a factor of 1.29 to reflect this improvement of laser power measurement accuracy.

3.3.3 Laboratory generated aerosols

This section presents the absorption and scattering coefficients measured for three different types of laboratory-generated aerosols. These include purely scattering salt (NaCl) aerosol, strongly absorbing kerosene soot aerosol, and short-wavelength absorbing incense aerosol. Besides functioning as instrument performance tests, these measurements provide an opportunity for the analysis of the wavelength dependence of absorption and scattering for a range of aerosols that might be representative of atmospheric aerosols in different locations and during different events.

Incense is used to produce fragrances for ceremonial purposes and in residential homes. A wide variety of substances are used to produce incense, including wild flowers, strawberries, sandal wood and other aromatic woods, and resins. Burning incense produces mostly organic compounds including polycyclic aromatic hydrocarbons

(PAHs), aromatic aldehydes, and aliphatic aldehydes, with a particle mass median aerodynamic diameter ranging from 150 to 300 nm (Ji et al., 2010; Yang et al., 2007). The incense used for this study was manufactured in India by coating the pulverized wooden materials and other ingredients on a supporting wooden core and had brown color. One incense stick was ignited in a chamber and the flame was immediately extinguished to obtain smoke from the smoldering phase. Incense is a good aerosol source that has strong absorption at shorter wavelengths due to BrC and can be used as surrogate for smoldering biomass combustion.

Kerosene soot aerosol has been employed extensively in the laboratory to calibrate the PA absorption measurements, to evaluate the measurements and precision of aerosol light absorption measuring instruments, and to study the aerosol absorption and scattering in external and internal mixing states (Arnott et al., 2000, 2005a; Petzold et al., 2005; Sheridan et al., 2005). It is a surrogate for diesel soot and exhibits nearly inverse wavelength dependence of the aerosol light absorption coefficient (Sheridan et al., 2005a).

3.3.3.1 Calculation of Ångström exponent of absorption (AEA), Ångström exponent of scattering (AES) and single scattering albedo (SSA)

AEA is used to analyze the spectral dependence of aerosol light absorption, to characterize the aerosol composition, and to model aerosol radiative forcing. The aerosol light absorption at a single wavelength can be extrapolated to other wavelengths by a power law relationship as

$$\beta_{abs}(\lambda) = C * \lambda^{-\alpha_{abs}} \quad , \qquad (4)$$

where $\beta_{abs}(\lambda)$ is the aerosol absorption coefficient at the wavelength λ of the light, C is a constant independent of wavelength, and α_{abs} is the AEA. The AEA, $\alpha_{abs}(\lambda_1, \lambda_2)$ can be calculated from the aerosol light absorption coefficient measured at two different wavelengths λ_1 and λ_2 as (Moosmüller et al., 2011)

$$\alpha_{abs}(\lambda_1, \lambda_2) = \frac{\ln\left(\beta_{abs}(\lambda_1) / \beta_{abs}(\lambda_2)\right)}{\ln(\lambda_2 / \lambda_1)} . \tag{5}$$

For small size parameter, absorbing spherical particles with a wavelength independent refractive index, AEA= 1 (Moosmüller and Arnott, 2009; van de Hulst, 1981).

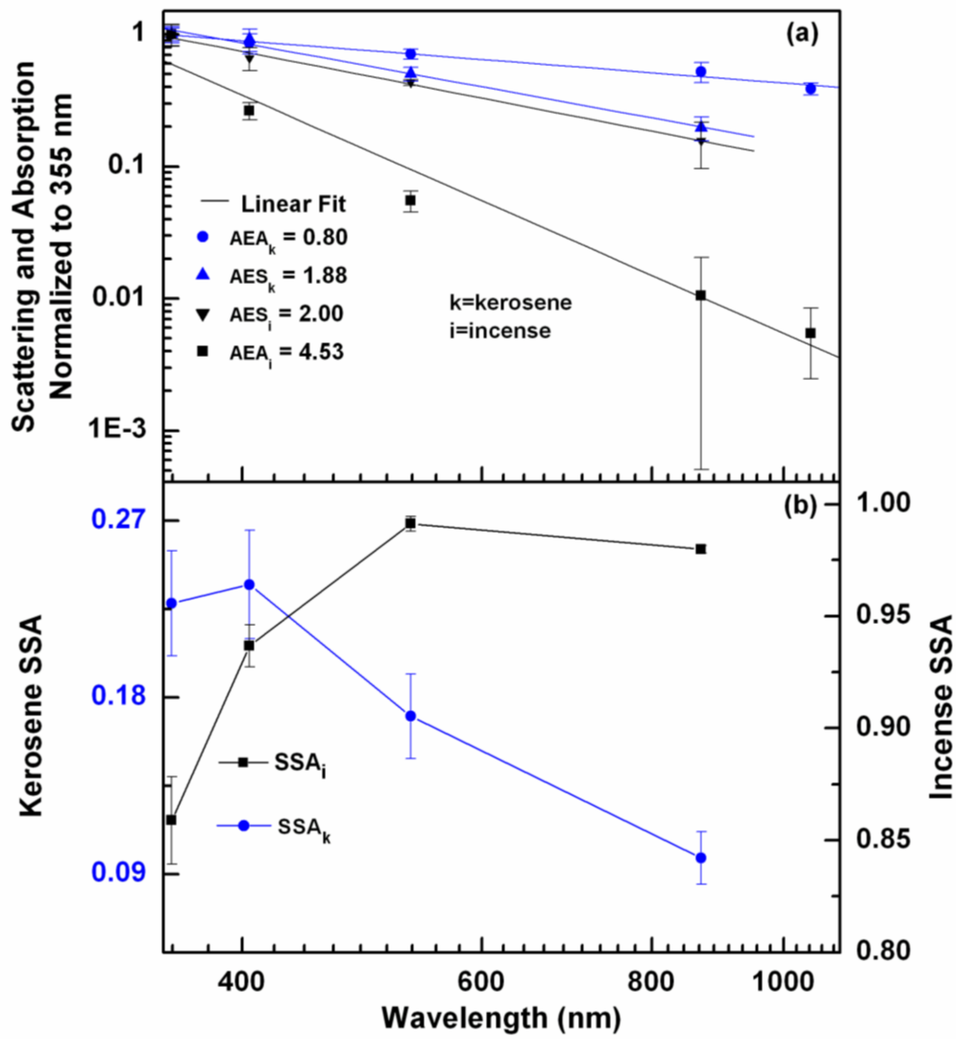

Figure 3.2 Intensive aerosol optical properties for kerosene and incense smoke. Ångström exponents of (a) scattering (AES) and absorption (AEA), where error bars indicate the standard deviation of the mean and (b) single scattering albedo (SSA). Uncertainty on SSA was determined by assuming 5% relative uncertainty in photoacoustic absorption coefficient measurements and 15% relative uncertainty in scattering coefficient measurements.

The Ångström exponent of scattering (AES) is used to characterize aerosol size. Like AEA, AES is also a power law relationship and can be calculated as the equations (4) and (5) by using aerosol scattering coefficients (β_{sca}). The magnitude of AES approaches a value of 4 for small particles and approaches 0 for large particles with a wavelength-independent refractive index (Bohren and Huffman, 1998). Another calculated optical property is the single scattering Albedo (SSA), which is defined as the ratio of scattering coefficient β_{sca} to the extinction coefficient, $\beta_{abs} + \beta_{sca}$ as

$$SSA = \frac{\beta_{sca}}{\beta_{sca} + \beta_{abs}} \ . \tag{6}$$

Power law relationships, Eqs. (4) and (5), were used to calculate AEA and AES to study the spectral variations of these quantities for laboratory aerosol and are plotted in Fig. 3.2a. Here, the AEA is the negative slope of the β_{abs} as a function of available wavelengths: 355, 405, 532, 870, and 1047 nm in a log-log plot. The AES is the negative slope of a similar plot excluding the 1047 nm wavelength where scattering was not measured. The value of AEA is 0.80 for kerosene and 4.53 for incense aerosols. Our AEA of kerosene is comparable the value of 1.01 measured by Schnaiter et al. (2006) for a propane diffusion flame at C/O=0.29. Ajtai et al. (2010) presented a higher value of 1.24 for spectral range 266-1064 nm with the same C/O ratio but slightly different burner type than Schnaiter et al. (2006) by measuring the slope of the log-log plot, as applied in our study. The data shows a curvature of the incense absorption coefficients as a function of wavelength, resulting in a larger AEA for shorter wavelengths than for longer ones. Such a curvature has previously been described for AERONET extinction (Schuster et al., 2006), and for BrC absorption coefficients using a damped simple harmonic oscillator model (Moosmüller et al., 2011). Further, β_{abs} for incense aerosol at 355 nm was found to be nearly 20 times higher than the IR β_{abs} at 870 nm. Kerosene soot is a good example of black carbon while incense aerosol is a BrC example. Similarly, AES is 1.88

for kerosene soot and 2.0 for incense aerosols, indicating larger aerosol size for kerosene soot aerosol than for incense aerosol. AES of kerosene is very close to the value of 1.70 reported by Schnaiter et al. (2006). Figure 3.2b compares SSA for kerosene soot and incense burning aerosols. SSA decreases with wavelength for kerosene soot yet it increases for incense burning aerosol with wavelength, yielding positive and negative Ångström exponents of SSA (AESSA), respectively (Moosmüller and Chakrabarty, 2011). Incense smoke behaves optically similar to primary emissions from biomass burning that have a large OC fraction (Lewis et al., 2008).

3.4 Ambient Measurements

3.4.1 Meteorological conditions and classification of measurement events

In this study, we used meteorological data from http://www.wrcc.dri.edu/rcc.html and balloon soundings from http://weather.uwyo.edu/upperair/sounding.html pertaining to the Reno area. The data were analyzed from 18 December 2009 to 18 January 2010 to study the enhancement of β_{sca} and β_{abs} by freshly emitted traffic and wood burning aerosols trapped near the surface due to temperature inversion. Temperature generally decreases with altitude in the lower part of the atmosphere, but during certain meteorological situations, the surface may become colder than the air at higher elevations, leading to temperature inversion conditions, which tend to suppress the vertical mixing of air. During temperature inversion periods, the local health officials of Washoe County, Nevada announced air pollution alerts to encourage inhabitants to refrain from extended outdoor activities, and banned residential wood burning (see, http://www.co.washoe.nv.us/repository/print_pr.php?article=8510). The β_{abs} during these conditions was comparable to that of Reno, NV during the California wild fire season in the summer of 2008 and to that in Mexico City (Gyawali et al., 2009; Paredes-Miranda et al., 2009).

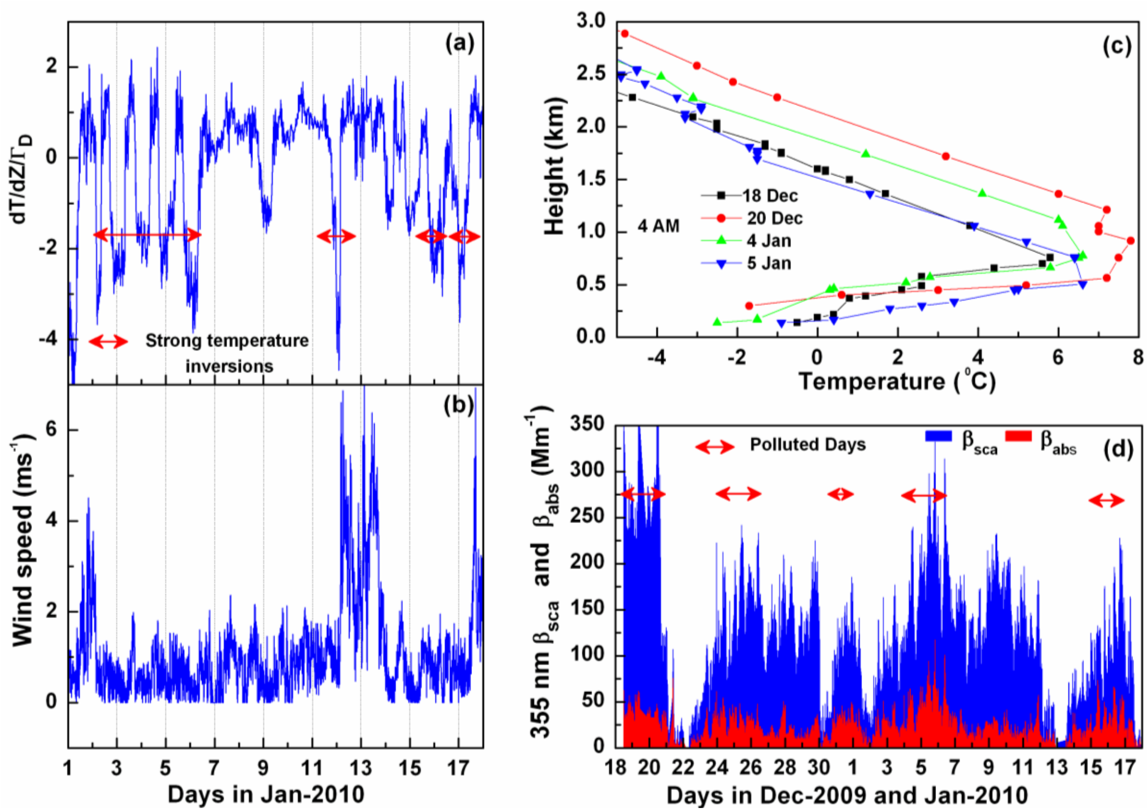

Figure 3.3 Meteorology and aerosol optics measurements at 355 nm during winter 2009/2010 at Reno, Nevada. (a) Temperature gradient normalized to dry adiabatic lapse rate (-9.8 0C), with negative values indicating temperature inversions, (b) wind speed, (c) temperature profiles from radiosonde launches, whereas the height is above the ground level (AGL). Strong temperature inversions are associated with the highly polluted events of the winter season, (d) two minute average of the ambient aerosol scattering and absorption coefficients.

Figure 3.3 presents the aerosol time-series of β_{sca} and β_{abs} at 355 nm in conjunction with meteorological parameters from two near surface stations in Reno separated by an altitude difference of 143 m. Figures 3.3a and b display the temperature gradient normalized by the dry adiabatic lapse rate (-9.8 $^{\circ}$C km^{-1}) and the wind speed, respectively. Large negative values of the normalized temperature gradient indicate the strength of the temperature inversion. Soundings balloons were launched from the National Weather Service office located about 150 meters above the valley floor. Thus the higher than valley floor balloon launch site may underestimate the inversion strength. The relatively high wind speed of 6 to 7 ms^{-1} breaks the temperature inversion on January 12. Figure 3.3c shows the temperature profiles from the morning balloon soundings for major temperature inversion events. Additional short-term temperature inversion of a similar nature took place during December and January. Figure 3.3d displays the two-minute average time-series of β_{sca} and β_{abs} at 355 nm. Four episodes of elevated β_{sca} and β_{abs} are centered on 19 and 25 December 2009, and 6 and 16 January, 2010, and are associated with temperature inversion and diminished wind speed (as shown in Figs. 3.3a, b, and c). These high pollution episodes were predominantly of local origin, with air trapped in the lower levels due to severe stagnation. Results presented here show that the 355 nm β_{sca} and β_{abs} of trapped emissions can be ten times greater than those for clean days. For such polluted days, the increased UV extinction slows down the formation of SOA and ozone (Barnard et al., 2008).

Based upon the meteorological parameters and the magnitude of β_{sca} and β_{abs}, we have classified the measurements made from 18 December to January18 into two groups: “clean days” and “polluted days.” Days were classified as polluted days if the average β_{abs} values at 355 nm for the particular days were about 40 Mm^{-1} or higher, such as 18 to 20, 24 to 26, and 31 December, 4 to 6 and 15 and 16 January. The $PM_{2.5}$ mass concentration during the polluted days was at least 40 μgm^{-3} (air quality public warning ''Sensitive") or as high as 90 μgm^{-3} (air quality public warning "Unhealthy"; see, http://alg.umbc.edu/usaq).

3.4.2 Particulate matter (PM) and gaseous pollutant concentrations, and their effects on aerosol optical properties

This section presents particulate matter (PM) and gaseous pollutant concentrations from an air quality monitoring station (South of the Truckee River, EPA ID#32-031-0016), ~0.9 miles from the Department of Physics, University of Nevada, Reno, USA, where the aerosol optics measurements were made. The purpose of this section is to investigate the source contributions to the PM and gaseous pollutants during clean and polluted days. Wood burning results in much more CO and less NO_x (NO_2 + NO) than vehicular emissions (Kirchstetter et al., 1999; Johansson et al., 2004), while diesel vehicles are important NOx sources because of high combustion temperature (Lloyd and Cackette, 2001). Biomass burning, especially high-temperature flaming combustion may also generate substantial NOx (Chen et al., 2010). Wood combustion is known to contain humic-like substances (Hoffer et al., 2006) or BrC (Chakrabarty et al., 2010) that strongly absorbs in the UV regions while BC emission from traffic exhibits inverse wavelength dependence of light absorption (Bond and Bergstron, 2006). These evidences have been used to identify the influence of wood burning and traffic emissions using the concurrent multispectral aerosol optical measurements and gaseous pollutant concentration measurements (Sandradewi et al., 2008 a, b).

Hourly $PM_{2.5}$ and PM_{10} mass concentrations were measured by Beta Attenuation Monitor (BAM) (MetOne SASS), whereas the Federal Reference Method (FRM) was used for 24-h speciation of $PM_{2.5}$ mass concentrations and additional instruments measured concentrations of gaseous pollutants. The operation of the BAMs has been described in detail elsewhere (Chow et al., 2006; Huang and Tai, 2008; Schwab et al., 2006; Takahashi et al., 2008). The working principle of FRM is described in BGI (2009a, b).

Diurnal concentrations of CO, NO, NO_2, $PM_{2.5}$, and coarse particles (PM_{10} - $PM_{2.5}$) averaged for clean days and polluted days are shown in Fig. 3.4. For CO and NO, the maximum values occurred during the morning rush hours, followed by a decrease in those quantities in the late morning due to dilutions of these pollutants and growth of the BL. The diurnal variations of CO and NO_x concentrations were strongly correlated with β_{abs} at all wavelengths, both for polluted and clean days. The correlation coefficient (R^2) varied from 0.65 (β_{abs} at 532 nm with CO) to 0.84 (β_{abs} at 355 nm with NO_x). The high correlation suggests that the CO and NO_x emitters might also be high particle emitters (Kirchstetter et al., 1999) that influence the multi-spectral aerosol light absorption and scattering. The fact that the mean AEA value increased from 1.03 to 1.14 (see Table 1) suggests a minor increase in BrC fraction in organics during relatively clean days. This does not necessarily mean the absence of biomass burning or residential wood burning during the study period, since BrC formation from wood/biomass burning highly depends on combustion efficiency (CE); low CE leads to BrC enrichment in the smoke (Chen et al., 2010); in many cases residential wood burning in Reno may be efficient enough to mitigate BrC emissions. Very low correlation coefficients (R^2~0.2) between AEA and CO and NO_x were found during the study periods, in contrast to a similar study in a Swiss alpine valley that found a much higher correlation (R^2=0.5) for substantial emissions from wood burning and traffic

(Sandradewi et al., 2008a). They reported AEA 1.1 for traffic emissions and 1.9 for wood burning. The lower than expected values of AEA during the study period are consistent with the findings that approximately two-thirds of NH_4NO_3 were associated with mobile source emissions and one-third with residential wood combustion emissions (Watson et al., 2011). Additionally, lower average values of AEA during polluted days (snow covered and strong temperature inversion episodes) can be associated with increased consumption of gasoline and diesel fuel (due to more frequent snow plowing and blowing) (Watson et al., 2011) that may emit more primary $PM_{2.5}$ and NO_x than during the drier periods.

The temperature inversions resulted in high concentrations of PM and gaseous pollutants, as shown in Fig. 3.4. $PM_{2.5}$ and coarse particle concentrations exhibited much higher concentrations with pronounced diurnal variation during polluted days. $PM_{2.5}$ primary emissions are likely influenced by traffic and residential wood combustion (Watson and Chow , 2002). The mid-day peaks of $PM_{2.5}$ and coarse particles, however, may result from the temporal overlap between the evening rush hour, the secondary aerosol produced during day time, wind-related dust, and traffic resuspension (Stephens et al., 2008).

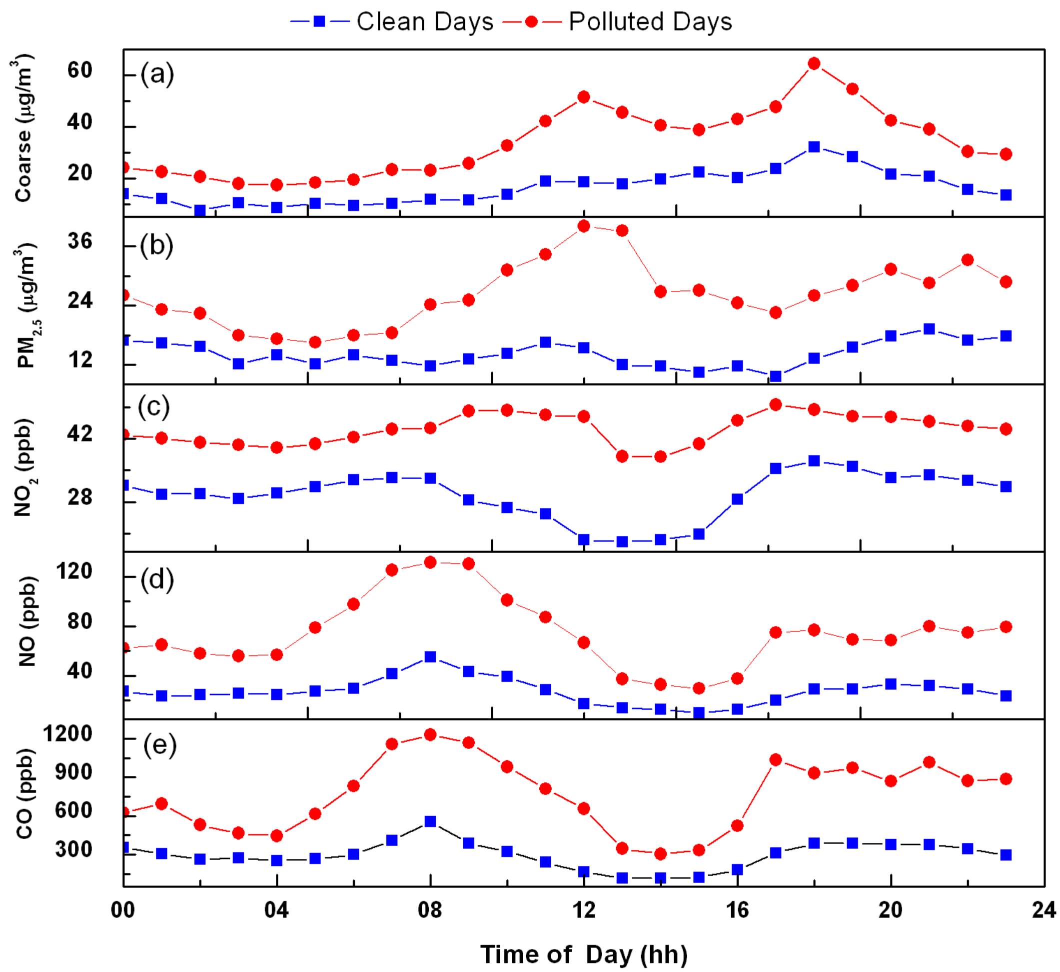

Figure 3.4 Diurnal variation of hourly average concentrations of (a) coarse particles, (b) PM2.5, (c) ni tric oxide, (d) nitrogen dioxide, and (e) carbon monoxide.

Figure 3.5 shows 24-h averages of $PM_{2.5}$ component mass concentrations for highly polluted days (18 and 24 December, and 5 January) and relatively clean days (21 December and 14 and 17 January). The comparison shows slightly higher concentrations of organic material, much higher quantities of ammonium nitrate (NH_4NO_3), and a higher

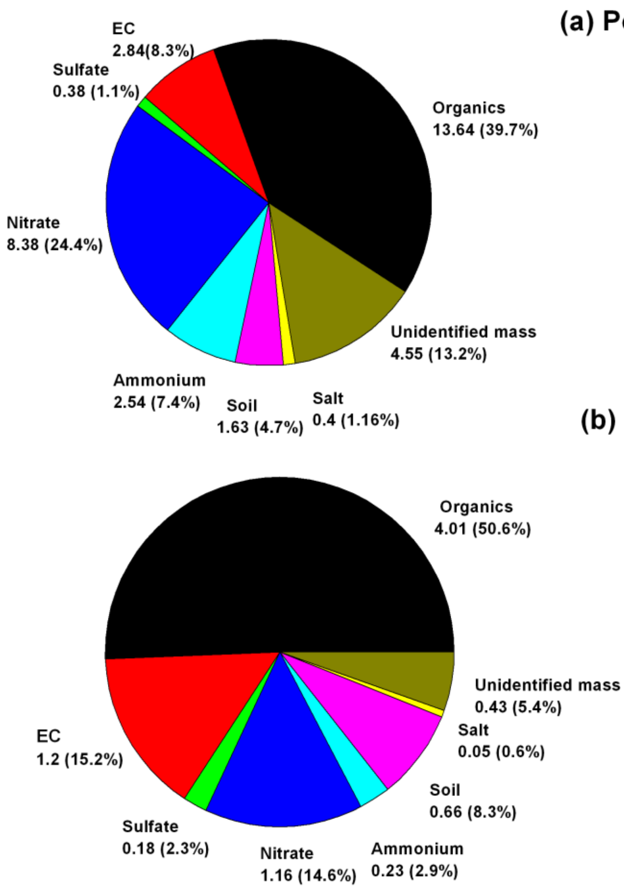

Figure 3.5 Twenty-four-hour average PM2.5 component concentrations ( ) for (a) polluted days (18 and 24 December and 5 January) and (b) clean days (21 December and 14 and 17 January).

amount of unexplained mass during the polluted days. The unexplained mass highly correlates with the NH_4NO_3. Furthermore, NH_4NO_3 was the primary cause of the lift in the $PM_{2.5}$ mass concentrations over the 35 μgm^{-3} threshold during polluted days. Nitric acid (HNO_3) is formed from oxidation of NO_x (NO_2 + NO) via either photochemical or nighttime reactions (Watson and Chow, 2002). NH_4NO_3 is formed by the reaction of HNO_3 and ammonia (NH_3) from agricultural activities. NH_4NO_3 exhibits higher hygroscopic growth, increasing the amount of light scattering and direct radiative forcing by ambient aerosols (Crosier et al., 2007). The consistently higher values of β_{sca} at all wavelengths during polluted episodes (see Fig. 3.6b) can be attributed to dominance of NH_4NO_3. In addition, there is a possibility of the formation of organic nitrates in the presence of nitrates and organic species in pollution plumes (Flowers et al., 2010). Particle phase organic nitrates are strong absorbers at UV wavelength (Jacobson, 1999). The strength of the absorption increases with the acidity of organic nitrates. However, consistently low values of AEA (i.e., less than 1.2) (Fig. 3.7d) for all pairs including the analysis of multispectral β_{sca} and β_{abs} (presented in the next section) does not support the presence of short wavelength absorbing acidic organic species during polluted days.

3.4.3 Ambient aerosol optical properties measurements

In this section, we present our findings on diurnal variation of half-hour average ambient extensive and intensive aerosol optical properties at wavelengths of 355, 405, 532, and 870 nm from 18 December 2009 to 18 January 2010. These measurements were obtained at the Physics building of the University of Nevada, Reno, USA. PA sampled from an inlet at a flow rate of ~3 lpm through a ~3 m insulated copper inlet line located ~10 m above the ground. Spectral and diurnal variations of β_{sca}, β_{abs}, AES, AEA, and SSA during the study periods were analyzed and classified for “clean days” and “polluted days”.

3.4.3.1 Spectral and diurnal variations of β_{sca} and β_{abs}

Figures 3.6a and b compare the diurnal and spectral variations of half-hour averages of β_{sca} during clean days and polluted days, respectively. These data describe common effects of the BL dynamics, daytime photochemical activity, and additional formation of non-light absorbing particles. Similarly, Figs. 3.6c and d compare the β_{abs} measurements. In comparison, peak values of β_{sca} and β_{abs} on stagnant days are nearly twice as large as those values measured on clean days. This can be attributed to the increased concentration of PM, specifically ammonium nitrate, soot, and organics during the polluted days. Additionally, during polluted days the peak of the scattering coefficient was 4 h later than the absorption coefficient peak possibly due to gas to particle formation of secondary aerosol that scatters light effectively, as previously seen in Mexico City (Paredes-Miranda et al. 2009).

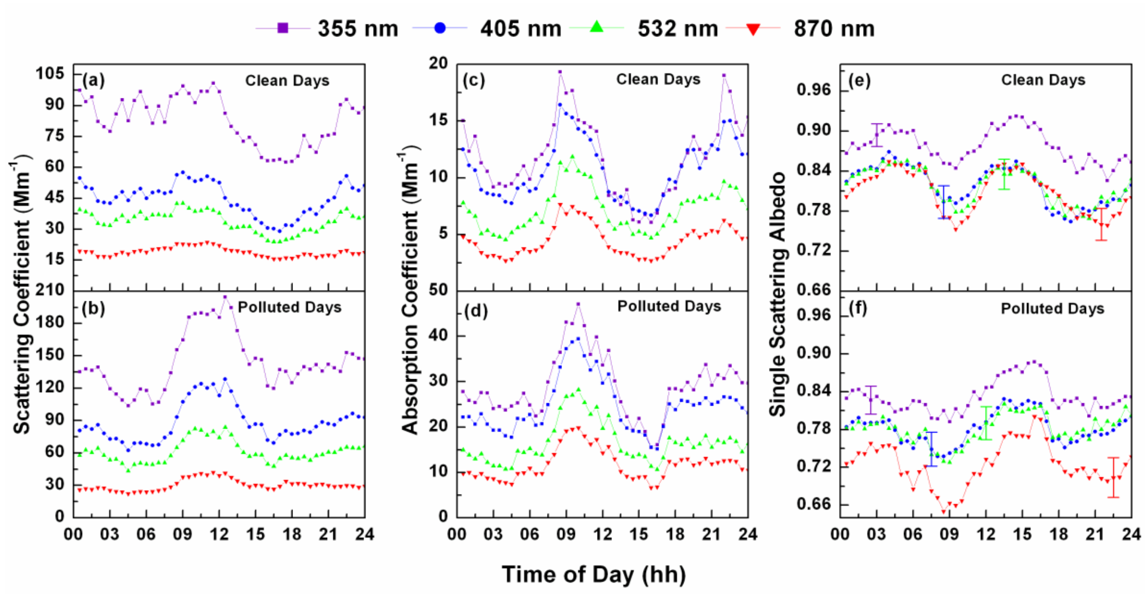

Figure 3.6 Diurnal variation of half-hour average ambient aerosol optical properties from 18 December, 2009 to 18 January, 2010 at wavelengths 355, 405, 532, and 870 nm for clean and polluted days. (a) and (b) are the scattering coefficients, (c) and (d) are the absorption coefficients, and (e) and (f) are the single scattering albedos (SSA). Uncertainty on SSA was determined by assuming 5% relative uncertainty in photoacoustic absorption coefficient measurements and 15% relative uncertainty in scattering coefficient measurements.

3.4.3.2 Spectral and diurnal variation of SSA

SSA is a crucial optical parameter for determining the sign of net radiative forcing by aerosol. The value of 0.85 represents an approximate boundary point. Values above 0.85 generally represent a cooling impact while values less than this quantity represent an heating impact (Hansen et al., 1981). While the temporal and spatial variations of SSA in the atmosphere are associated with BL mechanisms, rush hour activity, and other natural and anthropogenic events, the spectral variations of SSA are dependent on aerosol size, chemical composition, and mixing state. For dust and biomass burning aerosols that absorb significantly at shorter solar wavelengths, SSA generally increases with wavelength, while this tendency reverses for small-particle BC aerosol from vehicular exhaust (Bergstrom et al., 2002; Gyawali et al., 2009; Sokolik and Toon, 1999). Figures 3.6e and f show the diurnal and spectral changes in half-hour average of SSA computed with equation 6. The role of temperature inversion on the diurnal evolution of aerosol size and composition is reflected in the magnitude of SSA. Minimum SSA is observed around 09:00 LT, coincident with morning peak traffic, while maximum SSA is observed at 15:00 LT, concurring with the low value of AES and dominance of larger particles as evidenced in Figs. 3.4a and b. Compared to the other wavelengths, diurnal half-hour SSA at 355 nm is the highest value, varying from 0.80 to 0.92. Other wavelengths exhibit a distribution from 0.65 at 870 nm to 0.88 at 532 nm. Polluted days show less diurnal variation and lower values of SSA due to the averaging effects of multiple days of stagnation.

Though our measurement techniques and approaches are for aerosol sampled close to ground level, it is worthwhile to compare our findings with other published data even if these data are mainly based on remote sensing and focus on the total atmospheric column.

Since SSA is an intensive parameter, for well-mixed conditions in-situ ground based and remote sensing measurements should have a similar relationship. Hofzumahaus et al. (2002) applied the best fit of modeled actinic fluxes to spectroradiometer measurements and came up with 0.87 and 0.95 for SSA at 355 nm for different days in Greece. Corr et al. (2009) found SSA variations from 0.73 to 0.85 at 368 nm using a multi-filter rotating shadowband radiometer (MFRSR) in Mexico City. Barnard et al (2008) reported SSA = 0.80 at 368 nm using a UV-MFRSR technique. These authors have also reported SSA for visible wavelengths and acknowledged that the observed lower value towards the UV region, when present, is due to the enhanced absorption by certain organic compounds in aerosols.

3.4.3.3 Spectral and diurnal variation of AES

The wavelength dependence of AES has been used to understand the dominant aerosol size distribution along with the optical properties of biomass burning, urban, and desert dust aerosols (Eck et al., 1999; Reid et al., 1999). Dubovik et al. (2002) described values of Ångström exponent of extinction (AEE) varying from -0.1 to 2.5 to identify aerosol sources including desert dust and biomass burning in their comprehensive survey of aerosol optical properties at locations around the globe (Dubovik et al., 2002). Values of AEE close to 0 occur when the scattering is dominated by large dust particles, and AEE close to 2.5 represents smoke particles. These values were reported from ground-based Sun photometer remote sensing measurement techniques. However, we note that the AEA and the AEE are only comparable when extinction is dominated by scattering.

Figures 3.7a and b present the variations of AES during the clean and polluted days. $\beta_{sca}(\lambda)$ was used in Eq. 5 for the calculations of AES, where 870 nm was taken as the reference wavelength. Values of AES are large in the early morning, with AES=1.8 for the 355/870 nm pair, and around 1.3 for longer-wavelength pairs (405/870 and 532/870 nm), a widely used value for the atmosphere of natural composition. On clean days, AES values for the longer-wavelengths pairs decline continuously after midnight and are at their minimum value of ~0.8 about four hours after the local noon, at the warmest, most diluted time of the day. The minimum

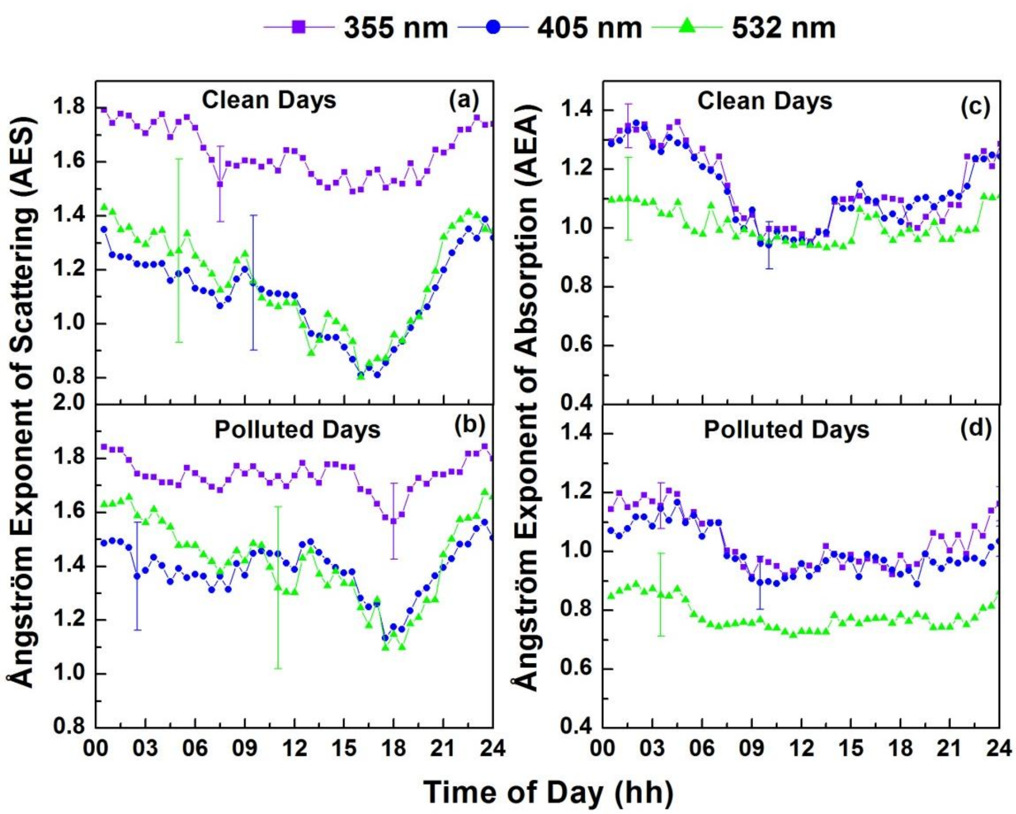

Figure 3.7 Diurnal variation of half-hour average ambient intensive aerosol optical properties for clean and polluted days from 18 December, 2009 to 18 January, 2010 at wavelengths 355, 405, and 532 nm using 870 nm as a reference. (a) and (b) Ångström exponent of scattering (AES), (c) and (d) Ångström exponent of absorption (AEA).

Uncertainty on AES and AEA were determined by assuming 5% relative uncertainty in photoacoustic absorption coefficient measurements and 15% relative uncertainty in scattering coefficient measurements.

on polluted days occurs six hours after local noon, corresponding to peak particle size. In comparison, AES varies more for all pairs of wavelengths for clean days than on polluted days. The significant diurnal change of AES implies a distinct diurnal cycle for particle size. The size of the freshly emitted particles increases over their atmospheric residence time due to the various phenomena present in atmospheric processing (Reid et al., 1998). As stated above, AES is at its minimum in the later part of the day, indicating the dominance of larger particles as a result of atmospheric aging of aerosols as found in the diurnal variations of particulate matters. Turbulent mixing at the BL thickness peak may enhance coagulation, and repeatedly expose aerosol and precursors to strong UV radiation at the top of the BL. The BL expansion, photo-oxidation, condensation, and coagulation processes smear out the dominance of freshly emitted sub-micron particles, shifting to the dominance of larger-sized aged aerosol as implied in the diurnal variation of AES and measurements of $PM_{2.5}$ and coarse particle mass concentrations.

The minimum of AES for the longer-wavelength pairs occurs two hours later than for clean days, likely as a result of the delay in photo-chemically driven condensational growth of primary aerosols on polluted days. The explanation for the vastly different behavior of AES for the wavelength pair, 355/870 nm, is currently unknown but maybe related to significant changes in refractive indices of different PM components between the visible (i.e. 405 and 532 nm) and the UV (i.e. 355 nm).

3.4.3.4 Spectral and diurnal variation of AEA

AEA responds to the composition, size, and the presence of coatings on aerosol. Recent analysis shows that AEA can be as high as 1.6 even with non-absorbing coatings on BC (Gyawali et al., 2009; Lack and Cappa, 2010). It has been shown that the core size, coating thickness, and complex refractive index of both components play a vital role in the spectral coating enhancement of absorption.

The diurnal variation of AEA is shown in Figs. 3.7c and d. The diurnal variations at wavelength pairs 355/870, and 405/870 nm exhibit similar behavior, displaying higher values in the early morning and then decreasing by noon and increasing thereafter. The value of AEA at 355/870 nm is as high as 1.4 on clean days during nighttime hours due to biomass burning. For the wavelength pair 532/870 nm AEA is close to one during clean days and has little variation, but remains around 0.8 during polluted days.

AEA depends on the wavelength pair as well as the mixing and coating state of the aerosols. Depending upon the nature of OA, its mass absorption coefficients towards UV is significantly higher (as high as 12 m^2g^{-1} at 350 nm) than at mid visible regions (Barnard et al., 2008; Lack and Cappa, 2010). Hence, 355 and 405 nm absorption is due to OA and BC, whereas 532 and 870 nm absorption is mainly due to BC. The maximum AEA was found around 1.4 for the pair 355/870 nm and it can be attributed to the presence of OA from wood burning. This value decreases to around 1.0 during morning rush hour when BC emissions from vehicles are dominant. After noon, the increase in AEA for all pairs is due to the atmospheric processing of aerosols, in which coating, mixing, and coagulation are taking place. We did not observe dramatic variation of AEA for the 355/870 nm pair compared with the 405/870 nm pair. On the other hand, it is interesting to see (Fig. 3.7d) that AEA remains nearly constant throughout the day. Restrictions against residential wood burning on polluted days may also result in lower AEA values at night than during clean days.

Table 3.1 Mean values of SSA, AEA, and AES for clean (C) and polluted (P) days. For AEA and AES the reference wavelength is 870 nm.

Wavelength	SSA C	SSA P	AEA C	AEA P	AES C	AES P
355 nm	0.87±0.02	0.83±0.02	1.14±0.12	1.03±0.09	1.63±0.09	1.73±0.06
405 nm	0.80±0.02	0.78±0.02	1.12±0.12	0.99±0.07	1.11±0.15	1.38±0.09
532 nm	0.82±0.03	0.78±0.02	1.00±0.05	0.78±0.04	1.16±0.18	1.42±0.15
870 nm	0.81±0.03	0.72±0.03				

Figures 3.8a and b show the variation of AES and AEA at 355 and 532 nm with SSA at 355 and 532 nm, respectively. Like SSA, values of AEA are generally larger and more scattered during clean days. Even though the error bars are overlapping or touching in most of the cases, there is the clear distinction between the mean values of intensive aerosol optical properties, i.e., AES, AEA, and SSA for clean days and polluted days (Figs. 3.8c, d, and e). The mean values of SSA, AEA, and AES are presented in table 1. The mean values of the AEA for clean days are comparable with the AEA values reported by Ajtai et al. (2011) from field measurements at suburban wintry conditions in Hungary. This demonstrates some similarity of spectral dependence of aerosol light absorption in these

two different places.

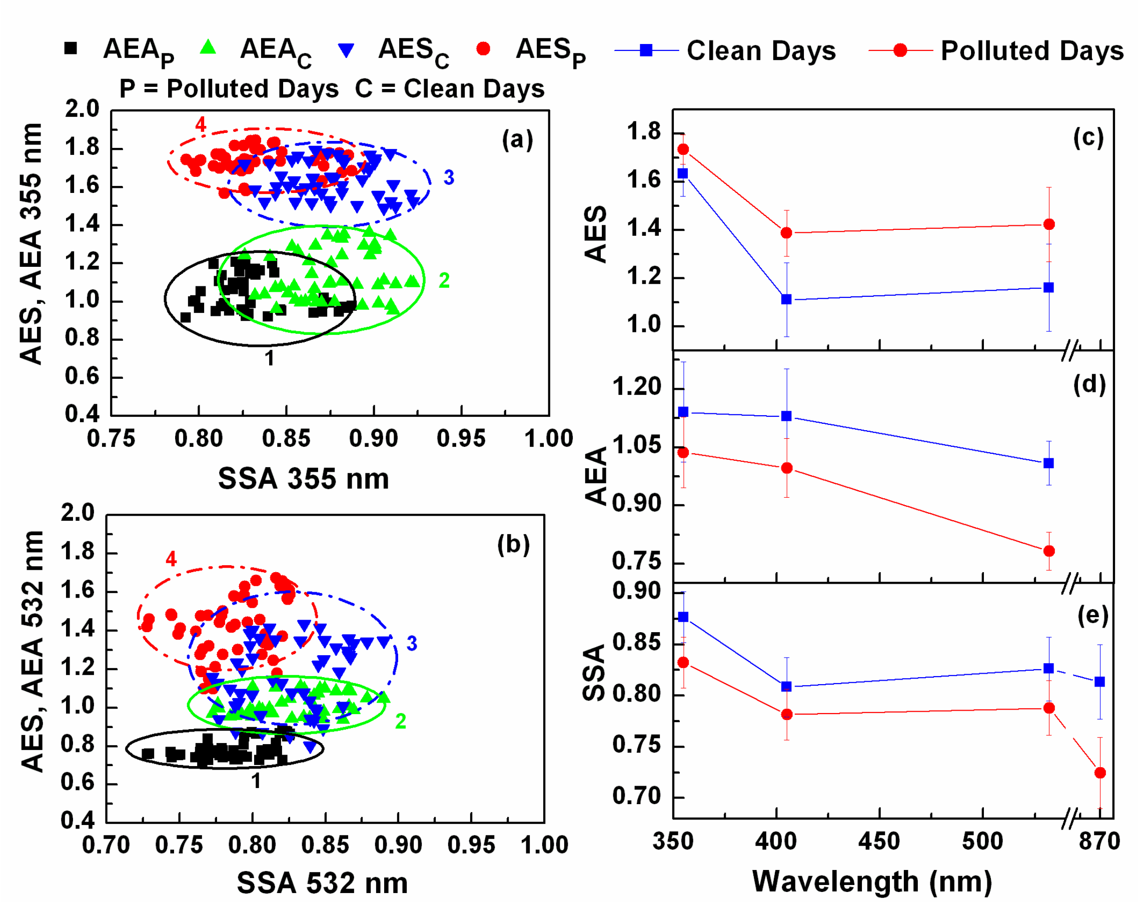

Figure 3.8 Ambient intensive aerosol optical properties from 18 December, 2009 to 18 January, 2010. Half-hour average AES and AEA versus single scattering albedo (SSA) for (a) 355 nm and (b) 532 nm. Averaged (c) AES and (d) AEA for “clean days” and “polluted days” using 870 nm as a reference wavelength. (e) similar plot for SSA.

3.5 Summary and Conclusions

A new photoacoustic instrument measuring aerosol light absorption and scattering at 355 nm was constructed to explore aerosol optical properties in the UV region and to investigate light absorbing organic aerosols. Multispectral photoacoustic measurements of laboratory-generated and ambient aerosols were performed in Reno, Nevada, USA to evaluate the aerosol light absorption and scattering from near UV to near IR. Particulate matter, gaseous pollutants, and meteorological data in combination with aerosol optical properties were used to get insights into the winter-time urban aerosol evolution and composition. Based upon these analyses, the measurement period, from 18 December 2009 to 18 January 2010 has been divided into "polluted days" (temperature inversion) and "clean days" (well-mixed air).

The results lead to the following remarks and conclusions. The AEA is very large for incense (i.e. 4.53) compared with that of kerosene soot (i.e. 0.80), highlighting its use as a surrogate for smoldering phase biomass combustion. The higher mass concentrations of $PM_{2.5}$ and coarse particles were associated with the intense ground level temperature inversions. The temporal variation of aerosol intensive parameters is much more pronounced on clean days than on polluted

days. The strong temperature inversions more than doubled the peak values of diurnal half-hour average of aerosol absorption (i.e. $\beta^{355nm}_{abs clean}$ = 18 Mm^{-1}, and $\beta^{355nm}_{abs\ polluted}$= 48 Mm^{-1}) and scattering coefficients (i.e. $\beta^{355nm}_{sca\ clean}$ = 105 $Mm^{-1}$and $\beta^{355nm}_{sca\ polluted}$=210 Mm^{-1}).

Organic species dominated the $PM_{2.5}$ component mass concentrations during the study periods; however, the low values of AEAs suggest that the light absorbing particles were not dominated by light absorbing organic carbon or BrC during polluted days. Our work with UV (355 nm) absorption does not show a strong signature of wood smoke for Reno, in contrast to what has been found in other places (e.g., Sandradewi et al., 2008a, b). Residential wood burning in Reno may be efficient enough to mitigate BrC emissions. It was concurrently found that approximately two-thirds of nitrate aerosols were associated with mobile source emissions and one-third with residential wood combustion emissions (Watson et al., 2011). The maximum scattering coefficient values during polluted days occurred 4 h later than the maximum scattering coefficient values on clean days, suggesting that formation of secondary organic aerosol is delayed by the strong temperature inversions during polluted days. The concurrent temporal maximum absorption values during clean and polluted days imply that traffic emissions are the dominant source of multispectral aerosol absorption. In general, SSAs are larger for all wavelengths on clean days (i.e. $SSA_{clean}^{355nm} = 0.87$) than on polluted days (i.e. $SSA_{polluted}^{355nm} =$ 0.83). This can be attributed to the increased use of gasoline and diesel engines in the snow removal process and the restrictions on residential wood burning (source of primary organic aerosol) on polluted days.

3.6 Acknowledgements

This material is based upon work supported by NASA EPSCoR under Cooperative Agreement No. NNX10AR89A, by NASA ROSES under Grant No. NNX11AB79G, and by the Pacific Northwest National Laboratory.

3.7 References

Abu-Rahmah, A., Arnott, W. P., and Moosmüller, H.: Integrating nephelometer with a low truncation angle and an extended calibration scheme, Meas. Sci. Technol., 17, 1723-1732, 2006.

Ajtai, T., Filep, À., Schnaiter, M., Linke, C., Vragel, M., Bozóki, Z., Szabó, G., and Leisner, T.:
A novel multi-wavelength photoacoustic spectrometer for the measurement of the UV-vis-NIR spectral absorption coefficient of atmospheric aerosols, Journal of Aerosol Science, 41, 1020-1029, 2010.

Ajtai, T., Filep, À., Utry, N., Schnaiter, M., Linke, C., Bozóki, Z., Szabó, G., and Leisner, T.:
Inter-comparison of optical absorption coefficients of atmospheric aerosols determined by a multi-wavelength photoacoustic spectrometer and an Aethalometer under sub-urban wintry conditions, Journal of Aerosol Science, 42, 859-866, 2011.

Andreae, M. O. and Gelencsér, A.: Black carbon or brown carbon? The nature of light-absorbing carbonaceous aerosols, Atmos. Chem. Phys., 6, 3131–3148, doi:10.5194/acp-6-3131-2006, 2006.

Arnott, W. P., Moosmüller, H., and Walker, J.: Nitrogen dioxide and kerosene-flame soot calibration of photoacoustic instruments for measurement of light absorption by aerosols, Rev. Sci. Instrum., 71, 4545–4552, 2000.

Arnott, W. P., Zielinska, B., Rogers, C. F., Sagebiel, J., Park, K., Chow, J., Moosmüller, H.,
Watson, J. G., Kelly, K., Wagner, D., Sarofim, A., Lighty, J., and Palmer, G.: Evaluation of 1047-nm Photoacoustic Instruments and Photoelectric Aerosol Sensors in Source-Sampling of Black Carbon Aerosol and Particle-Bound PAHs from Gasoline and Diesel Powered Vehicles, Environ. Sci. Technol., 39, 5398–5406, 2005a.

Arnott, W. P., Hamasha, K., Moosmüller, H., Sheridan, P., and Ogren, J.: Towards aerosol light-absorption measurements with a 7-wavelength Aethalometer: Evaluation with a photoacoustic instrument and 3-wavelength nephelometer, Aerosol Sci. Tech., 39, 17-29, 2005b.

Arnott, W. P., Moosmüller, H., and Walker, J.: Nitrogen dioxide and kerosene-flame soot calibration of photoacoustic instruments for measurement of light absorption by aerosols, Rev. Sci. Instrum., 71, 4545-4552, 2000.

Arnott, W. P., Moosmüller, H., Rogers, C., Jin, T., and Bruch, R.: Photoacoustic spectrometer for measuring light absorption by aerosols: Instrument description, Atmos. Environ., 33, 2845-2852, 1999.

Arnott, W. P., Walker, J., Moosmüller, H., Elleman, R., Jonsson, H., Buzorius, G., Conant, W., Flagan, R., and Seinfeld, J.: Photoacoustic insight for aerosol light absorption aloft from meteorological aircraft and comparison with particle soot absorption photometer measurements: DOE Southern Great Plains climate research facility and the coastal stratocumulus imposed perturbation experiments, J. Geophys. Res., 111, D05S02, doi:10.1029/2005JD005964, 2006.

Barnard, J. C., Volkamer, R., and Kassianov, E. I.: Estimation of the mass absorption cross section of the organic carbon component of aerosols in the Mexico City Metropolitan Area, Atmos. Chem. Phys., 8, 6665-6679, doi:10.5194/acp-8-6665-2008, 2008.

Bergstrom, R. W., Pilewskie, P., Russell, P. B., Redemann, J., Bond, T. C., Quinn, P. K., and Sierau, B.: Spectral absorption properties of atmospheric aerosols, Atmos. Chem. Phys., 7, 5937-5943, doi:10.5194/acp-7-5937-2007, 2007.

Bergstrom, R. W., Russell, P. B., and Hignett, P.: Wavelength Dependence of the Absorption of Black Carbon Particles: Predictions and Results from the TARFOX Experiment and Implications for the Aerosol Single Scattering Albedo, J. Atmos. Sci., 59, 567-577, 2002.

Bergstrom, R. W., Schmidt, K., Coddington, O., Pilewskie, P., Guan, H., Livingston, J., Redemann, J., and Russell, P. B.: Aerosol spectral absorption in the Mexico City area: results from airborne measurements during MILAGRO/INTEX B, Atmos. Chem. Phys., 10, 6333-6343, doi:10.5194/acp-10-6333-2010, 2010.

BGI.: PQ100 Portable PM_{10} / TSP / $PM_{2.5}$. Prepared by BGI Incorporated, Waltham, MA, USA, http://www.bgiusa.com/aam/portable.htm, last accessed: 06/09/2011, 2009a.

BGI.: PQ200 Ambient Fine Particulate Sampler. Prepared by BGI Incorporated, Waltham, MA, USA, http://www.bgiusa.com/aam/pq200.htm, last accessed: 06/09/2011, 2009b.

Bohren, C. F. and Huffman, D. R.: Absorption and scattering of light by small particles, John Wiley & Sons Inc., 530 pp., 1983.

Bond, T. C.: Spectral dependence of visible light absorption by carbonaceous particles emitted from coal combustion, Geophys. Res. Lett., 28, 4075-4078, 2001.

Bond, T. C. and Bergstrom, R. W.: Light absorption by carbonaceous particles: An investigative review, Aerosol Sci. Tech., 40, 27-67, 2006.

Chakrabarty, R. K., Moosmüller, H., Chen, L.-W. A., Lewis, K., Arnott, W. P., Mazzoleni, C., Dubey, M. K., Wold, C. E., Hao,W. M., and Kreidenweis, S. M.: Brown carbon in tar balls from smoldering biomass combustion, Atmos. Chem. Phys., 10, 6363–6370, doi:10.5194/acp-10-6363-2010, 2010.

Chen, L.-W. A., Verburg, P., Shackelford, A., Zhu, D., Susfalk, R., Chow, J. C., and Watson, J. G.: Moisture effects on carbon and nitrogen emission from burning of wildland biomass, Atmos. Chem. Phys., 10, 6617–6625, doi:10.5194/acp-10-6617-2010, 2010.

Chen, C.-L., Tsuang, B.-J., Tu, C.-Y., Cheng, W.-L., and Lin, M.-D.: Wintertime vertical profiles of air pollutants over a suburban area in central Taiwan, Atmos. Environ, 36, 2049-2059, 2002.

Chow, J.C., Watson, J.G.: Lowenthal, D.H., Chen, L.-W.A., Tropp, R.J., Park, K., and Magliano, K.L.: $PM_{2.5}$ and PM_{10} mass measurements in California's San Joaquin Valley, Aerosol Sci. Technol., 40(10): 796-810, 2006.

Clarke, A. D., Noone, K. J., Heintzenberg, J., Warren, S. G., and Covert, D. S.: Aerosol light absorption measurement techniques: Analysis and intercomparisons, Atmos. Environ, 21, 1455-1465, doi:10.1016/0004-6981(67)90093-5, 1987.

Corr, C., Krotkov, N., Madronich, S., Slusser, J., Holben, B., Gao, W., Flynn, J., Lefer, B., and Kreidenweis, S.: Retrieval of aerosol single scattering albedo at ultraviolet wavelengths at the T1 site during MILAGRO, Atmos. Chem. Phys., 9, 5813–5827, doi:10.5194/acp-9-5813-2009, 2009.

Crosier, J., Allan, J. D., Coe, H., Bower, K. N., Formenti, P., and Williams, P. I.: Chemical composition of summertime aerosol in the Po Valley (Italy), northern Adriatic and Black Sea, Q. J. R. Meteorol. Soc. 133: (S1) 61-75, doi: 10.1002/qj.88, 2007.

D'Alessio, A., D'Anna, A., Gambi, G., and Minutolo, P.: The spectroscopic characterization of UV absorbing nanoparticles in fuel rich soot forming flames, J. Aerosol Sci, 29, 397-409, 1998.

Dubovik, O., Holben, B., Eck, T. F., Smirnov, A., Kaufman, Y., King, M. D., Tanre, D., and Slutsker, I.: Variability of absorption and optical properties of key aerosol types observed in worldwide locations, J. Atmos. Sci., 59, 590-608, 2002.

Eck, T. F., Holben, B. N., Reid, J. S., Dubovik, O., Smirnov, A., O'Neill, N. T., Slutsker, I., and Kinne, S.: Wavelength dependence of the optical depth of biomass burning, urban, and desert dust aerosols, J. Geophys. Res., 104, D24, 31333-31349, 1999.

Flowers, B. A., Dubey, M. K., Mazzoleni, C., Stone, E. A., Schauer, J. J., Kim, S.-W., and Yoon,
S. C.: Optical-chemical-microphysical relationships and closure studies for mixed carbonaceous

aerosols observed at Jeju Island; 3-laser photoacoustic spectrometer, particle sizing, and filter analysis, Atmos. Chem. Phys., 10, 10387–10398, doi:10.5194/acp-10-10387-2010, 2010.

Grisdale, R. O.: The formation of black carbon, *J. Appl. Phys*, *24*, doi:10.1063/1.1721452, 1953.

Gillis, K. A., Havey, D. K., and Hodges, J. T.: Standard photoacoustic spectrometer: Model and validation using O_2 A-band spectra. Rev. Sci. Instrum., 81: 064902-1, 064902-13, 2010.

Gyawali, M., Arnott, W. P., Lewis, K., and Moosmüller, H.: In situ aerosol optics in Reno, NV,
USA during and after the summer 2008 California wildfires and the influence of absorbing and non-absorbing organic coatings on spectral light absorption, Atmos. Chem. Phys., 9, 8007–8015, doi:10.5194/acp-9-8007-2009, 2009.

Hansen, J., Johnson, D., Lacis, A., Lebedeff, S., Lee, P., Rind, D., and Russell, G.: Climate Impact of Increasing Atmospheric Carbon Dioxide, Science, 213, 957-966, doi:10.1126/science.213.4511.957, 1981.

Hoffer, A., Gelencsér, A., Guyon, P., Kiss, G., Schmid, O., Frank, G. P., Artaxo, P., and Andreae, M. O.: Optical properties of humic-like substances (HULIS) in biomass-burning aerosols, Atmos. Phys. Chem., 6, 3563–3570, doi:10.5194/acp-6-3563-2006, 2006.

Hofzumahaus, A., Kraus, A., Kylling, A., and Zerefos, C. S.: Solar actinic radiation (280–420 nm) in the cloud-free troposphere between ground and 12 km altitude: Measurements and model results, J. Geophys. Res., 107, doi:200210.1029/2001JD900142, 2002.

Horvath, H.: Atmospheric light absorption--A review, Atmos. Environ., 27, 293-317, 1993.

Huang, C. H. and Tai, C.Y.: Relative humidity effect on PM2.5 readings recorded by collocated beta attenuation monitors. Environmental Engineering Science, 25(7): 1079-1089. ISI:000259125600013, 2008.

Jacobson, M. C., Hansson, H.-C., Noone, K. J., and Charlson, R. J.: Organic atmospheric aerosols: Review and state of the science, Rev. Geophys., 38, 267-294, 2000.

Jacobson, M. Z.: Isolating nitrated and aromatic aerosols and nitrated aromatic gases as sources of ultraviolet light absorption, J. Geophys. Res., 104, 3527-3542, 1999.

Ji, X., Le Bihan, O., Ramalho, O., Mandin, C., D'Anna, B., Martinon, L., Nicolas, M., Bard, D., and Pairon, J.-C.: Characterization of particles emitted by incense burning in an experimental house, Indoor Air, 20, 147-158, doi:10.1111/j.1600-0668.2009.00634.x, 2010.

Kikas, U., Reinart, A., Vaht, M., and Veismann, U.: A case study of the impact of boundary layer aerosol size distribution on the surface UV irradiance, Atmos. Environ., 35, 5041-5051, 2001.

Kirchstetter, T. W., Novakov, T., and Hobbs, P.V.: Evidence that the spectral dependence of light absorption by aerosols is affected by organic carbon, J. Geophys. Res., 109, D21208, doi:10.1029/2004JD004999, 2004.

Kirchstetter, T. W., Harley, R. A., Kreisberg, N. M., Stolzenburg, M. R., and Hering, S. V.: On-road measurements of fine particle and nitrogen oxide emissions from light-and heavy-duty motor vehicles, Atmos. Environ.,33, 2955-2968, 1999.

Lack, D. A. and Cappa, C. D.: Impact of brown and clear carbon on light absorption enhancement, single scatter albedo and absorption wavelength dependence of black carbon, Atmos. Chem. Phys., 10, 4207-4220, doi:10.5194/acp-10-4207-2010, 2010.

Levoni, C., Cervino, M., Guzzi, R., and Torricella, F.: Atmospheric aerosol optical properties: a database of radiative characteristics for different components and classes, Appl. Opt., 36, 8031-8041, 1997.

Lewis, K., Arnott, W. P., Moosmüller, H., and Wold, C. E.: Strong spectral variation of biomass smoke light absorption and single scattering albedo observed with a novel dual-wavelength photoacoustic instrument, J. Geophys. Res., 113, D16203, doi:10.1029/2007JD009699, 2008.

Lewis, K. A., Arnott, W. P, Moosmüller, H., Chakrabarty, R. K., Carrico, C. M, Kreidenweis, S. M., Day, D. E., Malm, W. C., Laskin, A., Jimenez, J. L., Ulbrich, I. M. Huffman, J. A., Onasch, T. B.,Trimborn, A., Lui, L., and Mishchenko, M. I.: Reduction in Biomass Burning Aerosol Light Absorption upon Humidification: Roles of Inorganically-Induced Hygroscopicity, Particle Collapse, and Photoacoustic Heat and Mass Transfer. Atm. Chem. Phys., 9, 8949-8966, doi:10.5194/acp-9-8949-2009, 2009.

Lloyd, A. C. and Cackette, T. A.: Critical review- Diesel engines: Environmental impact and control, J. Air Waste Manage. Assoc., 51(6): 809-847, 2001.

Martins, J. V., Artaxo, P., Kaufman, Y. J., Castanho, A. D., and Remer, L. A.: Spectral absorption properties of aerosol particles from 350–2500nm, Geophys. Res. Lett., 36, L13810, doi:200910.1029/2009GL037435, 2009.

Moosmüller, H. and Chakrabarty, R. K.: Technical Note: Simple Analytical Relationships between Ångström Coefficients of Aerosol Extinction, Scattering, Absorption, and Single Scattering Albedo. Atm. Chem. Phys., 11,10677-10680, doi:10.5194/acp-11-10677-2011, 2011.

Moosmüller, H. and Arnott, W. P.: Particle Optics in the Rayleigh Regime. J. Air & Waste Manage. Assoc., 59, 1028-1031, 2009.

Moosmüller, H., Chakrabarty, R. K., Ehlers, K. M., and Arnott, W. P.: Absorption Ångström coefficient, brown carbon, and aerosols: basic concepts, bulk matter, and spherical particles, Atmos. Chem. Phys., 11, 1217-1225, doi: 10.5194/acp-11-1217-2011, 2011.

Moosmüller, H., Chakrabarty, R. K., and Arnott, W. P.: Aerosol light absorption and its measurement: A review, J. Quant. Spectrosc. Radiat. Transfer, 110, 844-878, 2009.

Moosmüller, H., Arnott, W. P., Rogers, C. F., Chow, J. C., Frazier, C. A., Sherman, L. E., and Dietrich, D. L.: Photoacoustic and filter measurements related to aerosol light absorption during the Northern Front Range Air Quality Study (Colorado 1996/1997), J. Geophys. Res., 103, D21, doi:10.1029/98JD02618,1998.

Paredes-Miranda, G., Arnott, W. P., Jimenez, J. L., Aiken, A. C., Gaffney, J. S., and Marley, N. A.: Primary and secondary contributions to aerosol light scattering and absorption in Mexico City during the MILAGRO 2006 campaign, Atmos. Chem. Phys., 9, 3721-3730, doi:10.5194/acp-9-3721-2009.

Petzold, A. and Schönlinner, M.: Multi-angle absorption photometry--a new method for the measurement of aerosol light absorption and atmospheric black carbon, J. Aerosol Sci., 35, 421-441, 2004.

Reid, J. S., Hobbs, P. V., Ferek, R. J., Blake, D. R., Martins, J. V., Dunlap, M. R., and Liousse, C.: Physical, chemical, and optical properties of regional hazes dominated by smoke in Brazil, J. Geophys. Res., 103, 32059-32080, 1998.

Reid, J. S., Eck, T., Christopher, S., Hobbs, P. V., and Holben, B. N.: Use of the Angstrom exponent to estimate the variability of optical and physical properties of aging smoke particles in Brazil, J. Geophys. Res., 104, 27473-27489, 1999.

Roden, C. A., Bond, T. C., Conway, S., Benjamin, A., and Pinel, A. B. O.: Emission factors and real-time optical properties of particles emitted from traditional wood burning cookstoves, Environ. Sci. Technol., 40, 6750-6757, 2006.

Sandradewi, J., Prévôt, A. S. H., Szidat, S., Perron, N., Alfarra, M. R., Lanz, V. A., Weingartner, E., and Baltensperger, U.: Using aerosol light absorption measurements for the quantitative de- termination of wood burning and traffic emission contributions to particulate matter, Environ. Sci. Technol., 42, 3316–3323, doi:10.1021/es702253m, 2008a.

Sandradewi, J., Prévôt, A. S. H., Weingartner, E., Schmidhauser, R., Gysel, M., and Baltensperger, U.: A study of wood burning and traffic aerosols in an Alpine valley using a multi-wavelength Aethalometer, Atmos. Environ., 42, 101–112, 2008b.

Schuster, G. L., Dubovik, O., and Holben, B. N.: Angstrom exponent and bimodal aerosol size distributions, J. Geophys. Res., 111, D07207, doi: 10.1029/2005JD006328, 2006.

Schwab, J. J., Felton, H. D., Rattigan, O. V., and Demerjian, K. L.: New York state urban and rural measurements of continuous $PM_{2.5}$ mass by FDMS, TEOM, and BAM. J. Air Waste Manage. Assoc., 56(4): 372-383, 2006.

Schnaiter, M., Gimmler, M., Llamas, I., Linke, C., Jäger, C., and Mutschke, H.: Strong spectral dependence of light absorption by organic carbon particles formed by propane combustion, Atmos. Chem. Phys., 6, 2981–2990, 2006, http://www.atmos-chem-phys.net/6/2981/2006/.

Seinfeld, J. H. and Pandis, S. N.: Atmospheric Chemistry and Physics: From Air Pollution to Climate Change, 2nd ed., Wiley, Hoboken, NJ, USA, 2006.

Sheridan, P., Arnott, W. P., Ogren, J., Andrews, E., Atkinson, D., Covert, D., Moosmüller, H., Petzold, A., Schmid, B., Strawa, A., Varma, R., and Virkkula: The Reno Aerosol Optics Study: An evaluation of aerosol absorption measurement methods, Aerosol Sci. Tech., 39, 1-16, doi:10.1080/027868290901891, 2005.

Silva, P., Vawdrey, E., Corbett, M., and Erupe, M.: Fine particle concentrations and composition during wintertime inversions in Logan, Utah, USA, Atmos. Environ., 41, 5410-5422, doi:10.1016/j.atmosenv.2007.02.016, 2007.

Sokolik, I. and Toon, O.: Incorporation of mineralogical composition into models of the radiative properties of mineral aerosol from UV to IR wavelengths, J. Geophys. Res., 104, 9423-9444, 1999.

Stephens, S., Madronich, S., Wu, F., Olson, J.B., Ramos, R., Retama, A., and Munoz, R.: Weekly patterns of Mexico City's surface concentrations of CO, NOx, PM10 and O3 during 1986–2007, Atmos. Chem. Phys., 8, 5313-5325, 2008.

Sun, H., Biedermann, L., and Bond, T.: Color of brown carbon: A model for ultraviolet and visible light absorption by organic carbon aerosol, Geophys. Res. Lett. 34, L17813, doi:10.1029/2007GL029797, 2007.

Taylor, T., L'Ecuyer, T., Slusser, J., Stephens, G., and Goering, C.: An operational retrieval algorithm for determining aerosol optical properties in the ultraviolet, J. Geophys. Res., 113, D03201, doi:10.1029/2007JD008661, 2008.

Tian, G., Moosmüller, H., and Arnott, W. P.: Simultaneous photoacoustic spectroscopy of aerosol and oxygen A-band absorption for the calibration of aerosol light absorption measurements. Aerosol. Sci. Technol., 43: 1084-1090, 2009

van de Hulst, H. C.: Light Scattering by Small Particles, Dover Publications, Inc., New York, USA, 453 pp., 1981.

Watson**,** J. G., Chow, J.C., Lowenthal, D. H., and Magliano, K. L.: Estimating aerosol light scattering at the Fresno Supersite, Atmos. Environ, 42, 1186-1196, 2008.

Watson, J.G. and Chow, J.C.: A wintertime $PM_{2.5}$ episode at the Fresno, CA, supersite, Atmos. Environ, 36(3), 465-475, 2002.

Watson, J. G., Chow, J. C., Chen, L.-W. A., Green, M. C., Kohl, S. D.: Wintertime $PM_{2.5}$ source contributions in Reno, NV. A report prepared by Desert Research Institute, Reno, NV, for Washoe County Health District, Air Quality Division, Reno, NV, 2011.

Wentzel, M., Gorzawski, H., Naumann, K., Saathoff, H., and Weinbruch, S.: Transmission electron microscopical and aerosol dynamical characterization of soot aerosols, J. Aerosol Sci., 34, 1347-1370, 2003.

Yang, C., Lin, T., and Chang, F.: Particle size distribution and PAH concentrations of incense smoke in a combustion chamber, Environmental Pollution, 145, 606-615, doi:10.1016/j.envpol.2005.10.036, 2007.

Zaveri, R. A., Berkowitz, C. M., Brechtel, F. J., Gilles, M. K., Hubbe, J. M., Jayne, J. T., Kleinman, L. I., Laskin, A., Madronich, S., Onasch, T. B., Pekour, M. S., Springston, S. R., Thornton, J. A., Tivanski, A. V., and Worsnop, D. R.: Nighttime chemical evolution of aerosol and trace gases in a power plant plume: Implications for secondary organic nitrate and organosulfate aerosol formation, NO_3 radical chemistry, and N_2O_5 heterogeneous hydrolysis, J. Geophys. Res., 115, D12304, doi:10.1029/2009JD013250, 2010.

4 Influence of Chemical Transformation and Meteorological Transport on Multispectral Aerosol Light Scattering, Absorption, and Extinction during the 2010 CARES campaign

4.1 Abstract

As a part of the Carbonaceous Aerosol and Radiative Effects Study (CARES) in June 2010, a study was conducted in the area of Sacramento to investigate the evolution of multispectral aerosol optical properties resulting from physical and chemical transformations. Spectral absorption (β_{abs}) and scattering (β_{sca}) coefficients for wavelengths ranging from 355 to 1064 nm were measured using photoacoustic (PA) instruments with integrating nephelometers and cavity ring down (CRD) instruments. This study presents the measurements carried out at two sites; the first site, named T0, was in Roseville, Sacramento and the second site, named T1, was located in the Sierra Nevada foothills, ~40 km northeast of site T0. From the 2nd to 22nd of June, T1 scattering measurements followed the same patterns of T0 scattering measurements but were slightly delayed, suggesting regional air mass influence. The short wavelength scattering at both sites gradually increased during the second half of the campaign (from the 22nd to 28th of June), due to the continuous growth of ultrafine and submicron (PM_1) particles. Measurements also showed a steady increase of secondary organic aerosol (SOA) concentration during this period. This particle growth was concurrently measured by a scanning mobility particle sizer (SMPS) and an aerosol mass spectrometer (AMS). Ångström exponent of absorption (AEA) was ~1.6 and was associated with the average β_{abs} of ~3.9 Mm^{-1} at 405 nm for T0. Similarly, AEA was 1.5 and was associated with average β_{abs} of ~4.5 Mm^{-1} at 355 nm for T1. These measurements were collected from

the period of enhanced SOA formation (from 22nd to 28th of June), indicating a modest wavelength-dependent enhancement of absorption by SOA at both sites. ‘Fresh’ local aerosol under northwesterly (NW) flows exhibited low single scatter albedo (SSA) and low concentration, compared with ‘aged’ aerosol from long range transport under southwesterly (SW) flows from the Francisco Bay Area. At T0 and T1 SSA decreased to 0.45 and 0.50 at 532 and 355 nm, respectively, during NW flows, while SSA increased consistently during the second half of the campaign at both sites. Multispectral aerosol light scattering β_{sca} was estimated by using Mie theory calculations on SMPS measurements of sub-micron particles. The estimated β_{sca} was underestimated by 13-90% depending upon the wavelengths and measurements sites, due to the exclusion of super-micron aerosol in the model.

4.2 Introduction

The Carbonaceous Aerosols and Radiative Effects Study (CARES) field campaign was undertaken to better understand the evolution of aerosol properties resulting from the various interactions between anthropogenic and biogenic emissions. The CARES field campaign took place near Sacramento, CA, USA, and employed a wide range of ground-based and airborne instruments that monitored comprehensive aerosol properties including meteorological variables and gaseous species. This campaign was designed to involve two ground sites inside and downwind from the Sacramento Valley. This was done to study the evolution of the properties of aerosols and trace gases as they drifted and diluted from the urban plume downwind through the biogenic emissions from pine forest to Cool, CA. Zaveri et al. (2012) presented detailed explanations of the instrumentation, sampling sites, and overall research objectives of the campaign.

Atmospheric aerosols have considerable impact on the Earth's radiation budget by the scattering and absorption of solar radiation, which is referred to as direct effect (Charlson et al., 1992; Schwartz, 1996). This can lead to heating or cooling of the climate depending on the magnitude of absorption and scattering. In addition to these direct effects, aerosols can also have indirect effects on radiation balance by changing the microphysical properties of clouds, thus influencing their optical properties and lifetime (Twomey, 1977; Coakley et al., 1987). Inorganic salt, such as sulfate, is known as an important aerosol species that strongly scatters and backscatters visible solar radiation, usually cooling the climate (Charlson et al., 1992; Haywood and Ramaswamy, 1998). Black carbon (BC) is the dominant absorber over the solar spectrum (Bond and Bergstrom, 2006), and usually warming the climate (Haywood and Ramaswamy, 1998; Ramanathan et al., 2005). In addition, the coating on BC particles increases its ability to absorb solar radiation (Fuller et al.,1999; Schnaiter et al., 2003; Saathoff et al., 2003; Moffet and Prather, 2009; Gyawali et al., 2009; Lack and Cappa, 2010; Shiraiwa et al., 2010), and also changes the lifetime of BC particles in the atmosphere (Lammel and Novakov, 1995; Weingartner et al., 1997). Furthermore, a number of studies (Andreae and Gelencser, 2006; Barnard et al., 2008; Gyawali et al., 2009; Kirchstetter et al., 2004; Sun et al., 2007) have identified some organic aerosols (OA) as the major absorbers particularly at shorter wavelengths. OA constitutes a large fraction of atmospheric aerosols, 20-90% of sub-micron aerosol mass (Zhang et al., 2007). These aerosols are efficient for light scattering because their size is similar to the wavelength of the visible solar radiation and their real part of refractive index is about 1.5. Additionally, they are transported far from the source region; hence, their climatic impact is not limited to the source region. However, the role of OA on the Earth's radiation budget is poorly understood and warrants more study (Intergovernmental Panel on Climate Change, 2007).

The Sacramento area occupies the centre of California's Sacramento Valley, which covers the northern third of the broad and agriculturally rich Central Valley. The Sacramento Valley is surrounded by the Sierra Nevada Mountains to the east, the California Coast Ranges to the west, and it merges with the San Joaquin Valley to the south. The evolutions of urban plumes, chemical transformation of trace gaseous species, and the evolutions of particulate matter are factors in the analysis of aerosols in the Sacramento area. The effect of biogenic emissions on the formation and processing of the aerosols in the forested ecosystem has been analyzed in past studies (Cahill et al., 2011; Dillon et al., 2002; Worton et al., 2011; Lunden et al., 2006). These studies have focused on the effect of biogenic emissions on aerosol formation and processing, as well as growth events and emission patterns, i.e. physical and chemical properties of ambient aerosols. In addition to these studies, we focused on light absorption and scattering measurements to study aerosol extinction and single scattering albedo from 355 nm to 1064 nm.

The prevailing wind in this region is from the west, which flows into the Central valley at the Carquinez Strait (the gap in the western mountain range) and is then moved up the Sacramento Valley and down the San Joaquin Valley (Bao et al., 2008; Zaremba and Carroll, 1999; Zhong et al., 2004). Especially during the summer, the lower surface pressure in the valley draws oceanic aerosols, and the urban plume including emissions from petrochemical industrial sites (near at the Carquinez Strait) into the valley. During the day, the Sacramento urban plume is driven by upslope winds that draw polluted air northeast over oak and pine trees in the Blodgett Forest area (approximately 75 km downwind of Sacramento), and further to the Sierra Nevada Mountains by late afternoon. At night, recirculation transports aged aerosols and gaseous species over Sacramento (Fast et al., 2012). The CARES campaign was designed to observe these flows as well as the evolution of the urban plume and its interaction with the biogenic emission at two ground sites, named T0 in the Roseville, Sacramento urban area, and T1 at Cool, a forested foothills region.

In the following section we provide descriptions of the measurement sites and instruments. Following that, we discuss the time series of aerosol light absorption and scattering coefficients obtained at the T0 and T1 sites using photoacoustic (PA) and cavity ring down (CRD) instruments. These results were analyzed in combination with the collocated measurements of aerosol chemical and meteorological parameters (i.e. temperature, wind speed, and wind direction). Also reported here is a scanning mobility particle sizer (SMPS) measurement of the size distribution of submicron particles (PM_1). These measurements were analyzed with Mie theory to estimate the submicron particle contribution of aerosol light scattering from UV to near IR regions at both T0 and T1 sites. These estimated aerosol light scattering coefficients were then compared with the measured values. Finally, the time series of aerosol optical properties at both sites are discussed in the context of synoptic wind flow patterns that govern the transport of aerosols (Fast et al., 2012; Zaveri et al., 2012).

4.3 Experimental

4.3.1 Ground sites and Instrumentation

The CARES campaign took place in the Sacramento valley from 2nd to 28th of June, 2010. Figure 4.1 presents the location of the ground sites of the campaign overlaid with the dominant day time patterns of summer wind movement. This consistent flow of air brings anthropogenic emissions from Sacramento to the Sierra Nevada foothills in the afternoon (Dillon et al., 2002; Lamanna and Goldstein, 1999). Two ground sites were strategically chosen to study the evolution and transport of urban emissions and their interaction with biogenic emissions in the relatively clean forested area. The urban site, T0 (altitude ~ 30 m ASL), was located on the American River College campus, ~14 km northeast of the downtown Sacramento area. The rural site, T1 (altitude ~450 m ASL), was located ~40 km northeast of the T0 site on the Northside School campus in Cool, CA. While vehicular emissions are the dominant source of air pollution around the T0 site, petrochemical refineries represent the major industrial emission directly upwind of Sacramento. During the course of the study, there was no significant industrial activity in the vicinity of the T1 site, though the nearest highway, California State Route 49, is within ~200 m, and I-80 connects nearby Auburn and Sacramento.

All measurements are reported at ambient temperature and pressure, and in Pacific Daylight Time (PDT), the local time in Sacramento, CA.

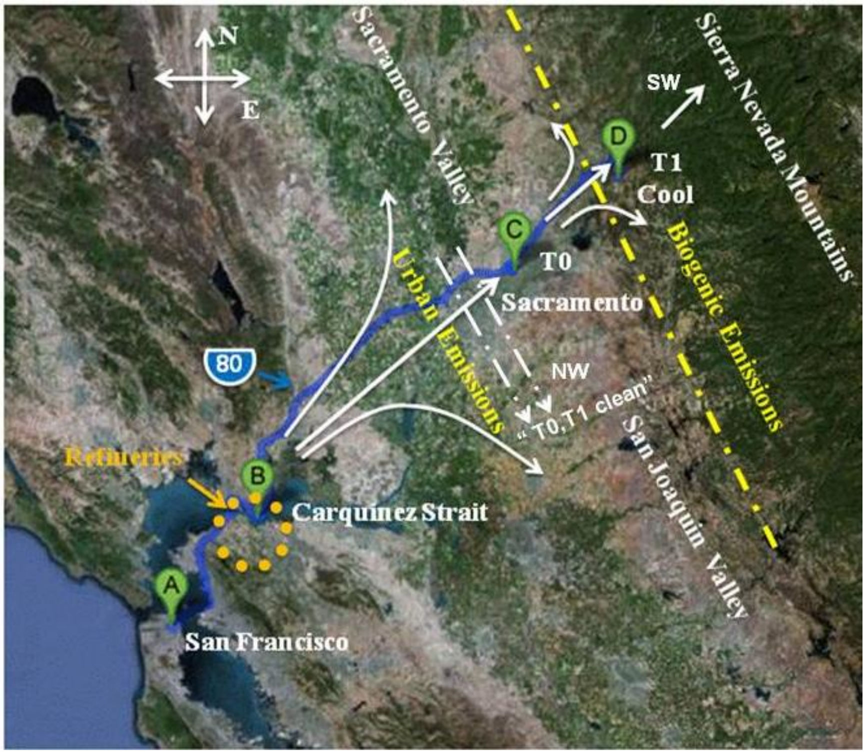

Figure 4.1 Locations of the ground sites of the campaign with the dominant day time patterns of summer wind movement.

4.3.2 Aerosol optical properties measurements

During the CARES campaign, a number of photoacoustic instruments (PA) were deployed both at T0 and T1 sites to study the spectral dependence of aerosol light absorption coefficient (β_{abs}) and scattering coefficient (β_{sca}). These coefficients expressed, in units of Mm^{-1} ($1Mm^{-1}=10^{-6}m^{-1}$), characterize the dissipation of electromagnetic radiation while traversing a unit distance. The process of atmospheric scattering takes place when a particle redistributes part of the incoming solar radiation in random directions without any change to its wavelength. In the absorption process, the solar radiation is absorbed by a particle and converted to heat energy. Although black carbon or elemental carbon accounts for most of the light absorption by atmospheric aerosols, there are other classes of organic compounds such as polycyclic aromatics (Jacobson, 1999) and humic-like substances (Hoffer et al., 2006) that also contribute to light absorption by atmospheric aerosols, particularly in the shorter wavelengths. In addition, aerosol species often combine to form mixed particles after emission from their sources during atmospheric processing, meaning that β_{abs} and β_{sca} of a mixed particle differ from those of their individual components, resulting in a corresponding change in the spectral dependence of absorption and scattering. Of special interest to the present study is the evolution of multi-spectral β_{abs} and β_{sca} in a mixed urban-biogenic environment. To accomplish this goal, our group from the University of Nevada, Reno (UNR), and Los Alamos National Laboratory, New Mexico (LANL) deployed PA operating at various wavelengths. At T0, we operated at 375, 405, 532, 781, 870, and 1047 nm, while at T1, we operated at 355, 405, 532, 781, and 870 nm.

PA techniques provides real time in-situ measurements of ambient aerosol light absorption (Arnott et al., 1999; Moosmüller et al., 2009) without changing the physical characteristics of the particles in the sampling process. In this method, aerosol samples are illuminated in an acoustic resonator by a modulated laser beam; the absorbed energy heats the aerosol, which is then released to its surroundings, producing a periodic variation in pressure (i.e. sound wave). The intensity of the sound wave is measured with a calibrated microphone located in the resonator. The PA simultaneously measures the aerosol light scattering coefficients using a reciprocal nephelometer (Abu-Rahmah et al., 2006). PA methods can determine the mixing and coating state of the aerosols, as opposed to measuring aerosol absorption by filter-based measurements. Filter-based methods can be complicated by the change of physical characteristics of the aerosols accumulating on the filter, as well as by the wetting of the filter substrate by certain organic aerosols (Subramanian et al., 2007).

Since PAs are designed for the concurrent measurement of aerosol light absorption and scattering coefficients, we can obtain the direct calculation of the extinction coefficient ($\beta_{ext} = \beta_{abs} + \beta_{sca}$), including other optical parameters like single scattering albedo (SSA) and Ångström exponent of absorption (AEA), which dictate both the magnitude and direction of the direct radiative forcing. The SSA is the ratio of aerosol scattering coefficient to the extinction coefficients and is expressed mathematically as

$$\text{SSA} = \frac{\beta_{sca}(\lambda)}{\beta_{abs}(\lambda) + \beta_{sca}(\lambda)} \qquad (1)$$

The spectral dependence of SSA at T0 was studied at $\lambda = 405$, 532, and 870 nm, and at T1 at $\lambda = 355$, 532, and 870 nm. Similarly, the AEA expressed by:

$$\text{AEA} = -\frac{\ln\left(\beta_{abs}(\lambda_1) / \beta_{abs}(\lambda_2)\right)}{\ln\left(\lambda_1 / \lambda_2\right)} \qquad (2)$$

characterizes the spectral dependence of aerosol light absorption within the wavelengths λ_1 and λ_2. The AEA at T0 was derived from the PA measurements of β_{abs} at λ_1 = 405 and at λ_2 = 870 nm, while at T1 it was derived from measurements of β_{abs} at λ_1 = 405 and at λ_2 = 870 nm.

Aerosol light extinction data was also obtained with the CRD operating at 1064 nm at both T0 and T1 sites. The operational mechanism and design of the CRD is described in detail in previous studies (Smith and Atkinson, 2001; Radney et al., 2009). It utilizes highly reflective mirrors to achieve a path length of several kilometers in a small cell. A laser pulse bounces between the mirrors inside the CRD which is analogous to the decay of sound from a tuning fork with time. The decay time in the CRD is measured for both the empty cell and for the aerosol laden cell, and the difference in these times is used to calculate the aerosol extinction coefficient.

4.3.3 Collocated measurements used in this study

Scanning mobility particle sizer (SMPS; Wiedensohler et al., 2010) measurements were collected at T0 (Zaveri et al., 2012) and T1 (Setyan et al., 2012). Within a particle diameter range from 8 to 858 nm, the particle size distributions were measured at T1 over 70 channels by a SMPS system consisting of a differential mobility analyzer (DMA) and a condensation particle counter (CPC; TSI Inc., MN; model 3772). Similar measurements were conducted at T0 for particle diameters from 12 to 736 nm over 115 channels. These measurements were used in Mie theory calculations for estimations of β_{sca}.

Measurements of size-resolved chemical composition of non-refractory particles of an aerodynamic diameter less than 1 μm (PM_1) were simultaneously acquired with a high resolution aerosol mass spectrometer (HR-AMS; Setyan et al. 2012). The HR-AMS provides mass concentration of inorganic and organic aerosols (OA).

4.3.4 Mie model to calculate β_{sca}

The interaction of a single homogeneous spherical particle with electromagnetic radiation can be computed from Mie theory (Kerker, 1969; Hulst, 1981). A model assuming spherical aerosols was applied (Wiscombe, 1980), which required particle number size distributions and complex refractive indices: $m = n_r + i\,n_i$. However, atmospheric aerosols widely vary in composition and size (a few nanometers to 100 μm ; Seinfeld and Pandis, 2006); the Mie model used here assumes a size-independent refractive index with externally mixed aerosol. The refractive index was assumed to be $1.53+i\ 10^{-6}$. This assumed value of the real part is often used for $(NH4)_2SO_4$, and is nearly constant for the wavelength range from 450 to 700 nm (Solane, 1984; Redemann et al., 2001; Fierz-Schmidhauser et al., 2010). Furthermore, recent study has suggested an increase in the real part of the refractive index from 1.48 to 1.55 of OA upon heterogeneous OH oxidation (Cappa et al., 2011).

From the aerosol size distribution of each SMPS channel (given by $\frac{dN}{d\log D_p}$), the β_{sca} is estimated with the following equation (Kleefeld et al., 2002; Chamaillard and Jennings, 2006):

$$\beta_{sca} = \int_{D_{\min}}^{D_{\max}} \frac{\pi D_p^{\ 2}}{4} Q_{sca}(\lambda, m, D_p) \ \frac{dN}{d\log D_p}\ d\log D_p \tag{3}$$

where Q_{sca} is the Mie scattering efficiency. Q_{sca} is a function of the refractive index *m*, wavelength λ, and mean diameter of the particle D_p. For each SMPS channel, D_p and $d\log D_p$ are calculated from equations (4) and (5):

$$\log D_p = \frac{1}{2}\left(\log D_{p,upper} + \log D_{p,lower}\right) \tag{4}$$

$$d\log D_p = \log D_{p,upper} - \log D_{p,lower}. \tag{5}$$

The SMPS at T0 measured the particle mobility diameter from 12 to 737 nm in 115 channels, while at T1 the measured particle diameter varied from 8 to 858 nm in 70 channels.

4.4 Results and discussion

4.4.1 Aerosol transport and meteorology

Figure 4.2 shows the time series of the aerosol optical properties and the meteorological conditions at sites T0 and T1 from the 2nd to 28th of June 2010. Traffic emission patterns in and around the sites alone cannot explain the features of the SSA and β_{sca}. Wind flow patterns and temperature were the primary contributors to the observed variations in aerosol optical properties. A study of the meteorological parameters characterizing the transport of aerosols during the CARES campaign is described by Fast et al. (2012). In brief, near-surface thermally-driven upslope flows supported by synoptic southwesterly (SW) winds were favorable for transport of urban plume from Sacramento to the T1 site near Cool. These patterns were occasionally interrupted by northwesterly (NW) flow, which carried the urban plume southeast to the San Joaquin Valley (Fig.4.1), thereby reducing the interaction of urban plume with the biogenic emissions en-route to T1. During these periods (10th-13th, 16th-17th, and 20th-21st of June 2010), the measured β_{sca} at both sites were significantly lower in comparison to measurements from the rest of the campaign. The NW flows in Fig. 4.2 are indicated by the shaded areas.

Four occurrences of lower values of SSA at both sites were centered on the 5th, 12th, 17th, and 21st of June, concurrent with the NW flows. The 30-min average values of the SSA for these episodes at T0 and T1 were around 0.50, 0.45, 0.65, and 0.77, respectively.

NW flows significantly reduced the aerosol concentration at T0 and T1. During these periods, SSA was reduced due to fresh local emissions which contributed to aerosol scattering and absorption likely due to motor vehicles emissions. Since measurements at T0 were more affected by the constant traffic emission of BC than measurements at T1, the SSA at T0 was slightly lower than that at T1. The SSA was as high as 0.98 at both sites during periods of significant southwesterly (SW) flow patterns and high temperatures.

Between days 1 and 22, T1 scattering measurements were a slightly delayed replica of T0 scattering measurements, suggesting regional air mass influence. The inset panel (Fig. 4.2b) presents the spatial and temporal features of aerosol transport from T0 to T1 during the 15th and 16th of June, representing the direct transport of the Sacramento plume through the biogenic foothills to Cool (Fast et al., 2012). The study of the β_{sca} reveals that the scattering feature was delayed by about five hours at T1 during the 16th of June. The transport ceased to be significant at around 07:00 at T0 and at 12:00 PDT at T1. According to Fast et al. (2012), on days with SW flows the transport time between the T0 and T1 varied from 2 to 8 hours with the longer times associated with urban plumes originating from downtown Sacramento. During these days, 532 and 355 nm β_{sca} at T0 and T1 were as high as 35 and 45 Mm^{-1}, respectively. Furthermore, diurnal characteristics such as morning and evening rush-hour traffic emissions were almost indistinguishable in β_{sca} measurements at T0 and T1 during SW flows. This suggests the facts that the pollution levels in the Sacramento and Cool regions were dependent on transport from the Bay Area rather than only on local emissions. In addition, episodes of elevated β_{sca} were observed only during the SW flows. During NW flows, β_{sca} measurements were close to the background levels of 3-4 Mm^{-1}, primarily due to the transport of cleaner air from the northern part of the Central Valley to T0 and T1 (Fast et al., 2012).

During the final six days of the campaign (22nd-28th of June), the 355 nm scattering at T1 was enhanced relative to the 532 nm scattering measured at T0 as a consequence of the ultrafine and submicron aerosol which began to grow vigorously in the size range where scattering at shorter wavelengths begins to increase. For instance, during this period, β_{sca} at 355 nm increased on average from 15 to 37 Mm^{-1} (147%), while β_{sca} at 532 nm increased from 12 to 19 Mm^{-1} (58%). Similarly, during the same period, β_{abs} at 355 nm increased from 2.1 to 4.4 Mm^{-1} (107%) and at 532 nm from 1.5 to 2.3 Mm^{-1} (58%). This period was the most favorable for the formation of secondary organic aerosols (SOA) due to the changing meteorological conditions such as maximum temperature around 39 ^{0}C at T0 and T1 sites (Fig. 4.2c). Higher temperature results in a higher emission rate of biogenic volatile organic compounds (VOC): isoprene, monoterpenes (Holzinger et al., 2007; Worton et al., 2011). Enhanced SOA formation was observed when the urban plume interacted with biogenic emissions during the campaign (Setyan et al., 2012).

Setyan et al. (2012) described the PM_1 chemical composition and size distribution of species at T1, including the OA components. In brief, PM_1 mass was dominated by OA (80%) and followed by sulfate (9.9%). Furthermore oxygenated OA (OOA) comprised 90% of the total mass distribution, while hydrocarbon-like OA (HOA) comprised 10%. The OOA factors correspond to the SOA and HOA to traffic-related primary emissions.

From this PM_1 classification, it is apparent that the enhanced scattering at T0 of 355 nm radiation was dominated by the OOA components of the SOA. We also note that the multispectral aerosol optical measurements from the 22nd of June through the end of the campaign were largely affected by the steady buildup of aged pollutants due to the recirculation of mixed urban and biogenic emissions.

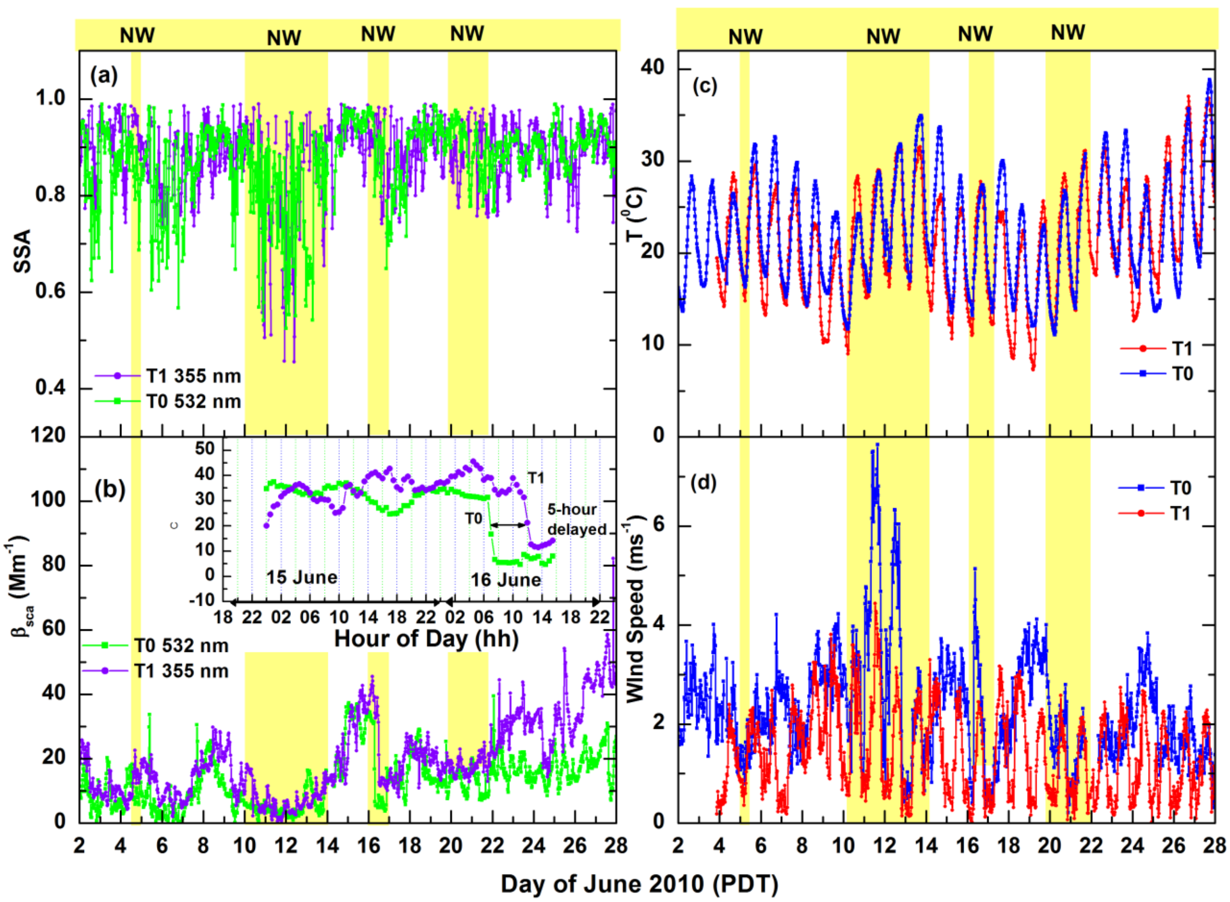

Figure 4.2 T0 and T1 time series plots of (a) single scattering albedo (SSA), (b) aerosol light scattering coefficient (β_{sca}) at 532 and 355 nm , (c) temperature, and (d) wind speed from the 2nd to 28th of June 2010. The inset panel highlights the aerosol transport from T0 to T1 and the associated time difference during the 15th and 16th of June 2010. Each point is a 30-min average of the measurements. The northwesterly (NW) flows are indicated by the shaded areas.

4.4.2 Diurnal cycles of aerosol chemical, physical, and optical properties

4.4.2.1 Site T0

Figure 4.3a-b shows the diurnal cycles of PM_1 organics and particle diameters analyzed by the AMS and SMPS at T0 from the 12th to 28th of June. Also presented in Fig. 4.3 are the PA measurements of β_{sca} (at 405, and 870 nm) and β_{abs} (at 405, 870, and 1047 nm) during the same period. The vertical bars represent one standard deviation of the averaged measurements during daylight hours (06:00 to 18:00 PDT). PM_1 organic data were available only from the 17th to 25th of June. There was a close diurnal cycle relationship between the PM_1 diameter and the aerosol scattering. Scattering at 405 nm especially agreed with the diameter of PM_1 after the 22nd of June to the end of the campaign, when PM_1 particle growth contributed to enhanced scattering at 405 nm relative to 870 nm. The maximum average PM_1 diameter was 68 nm with β_{sca} of 50 Mm^{-1} for the 28th of June, while the β_{sca} at 870 nm remained constant at around 11 Mm^{-1}.

Though β_{sca} at 405 nm and aerosol PM_1 diameter exhibited similar growth after the 22nd of June, there were some episodes before this date when the β_{sca} at 405 and 870 nm were increasing while PM_1 diameter was simultaneously decreasing during predominately SW winds. For example, on the 15th of June, we measured the highest value of β_{sca} at 870 nm of the campaign at 30 Mm^{-1}; on 16th and 18th of June it reached to a value from 8 to 18 Mm^{-1}. During these periods, the β_{sca} at 355 nm and 870 nm were comparable, while the PM_1 diameter decreased to around 40 nm, the lowest diameter observed during the campaign. Aerosol particle sizer (APS) measurements (not reported here) at T0 and T1 showed a higher concentration of coarse mode particles (Zaveri et al., 2012) due to the enhanced transport of sea salt from the Pacific Ocean into Sacramento through the Carquinez Strait. These coarse mode aerosols were responsible for the relative increase of scattering at 870 nm.

Figure 4.3d-f shows the diurnal cycle of SSA, AEA (at 405, and 870 nm), and the β_{abs}. The SSA was lower for both 405 and 870 nm during NW flows due to the effect of fresh traffic emissions. The difference between the SSA at 405 and 870 nm decreased continuously as the campaign progressed due to the enhanced formation of SOA and recirculation of aged aerosols. The diurnal variation of the SSAs was also decreasing as a result of steady buildup of aged aerosols (Zaveri et al., 2012). The SSA exhibited a similar value of ~0.90 at 405 and 870 nm after the 25th of June. The average AEA was nearly constant at ~1.5, indicating the presence of aerosols that absorb at shorter wavelengths at T0, even in the background air. However, the wider distribution of the AEA (from 0.1 to 3) suggested that absorption was strongly dependent on the diurnal cycle. The β_{abs} plotted for three wavelengths (Fig. 4.3f) demonstrates the nature of various light absorbing aerosols at T0. Since the absorption at 1047 nm is almost entirely due to BC, the nearly constant value at 0.3 Mm^{-1} of β_{abs} for 1047 nm suggests steady traffic emissions during this period. However, the comparatively higher variations of β_{abs} at 405 nm were due to the contribution of other shorter wavelength absorbing species like OA or brown carbon (BrC). The spikes in β_{abs} at 405 and 870 nm at T0 around the 14th and 17th of June might be due to the low wind speed.

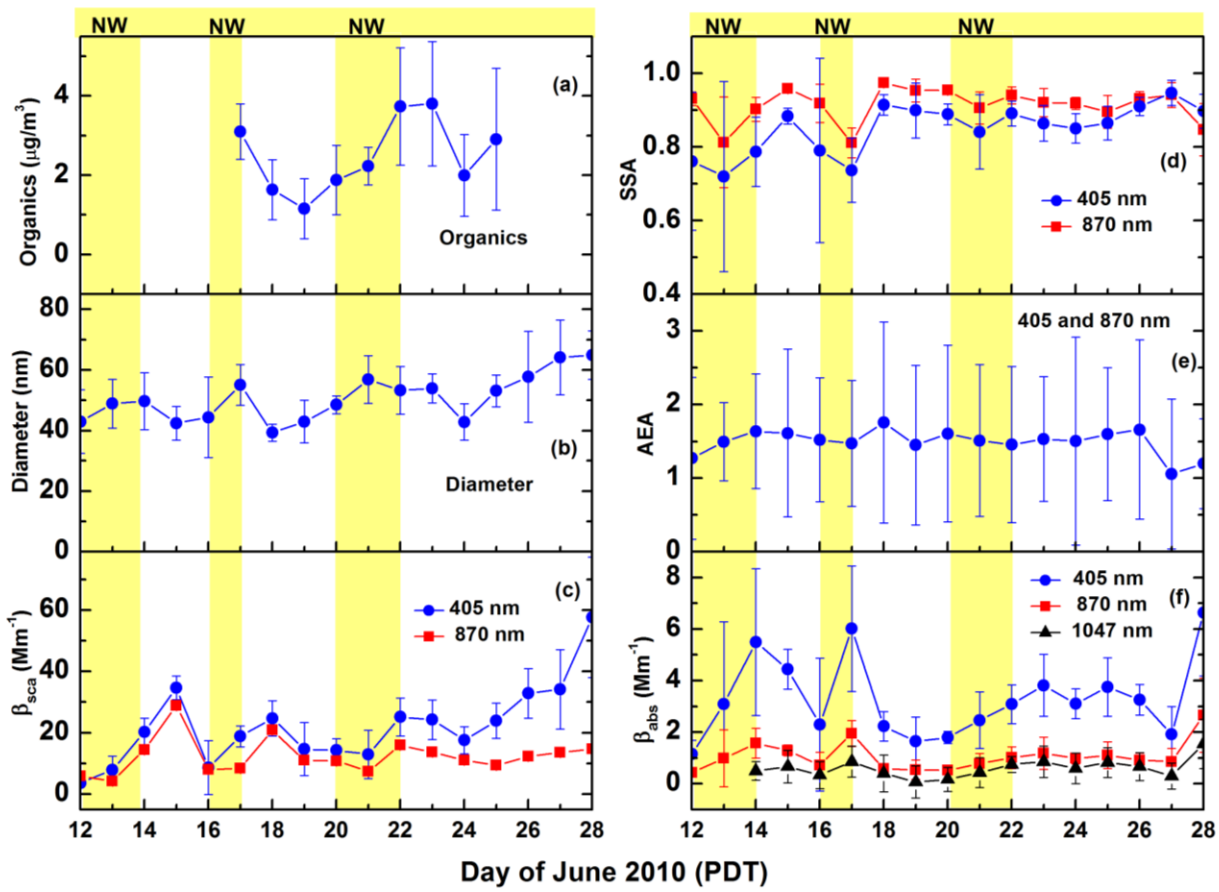

Figure 4.3 Daily variations of (a) concentration of organics (PM_1), (b) PM_1 particle diameter, (c) aerosol scattering coefficient (β_{sca}), (d) single scattering albedo (SSA), (e) Ångström exponent of absorption (AEA), and (f) absorption coefficients (β_{abs}) at 405, 870, and 1047 nm at T0 from the 12th to 28th of June 2010. Vertical bars represent one standard deviation of measurements. Each point is averaged from 06:00 to 18:00 PDT. The northwesterly flows (NW) are indicated by the shaded areas.

4.4.2.2 Site T1

Figure 4.4 presents the same measurements as plot 4.3 for the T0 site, but at wavelengths 355 and 870 nm and from the 2nd to 28th of June. The chemical, physical, and optical properties of the aerosols were more influenced by the NW flows in comparison to site T0. For example, between the 8th and 11th of June, the average concentration of PM_1 organics decreased from 4 to 1 $\mu g\, m^{-3}$, while the diameter of these particles decreased from 64 to 40 nm. As mentioned previously, the NW flows disrupted the transport of the urban plume to the T1 site, which would otherwise have gone through photochemical and physical processing. The size of the aerosol increases during atmospheric processing as a result of the coagulation and condensation of both organic and inorganic species, effecting aerosol optical properties (Reid et al., 1998). After the 22nd of June, the growing PM_1 diameter resulted in enhanced β_{sca} at 355 nm at T1 and also 405 nm at T0 (as previously mentioned), though the effect was more pronounced at 355 nm. The maximum PM_1 diameter at T1 reached around 98 nm while β_{sca} at 355 nm peaked at 55 Mm^{-1} on the 28th of June. The β_{sca} at 870 nm was slightly higher after the 22nd of June, but remained nearly constant around 10 Mm^{-1}.

According to Setyan et al. (2012), organics (OA+HOA) dominated the average chemical composition with 80% of PM_1 mass, followed by sulfate (9.9%), ammonium (4.5%), nitrate (3.6%), and BC (1.6%). In addition to BC, organic species emitted directly from combustion processes or formed via the oxidation of biogenic emissions are the only light absorbing carbonaceous aerosols in the atmosphere (Andreae and Crutzen, 1997). Figure 4.5 shows the scanning electron microscope (SEM) image of the particles collected at the T1 site. The SEM image displays the open fractal soot aggregates (left), spherical particles (center), collapsed soot aggregates (right), and soot mixed with the spherical particle (top). As the day progresses, the fractal soot particles begin to increase in mass and collapse into a more spherical form upon coating by organics, sulfate, ammonium, nitrate, and water (Moffet and Prather, 2009). The coating on the BC particles leads to absorption enhancement up to 1.6 (Moffet and Prather, 2009), while the AEA can be as high as 1.6 due to the non-absorbing coating (Gyawali et al., 2009; Lack and Cappa, 2010). This shows a significant deviation from the typical value of 1 for uncoated BC particles.

Figure 4d-f presents the diurnal cycles of the SSA, AEA, and β_{abs} at 355 and 870 nm. Days with NW flows exhibited lower SSA both at 355 and 870 nm with values 0.70 and 0.80, respectively. As observed at the T0 site, the SSA at both wavelengths became increasingly similar after the 22nd of June with values around 0.90. This was consistent with the concurrently observed increasing mass of PM_1 organics and the diameter of the particles. The diurnal average of AEA varied from 1.1 to 2.1, but the values decreased to around 1.5 after the 22nd of June, suggesting enhanced absorption due to the non-absorbing to mildly-absorbing coating of organic species on the BC. The β_{abs} at 355 nm varied from 1 to 5.8 Mm^{-1}, while at 870 nm it remained around 0.2 Mm^{-1} until the 20th of June, and then slightly increased to 0.5 Mm^{-1}. Similar results have been described in the Amazon Basin in a remote forested site during the dry season where the biogenic emission and soil dust (including soot) accounted for about 75% and 13%, respectively, of the total aerosol mass (Rizzo et al., 2011). Rizzo et al. (2011) reported the AEA at 370 and 880 nm below 1.5 (90% of the data), and less than 15 Mm^{-1} of the average β_{abs} at 450 nm. Though steadily increasing organic mass at T1 showed strong impact on aerosol light scattering at 355 nm, the same cannot be said of the aerosol light absorption at 355 nm. The SOA formed from the oxidation of biogenic emissions in the forested region (T1) was not ‘brown carbon’; i.e. did not have strong intrinsic UV absorption. These results are comparable with the analysis of the aerosol optical properties at the Amazon by Rizzo et al. (2011), who found no relative enhancement of aerosol light absorption at UV regions by the biogenic aerosols in comparison to the biomass burning aerosols.

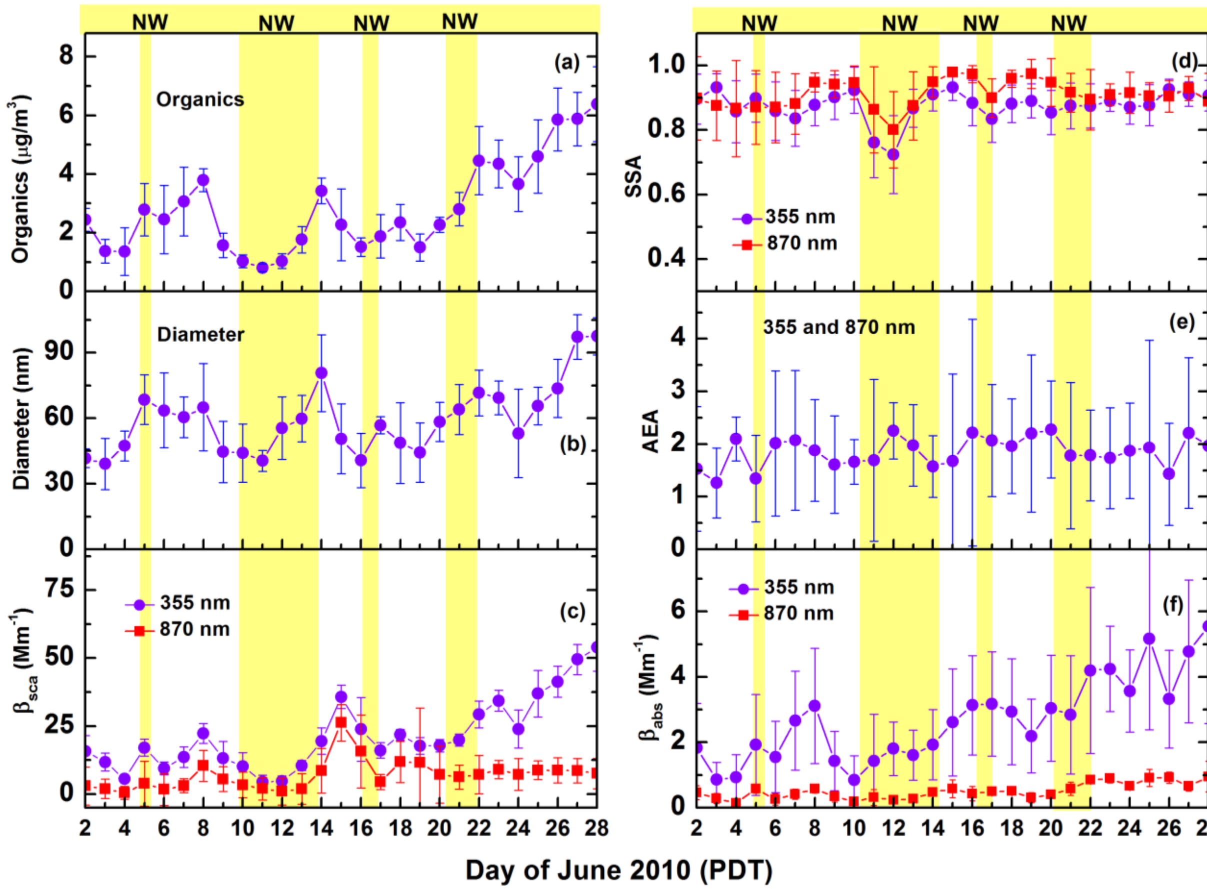

Figure 4.4 Daily variations of (a) mass concentration of PM_1 organics, (b) PM_1 particle diameter, (c) aerosol scattering coefficient (β_{sca}), (d) single scattering albedo (SSA), (e) Ångström exponent of absorption (AEA), and (f) absorption coefficients (β_{abs}) at 355 and 870 nm at T1 from the 2nd to 28th of June 2010. Bars represent one standard deviation. Each point is averaged from 06:00 to 18:00 PDT. The northwesterly flows (NW) are indicated by the shaded areas.

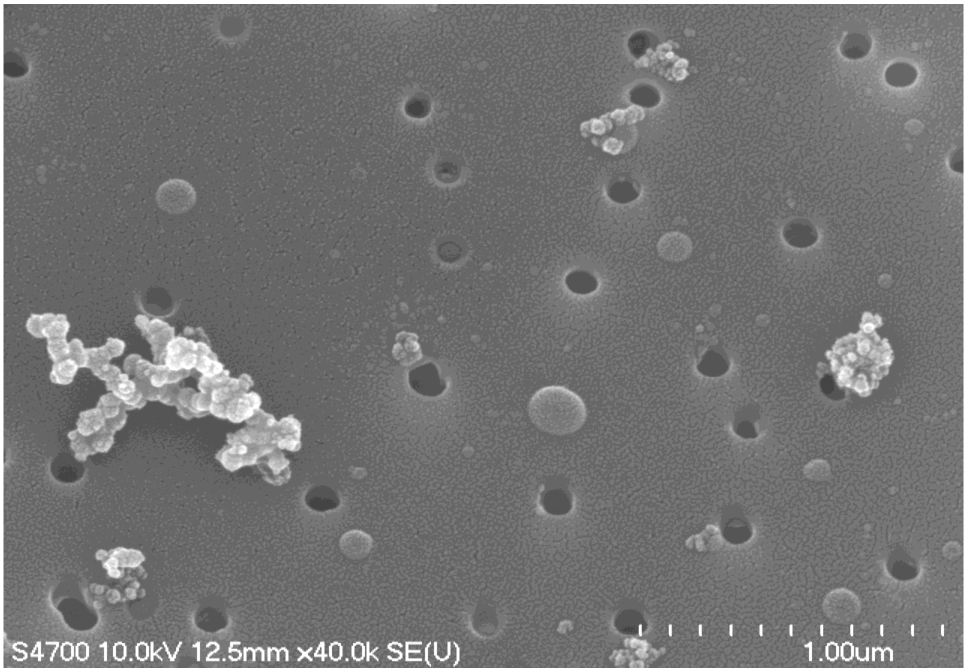

Figure 4.5 Scanning electron microscope (SEM) images of particles collected at T1 site. Open fractal soot aggregates (left), spherical particles (center), collapsed soot aggregates (right), and soot mixed with a spherical particle (top).

4.4.3 Measured and modeled aerosol light scattering

Figure 4.6a-b presents the time series of β_{sca}, which compares the measured and estimated β_{sca} at 532 nm for T0 and T1 from the 2nd to 28th of June. The time series plot helped to identify the origin of air mass that influenced the aerosol optical properties at both sites. PM_1 particle diameters and refractive index characterizing mixed OA and $(NH4)_2SO_4$ were used in the Mie model, so the deviation between the measured and estimated β_{sca} was mainly due to the change in particle size and composition. As mentioned previously, the concentration of the coarse particles was very low during the NW flows and enhanced formations of PM1 SOA were observed after the 22nd of June. The measured and the estimated β_{sca} were comparable during periods of NW flows including the last six days of the campaign, while the deviations were appreciable during the 8th , 14th-15th , and 18th of June. For example, the difference between these quantities was as high as 19 and 7 Mm^{-1} on the 8th of June at T0 and T1, respectively. During these days, significant amounts of coarse mode particles consisting of sea salt mixed with some dust particles were transported from the Pacific Ocean to the Sacramento area (Zaveri et al., 2012; Fast et al., 2012).

Figure 4.6c-d depicts the ratio of multispectral scattering contribution due to the super-micron aerosols, i.e. the ratio of the scattering due to super-micron particles $(\beta_{sca}^{Mea}(\lambda) - (\beta_{sca}^{Est}(\lambda))$, to the total scattering $((\beta_{sca}^{Mea}(\lambda))$. The scattering contribution from super-micron aerosols increased strongly as a function of wavelength for both T0 and T1 sites. For the shorter wavelengths (i.e. at 355 and 405 nm), super-micron particles contributed some aerosol light scattering at T0, while at T1 it was almost negligible.

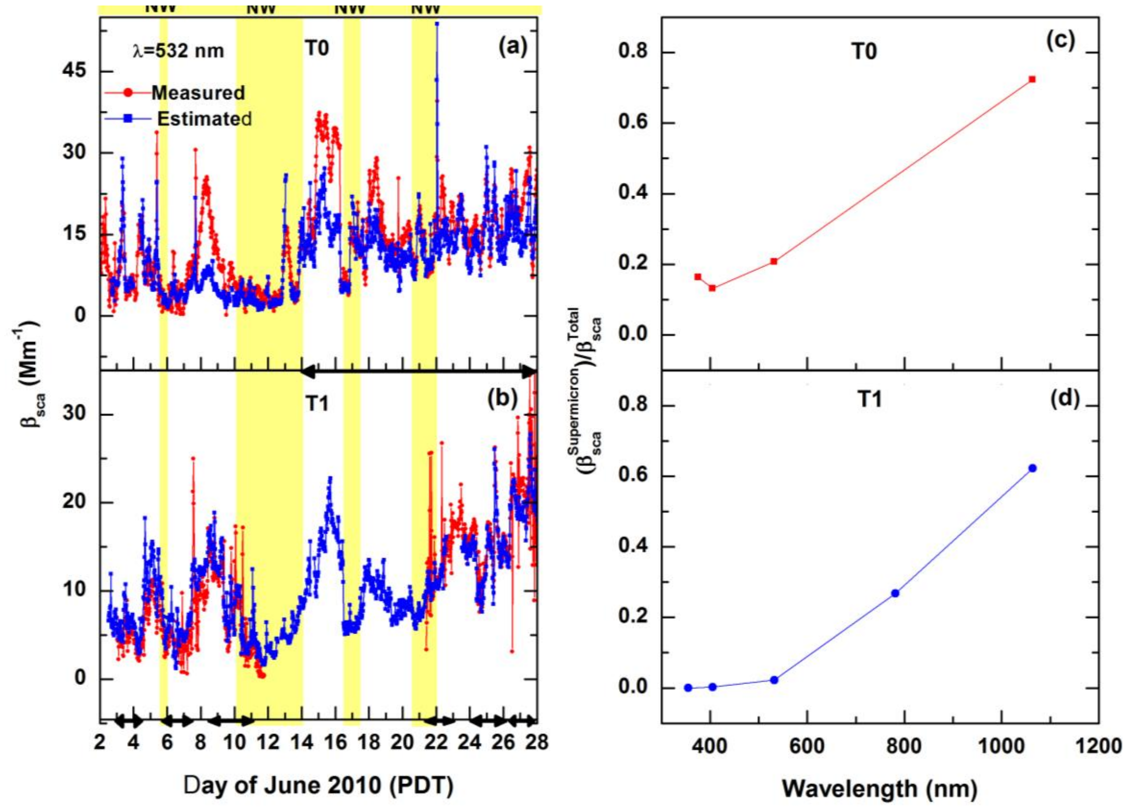

Figure 4.6 Time series of measured and modeled (Mie theory calculations of PM_1) aerosol scattering coefficient (β_{sca}) at 532 nm, (a) at T0 and (b) at T1. Each point is a 30-min average. The northwesterly flows (NW) are indicated by the shaded areas. The scattering contribution from super-micron aerosol (c) at T0 and (d) at T1. Each point is the average for the interval indicated by the arrows on the corresponding left panels.

4.4.3.1 Site T0

The measured β_{sca} was compared with the estimated scattering coefficient (β_{sca}^{Est}) for PM_1 SMPS measurements using Mie theory to study how well the PM_1 scattering can be associated with the measured aerosol light scattering from UV to near-IR wavelengths. The statistical analyses for all wavelengths presented in this section were taken for the same time periods of the measurements (as indicated in Fig. 4.6a). Note that PA β_{abs} at 870 nm was used with 1064 nm CRD extinction measurements ($\beta_{ext} = \beta_{sca} + \beta_{abs}$) to calculate 1064 nm β_{sca} by assuming an inverse wavelength dependence of BC absorption.

The correlation coefficient (R^2) and the slope of the regression between the measured and estimated scattering coefficients (β_{sca}^{Est}) for 593 data points at four wavelengths (λ = 375, 405, 532, and 1064 nm) are presented in Fig. 4.7a-d. For example, the linear relationship between β_{sca}^{Est} and β_{sca} at 375 nm is given by the equation (4)

$$\beta_{sca}^{Est} = 0.66\,\beta_{sca} + 5.26. \tag{4}$$

From equation (4), the model suggests that a unit increase in β_{sca} is associated with a 0.66 unit increase in the mean of β_{sca}^{Est} at 375 nm. Further, the value of R^2_{375nm} implied that the linear regression model explained approximately 76% of the variation in β_{sca}^{Est}. The R^2 values (as well as the slopes of the regression lines) were continuously decreasing with wavelength, i.e. $R^2_{405\,nm} = 0.70$, $R^2_{532nm} = 0.56$, *and* $R^2_{1064nm} = 0.32$. The deviation between the measured and estimated β_{sca} was determined by calculating the average error (AE) (Watson et al., 2008):

$$\text{AE (\%)} = 100\% \sum_1^{593} \frac{\beta_{sca}^{Est} - \beta_{sca}}{\beta_{sca}}. \tag{5}$$

Calculations reflect that β_{sca} was underestimated by an average of 17% and 90% at 375 and 1064 nm, respectively, and 21% and 24% at 405 and 870 nm, respectively.

In general, discrepancies between the measured and estimated β_{sca} for the shorter wavelengths are understandable if we consider 5% uncertainty for absorption measurements and 15% uncertainty for scattering measurements when using PA (Lewis et al., 2008), including other errors linked to the measurements of aerosol size and concentrations. It is apparent that great underestimation of β_{sca}, especially at 1064 nm, was due to considering only the PM_1 size distribution, as measured by SMPS, in Mie theory. Scattering at this wavelength is strongly influenced by particles larger than PM1. In addition, comparatively lower value of R^2 at 1064 nm ($R^2 = 0.32$) was likely due to temporal variations of particle concentration as a function of size, i.e. sub-micron (PM_1) and super-micron particle concentration might follow slightly different diurnal cycles. Other possible causes of these discrepancies are discussed in the next section (3.3.2).

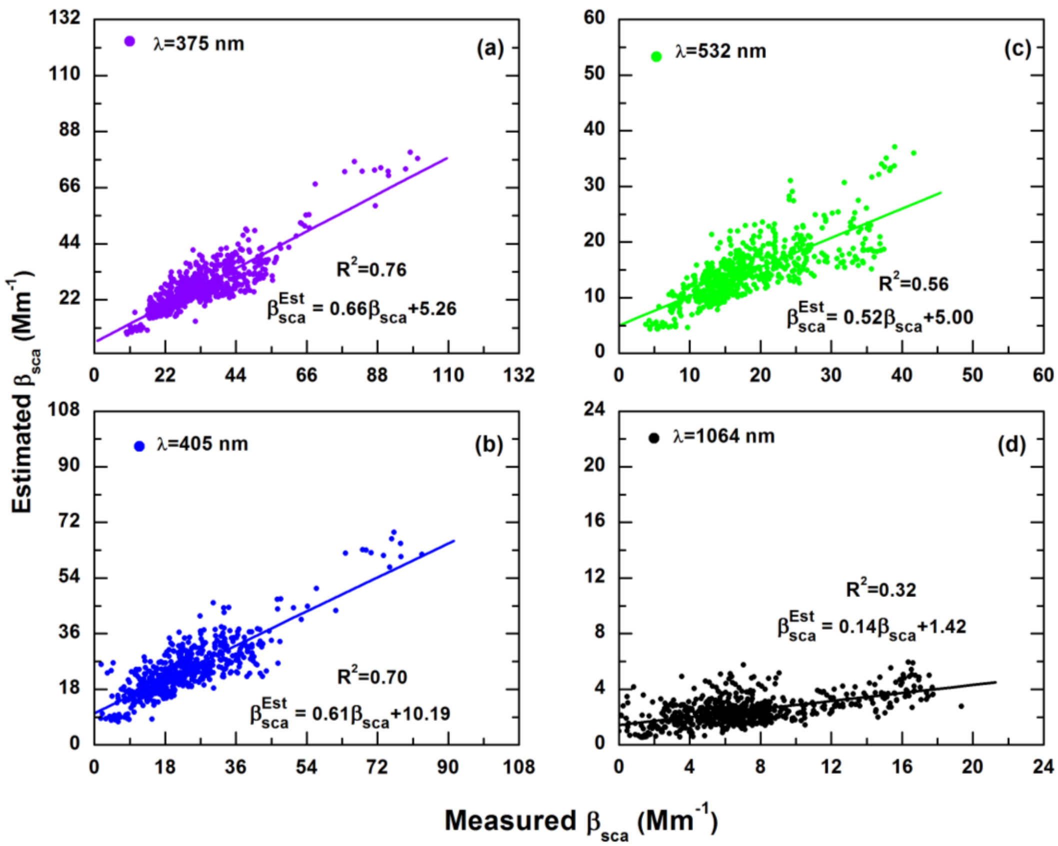

Figure 4.7 Scatter plots of multi-spectral measured and estimated (Mie calculations for PM_1) scattering coefficient (β_{sca}) at T0. The straight lines are least-squares fits to the data. Each point represents a 30-min average of all instruments measuring simultaneously.

4.4.3.2 Site T1

Figure 4.8a-d presents the comparisons of the measured and estimated β_{sca} at T1 for slightly different time periods (indicated by arrows in Fig. 4.6b) than at T0. The R^2 values and slopes of the regression lines are larger than those at T0 and also decreasing as a function of wavelength. To illustrate, the regression model shows β_{sca}^{Est} is related to β_{sca} at 355 nm by equation (5):

$$\beta_{sca}^{Est} = 0.81\,\beta_{sca} + 4.5. \qquad (5)$$

This reflects the fact that a unit increase in β_{sca} results in a 0.81 unit increase in the mean of β_{sca}^{Est} at 355 nm. In addition, the value of R^2_{355nm} suggests that the linear regression model explains 95% of the variation in β_{sca}^{Est}, which was higher by 19% than at 375 nm at site T0. Similarly, for measurements at both sites at 405, 532, and 1064 nm, R^2 was higher by 23%, 27%, and 29%, respectively, at T1 than at T0. Further, the AE calculations for 560 data points using equation (4) provide evidence that the underestimation of β_{sca} was lower at T1 than at T0 for all wavelengths. At T1, β_{sca} was underestimated by 13%, 15%, 17%, 34%, and 54% at 355, 405, 532, 781, and 1064 nm, respectively.

As explained in the previous section, the higher underestimation of β_{sca} at longer wavelengths such as at 781 and 1064 nm can be attributed to the super-micron particles that were not considered in the Mie theory model. Also, Mie theory assumes particles to be spherical, which leads to an error of 5% on β_{sca} for PM_1 particles (Chamaillard et al., 2006). At T0 and T1 sites, β_{sca} was underestimated to a lesser extent for shorter wavelengths than longer wavelengths, within the measurement uncertainties of PA and SMPS, though some contribution of super-micron size particles cannot be ignored. Furthermore, between T0 and T1 sites, the Mie theory calculations resulted in lower underestimations of β_{sca} with higher R^2 at T1 than at T0 for the same wavelengths. This might be due to the different range of particle diameters and different resolution of the SMPS instruments at T0 (12-737 nm diameter, 115 channels) and at T1 (8-858 nm diameter, 70 channels). The other possible source of error might be due to the changing air mass at T0 and T1, including the considerations of slightly different time periods applied to the Mie theory calculations at both sites, which are examined in Fig. 4.6. It can be seen from Fig. 4.6 that the measured and modeled β_{sca} agree well during NW flows but deviate widely during SW flows. The comparison agreed poorly for the occasional β_{sca} peak events exceeding 25 Mm^{-1} (mostly at T0) relating to enhanced transport episodes of coarse mode aerosols from the San Francisco Bay Area to downtown Sacramento. An assumed constant refractive index of $1.53 + i\ 10^{-6}$. (independent of wavelength) for both sites might have minor implications in the different values of estimated β_{sca}, since very similar values of refractive index have been used for clean air (1.54+i0) and polluted air (1.53+i0.02) (Fierz-Schmidhauser et al., 2010).

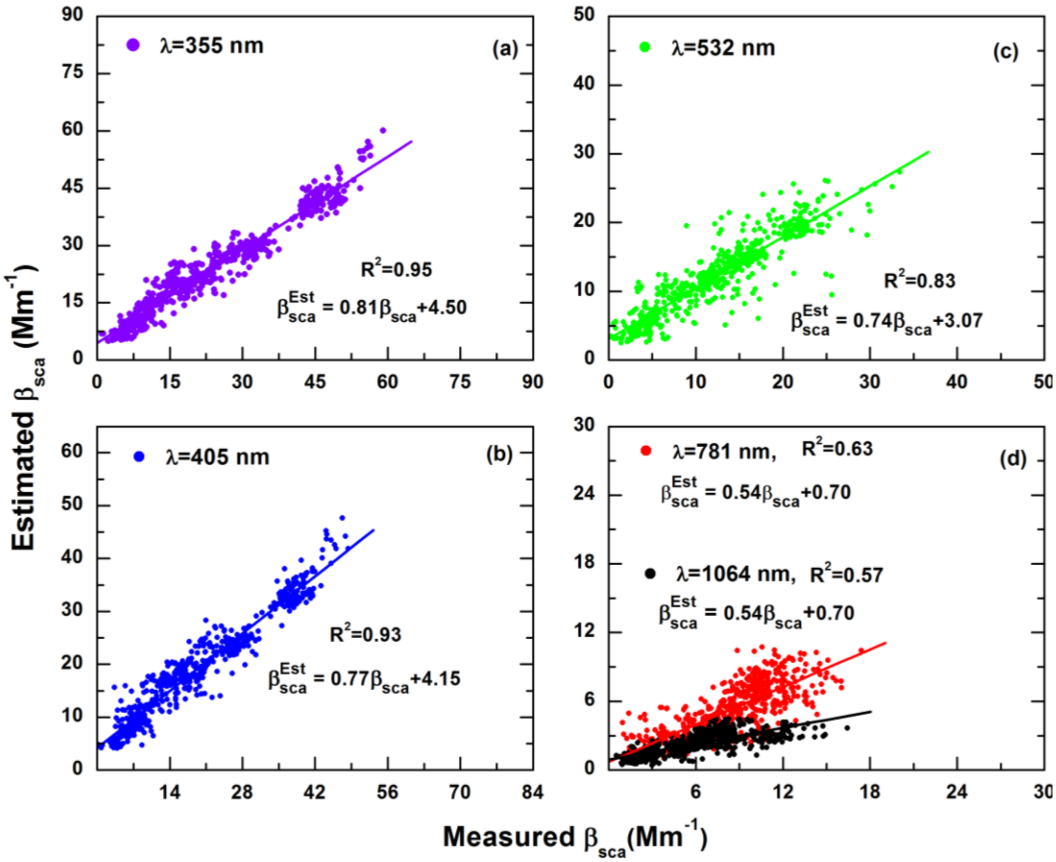

Figure 4.8 Scatter plots of multi-spectral measured aerosol light scattering coefficient (β_{sca}) and estimated (Mie calculations forPM_1) scattering coefficient β_{sca} at T1. The straight lines are least-squares fits to the data. Each point represents a 30-min average of all instruments measuring simultaneously.

4.5 Summary

Measurements of aerosol light absorption and scattering were obtained in downtown Sacramento at site T0, located on the American River College campus and in the Sierra Nevada foothills at site T1, located on the Northside School campus in Cool, CA. These measurements utilized PAs operating at 375, 405, 532, 870, and 1074 nm for T0 and at 355, 405, 532, 870 nm for T1. This instrument complimented measurements by other instruments including CRD and SMPS. Mie theory was used to analyze data gathered by these suites of instruments. Wavelength dependence of aerosol light absorption and aerosol light scattering enhancement factors and other aerosol optical properties were investigated. Additional instruments provided important meteorological parameters, such as air flow and temperature.

At both sites, during NW flows, average SSA decreased, in agreement with the shift from aged, photo-chemically processed aerosols mixed with biogenic emissions, to fresh local emissions, predominantly in fine mode. Secondary organic aerosol (SOA) mass concentration steadily increased in the latter half of the campaign, with strong impact on 355 nm light scattering; no relative enhancement of light absorption was found at 355 nm or 405 nm. Additionally, β_{abs} measured at the forest site (T1) during SW flows and higher ambient temperature indicated that low β_{abs} (below 5.8 Mm^{-1} at 355 nm), typically observed under enhanced formation of SOA, was associated with average AEA below 1.5. This finding suggests that biogenic aerosols from T1 may have a weak spectral dependence for absorption (the SOA was not 'brown carbon', i.e., did not have strong intrinsic near-UV absorption) when compared to biomass burning aerosols, i.e. light absorption was modestly enhanced at shorter wavelengths (355 nm, 375 nm, 405 nm, 532 nm) compared with 870 and 1047 nm.

The Mie theory model better predicted the measured β_{sca}, for shorter wavelengths at T1 (within the measurement uncertainty) than at T0. The underestimation of β_{sca} at T0 appeared to be related to differences in the conditions of the air mass, including the aerosol size and concentration measurements. The higher underestimation of β_{sca}, especially for wavelengths from the mid-visible to the near-IR, was due to the substantial contribution of super-micron aerosol to light scattering. Additionally, the lower values of R^2 at the longer wavelengths (i.e. 870 and 1064 nm) implied that the PM_1 and super-micron aerosols events evolved along slightly different diurnal cycles.

4.6 References

Abu-Rahmah, A., Arnott, W. P. and Moosmuller, H.: Integrating nephelometer with a low truncation angle and an extended calibration scheme RID F-8250-2011, Meas. Sci. Technol., 17(7), 1723–1732, doi:10.1088/0957-0233/17/7/010, 2006.

Andreae, M. O. and Crutzen, P. J.: Atmospheric Aerosols: Biogeochemical Sources and Role in Atmospheric Chemistry, Science, 276(5315), 1052–1058, doi:10.1126/science.276.5315.1052, 1997.

Andreae, M. O. and Gelencser, A.: Black carbon or brown carbon? The nature of light-absorbing carbonaceous aerosols RID B-1068-2008, Atmos. Chem. Phys., 6, 3131–3148, 2006.

Arnott, W., Moosmuller, H., Rogers, C., Jin, T. and Bruch, R.: Photoacoustic spectrometer for measuring light absorption by aerosol: instrument description RID F-8250-2011, Atmos. Environ., 33(17), 2845–2852, 1999.

Bao, J.-W., Michelson, S. A., Persson, P. O. G., Djalalova, I. V. and Wilczak, J. M.: Observed and WRF-simulated low-level winds in a high-ozone episode during the Central California Ozone Study, J. Appl. Meteorol. Climatol., 47(9), 2372–2394, doi:10.1175/2008JAMC1822.1, 2008.

Bond, T. and Bergstrom, R.: Light absorption by carbonaceous particles: An investigative review, Aerosol Sci. Technol., 40(1), 27–67, doi:10.1080/02786820500421521, 2006.

Cahill, T. A., Barnes, D. E., Spada, N. J., Lawton, J. A. and Cahill, T. M.: Very Fine and Ultrafine Metals and Ischemic Heart Disease in the California Central Valley 1: 2003-2007, Aerosol Sci. Technol., 45(9), 1123–1134, doi:10.1080/02786826.2011.582194, 2011.

Cappa, C. D., Che, D. L., Kessler, S. H., Kroll, J. H. and Wilson, K. R.: Variations in organic aerosol optical and hygroscopic properties upon heterogeneous OH oxidation, J. Geophys. Res., 116, 12 PP., doi:201110.1029/2011JD015918, 2011.

Chamaillard, K. and Jennings, S. G.: Particle counting and numerical models: Effect of instrumental size resolution and particle shapes on optical cross-sections, Journal of Quantitative Spectroscopy and Radiative Transfer, 100(1-3), 64–76, doi:10.1016/j.jqsrt.2005.11.064, 2006.

Chamaillard, K., Kleefeld, C., Jennings, S. G., Ceburnis, D. and O'Dowd, C. D.: Light scattering properties of sea-salt aerosol particles inferred from modeling studies and ground-based measurements, Journal of Quantitative Spectroscopy and Radiative Transfer, 101(3), 498–511, doi:10.1016/j.jqsrt.2006.02.062, 2006.

Change, I. P. on C. and I, I. P. on C. C. W. G.: Climate Change 2007: The Physical Science Basis : Contribution of Working Group I to the Fourth Assessment Report of the Intergovernmental Panel on Climate Change, Cambridge University Press., 2007.

Charlson, R., Schwartz, Hales, J., Cess, R., Coakley, J.,Hansen, J., and Hofman, D.: Climate forcing by anthropogenic aerosols, Science, 255(5043), 423–430, doi:10.1126/science.255.5043.423, 1992.

Coakley, J. A., Bernstein, R. L. and Durkee, P. A.: Effect of Ship-Stack Effluents on Cloud Reflectivity, Science, 237(4818), 1020–1022, doi:10.1126/science.237.4818.1020, 1987.

Dillon, M., Lamanna, M., Schade, G., Goldstein, A. and Cohen, R.: Chemical evolution of the Sacramento urban plume: Transport and oxidation RID A-6857-2011 RID A-8842-2011, J. Geophys. Res.-Atmos., 107(D5-6), doi:10.1029/2001JD000969, 2002.

Fast, J. D., Gustafson Jr., W. I., Berg, L. K., Shaw, W. J., Pekour, M., Shrivastava, M., Barnard, J. C., Ferrare, R. A., Hostetler, C. A., Hair, J. A., Erickson, M., et al.: Transport and mixing patterns over Central California during the carbonaceous aerosol and radiative effects study (CARES), Atmos. Chem. Phys., 12(4), 1759–1783, doi:10.5194/acp-12-1759-2012, 2012.

Fierz-Schmidhauser, R., Zieger, P., Vaishya, A., Monahan, C., Bialek, J., O'Dowd, C. D., Jennings, S. G., Baltensperger, U. and Weingartner, E.: Light scattering enhancement factors in the marine boundary layer (Mace Head, Ireland), J. Geophys. Res., 115, 11 PP., doi:201010.1029/2009JD013755, 2010.

Fuller, K. A., Malm, W. C. and Kreidenweis, S. M.: Effects of mixing on extinction by carbonaceous particles, J. Geophys. Res., 104(D13), PP. 15,941–15,954, doi:199910.1029/1998JD100069, n.d.

Gyawali, M., Arnott, W. P., Lewis, K. and Moosmüller, H.: In situ aerosol optics in Reno, NV, USA during and after the summer 2008 California wildfires and the influence of absorbing and non-absorbing organic coatings on spectral light absorption, Atmos. Chem. Phys., 9(20), 8007–8015, doi:10.5194/acp-9-8007-2009, 2009.

Haywood, J. M. and Ramaswamy, V.: Global sensitivity studies of the direct radiative forcing due to anthropogenic sulfate and black carbon aerosols, Journal of Geophysical Research, 103(D6), 6043–6058, doi:10.1029/97JD03426, 1998.

Hoffer, A., Gelencsér, A., Guyon, P., Kiss, G., Schmid, O., Frank, G. P., Artaxo, P. and Andreae, M. O.: Optical properties of humic-like substances (HULIS) in biomass-burning aerosols, Atmos. Chem. Phys., 6(11), 3563–3570, doi:10.5194/acp-6-3563-2006, 2006.

Holzinger, R., Millet, D. B., Williams, B., Lee, A., Kreisberg, N., Hering, S. V., Jimenez, J., Allan, J. D., Worsnop, D. R. and Goldstein, A. H.: Emission, oxidation, and secondary organic aerosol formation of volatile organic compounds as observed at Chebogue Point, Nova Scotia, J. Geophys. Res., 112, 12 PP., doi:200710.1029/2006JD007599, 2007.

Hulst, H. C. van de and Physics: Light Scattering by Small Particles, Dover Publications., 1981.

Jacobson, M.: Isolating nitrated and aromatic aerosols and nitrated aromatic gases as sources of ultraviolet light absorption, J. Geophys. Res.-Atmos., 104(D3), 3527–3542, doi:10.1029/1998JD100054, 1999.

Kerker, M.: The scattering of light, and other electromagnetic radiation, Academic Press., 1969.

Kirchstetter, T. W., Novakov, T. and Hobbs, P. V.: Evidence that the spectral dependence of light absorption by aerosols is affected by organic carbon, J. Geophys. Res., 109, 12 PP., doi:200410.1029/2004JD004999, 2004.

Kleefeld, C., O'Dowd, C. D., O'Reilly, S., Jennings, S. G., Aalto, P., Becker, E., Kunz, G. and Leeuw, G. de: Relative contribution of submicron and supermicron particles to aerosol light scattering in the marine boundary layer, J. Geophys. Res., 107, 13 PP., doi:200210.1029/2000JD000262, 2002.

Lack, D. A. and Cappa, C. D.: Impact of brown and clear carbon on light absorption enhancement, single scatter albedo and absorption wavelength dependence of black carbon, Atmospheric Chemistry and Physics Discussions, 10(1), 785–819, doi:10.5194/acpd-10-785-2010, 2010.

Lamanna, M. and Goldstein, A.: In situ measurements of C-2-C-10 volatile organic compounds above a Sierra Nevada ponderosa pine plantation RID A-6857-2011, J. Geophys. Res.-Atmos., 104(D17), 21247–21262, doi:10.1029/1999JD900289, 1999.

Lammel, G. and Novakov, T.: Water nucleation properties of carbon black and diesel soot particles, Atmospheric Environment, 29(7), 813–823, doi:10.1016/1352-2310(94)00308-8, 1995.

Lewis, K., Arnott, W. P., Moosmueller, H. and Wold, C. E.: Strong spectral variation of biomass smoke light absorption and single scattering albedo observed with a novel dual-wavelength photoacoustic instrument RID F-8250-2011, J. Geophys. Res.-Atmos., 113(D16), doi:10.1029/2007JD009699, 2008.

Lunden, M. M., Black, D. R., McKay, M., Revzan, K. L., Goldstein, A. H. and Brown, N. J.: Characteristics of fine particle growth events observed above a forested ecosystem in the Sierra Nevada Mountains of California RID A-6857-2011, Aerosol Sci. Technol., 40(5), 373–388, doi:10.1080/02786820600631896, 2006.

Moffet, R. C. and Prather, K. A.: In-situ measurements of the mixing state and optical properties of soot with implications for radiative forcing estimates, PNAS, 106(29), 11872–11877, doi:10.1073/pnas.0900040106, 2009.

Moosmueller, H., Chakrabarty, R. K. and Arnott, W. P.: Aerosol light absorption and its measurement: A review RID F-8250-2011, J. Quant. Spectrosc. Radiat. Transf., 110(11), 844–878, doi:10.1016/j.jqsrt.2009.02.035, 2009.

Radney, J. G., Bazargan, M. H., Wright, M. E. and Atkinson, D. B.: Laboratory Validation of Aerosol Extinction Coefficient Measurements by a Field-Deployable Pulsed Cavity Ring-Down Transmissometer, Aerosol Science and Technology, 43(1), 71–80, doi:10.1080/02786820802482536, 2009.

Ramanathan, V., Chung, C., Kim, D., Bettge, T., Buja, L., Kiehl, J., Washington, W., Fu, Q., Sikka, D. and Wild, M.: Atmospheric brown clouds: Impacts on South Asian climate and hydrological cycle, Proc. Natl. Acad. Sci. U. S. A., 102(15), 5326–5333, doi:10.1073/pnas.0500656102, 2005.

Redemann, J., Russell, P. and Hamill, P.: Dependence of aerosol light absorption and single-scattering albedo on ambient relative humidity for sulfate aerosols with black carbon cores, J. Geophys. Res.-Atmos., 106(D21), 27485–27495, doi:10.1029/2001JD900231, 2001.

Reid, J. S., Hobbs, P. V., Ferek, R. J., Blake, D. R., Martins, J. V., Dunlap, M. R. and Liousse, C.: Physical, chemical, and optical properties of regional hazes dominated by smoke in Brazil, Journal of Geophysical Research - Atmospheres, 103(D24), 32059–32080, doi:10.1029/98JD00458, 1998.

Rizzo, L. V., Correia, A. L., Artaxo, P., Procópio, A. S. and Andreae, M. O.: Spectral dependence of aerosol light absorption over the Amazon Basin, Atmospheric Chemistry and Physics Discussions, 11(4), 11547–11577, doi:10.5194/acpd-11-11547-2011, 2011.

Saathoff, H., Naumann, K.-H., Schnaiter, M., Schöck, W., Möhler, O., Schurath, U., Weingartner, E., Gysel, M. and Baltensperger, U.: Coating of soot and (NH4)2SO4 particles by ozonolysis products of α-pinene, Journal of Aerosol Science, 34(10), 1297–1321, doi:10.1016/S0021-8502(03)00364-1, 2003.

Schnaiter, M., Horvath, H., Mohler, O., Naumann, K., Saathoff, H. and Schock, O.: UV-VIS-NIR spectral optical properties of soot and soot-containing aerosols, J. Aerosol. Sci., 34(10), 1421–1444, doi:10.1016/S0021-8502(03)00361-6, 2003.

Schwartz, S.: The Whitehouse effect - Shortwave radiative forcing of climate by anthropogenic aerosols: An overview RID C-2729-2008, J. Aerosol. Sci., 27(3), 359–382, doi:10.1016/0021-8502(95)00533-1, 1996.

Seinfeld, J. H. and Pandis, S. N.: Atmospheric chemistry and physics: from air pollution to climate change, Wiley., 2006.

Setyan, A., Zhang, Q., Merkel, M., Knighton, W. B., Sun, Y., Song, C., Shilling, J. E., Onasch, T. B., Herndon, S. C., Worsnop, D. R., Fast, J. D., et al.: Submicron particles influenced by mixed biogenic and anthropogenic emissions: high-resolution aerosol mass spectrometry results from the Carbonaceous Aerosols and Radiative Effects Study (CARES), Atmospheric Chemistry and Physics Discussions, 12(2), 5601–5658, doi:10.5194/acpd-12-5601-2012, 2012.

Shiraiwa, M., Kondo, Y., Iwamoto, T. and Kita, K.: Amplification of Light Absorption of Black Carbon by Organic Coating RID A-6246-2010, Aerosol Sci. Technol., 44(1), 46–54, doi:10.1080/02786820903357686, 2010.

SLOANE, C.: OPTICAL-PROPERTIES OF AEROSOLS OF MIXED COMPOSITION, Atmos. Environ., 18(4), 871–878, doi:10.1016/0004-6981(84)90273-7, 1984.

Smith, J. D. and Atkinson, D. B.: A portable pulsed cavity ring-down transmissometer for measurement of the optical extinction of the atmospheric aerosol, Analyst, 126(8), 1216–1220, 2001.

Subramanian, R., Roden, C. A., Boparai, P. and Bond, T. C.: Yellow beads and missing particles: Trouble ahead for filter-based absorption measurements, Aerosol Sci. Technol., 41(6), 630–637, doi:10.1080/02786820701344589, 2007.

Sun, H., Biedermann, L. and Bond, T. C.: Color of brown carbon: A model for ultraviolet and visible light absorption by organic carbon aerosol, Geophys. Res. Lett., 34, 5 PP., doi:200710.1029/2007GL029797, 2007.

Twomey, S.: The Influence of Pollution on the Shortwave Albedo of Clouds, Journal of the Atmospheric Sciences, 34(7), 1149–1152, doi:10.1175/1520-0469(1977)034<1149:TIOPOT>2.0.CO;2, 1977.

Watson, J. G., Chow, J. C., Lowenthal, D. H. and Magliano, K. L.: Estimating aerosol light scattering at the Fresno Supersite, Atmospheric Environment, 42(6), 1186–1196, doi:10.1016/j.atmosenv.2007.10.040, 2008.

Weingartner, E., Burtscher, H. and Baltensperger, U.: Hygroscopic properties of carbon and diesel soot particles, Atmospheric Environment, 31(15), 2311–2327, doi:10.1016/S1352-2310(97)00023-X, 1997.

Wiedensohler, Birmili, W., Nowak, A., Sonntag, A., Weinhold, K., Merkel, M., Wehner, B., Tuch, T., Pfeifer, S., Fiebig, M., Fjäraa, A. M., et al.: Particle mobility size spectrometers: harmonization of technical standards and data structure to facilitate high quality long-term observations of atmospheric particle number size distributions, Atmospheric Measurement Techniques Discussions, 3(6), 5521–5587, doi:10.5194/amtd-3-5521-2010, 2010.

Wiscombe, W. J.: Improved Mie scattering algorithms, Appl. Opt., 19(9), 1505–1509, doi:10.1364/AO.19.001505, 1980.

Worton, D. R., Goldstein, A. H., Farmer, D. K., Docherty, K. S., Jimenez, J. L., Gilman, J. B., Kuster, W. C., de Gouw, J., Williams, B. J., Kreisberg, N. M., Hering, S. V., et al.: Origins and composition of fine atmospheric carbonaceous aerosol in the Sierra Nevada Mountains, California, Atmos. Chem. Phys., 11(19), 10219–10241, doi:10.5194/acp-11-10219-2011, 2011.

Zaremba, L. and Carroll, J.: Summer wind flow regimes over the Sacramento Valley, J. Appl. Meteorol., 38(10), 1463–1473, doi:10.1175/1520-0450(1999)038<1463:SWFROT>2.0.CO;2, 1999.

Zaveri, R. A., Shaw, W. J., Cziczo, D. J., Schmid, B., Alexander, M. L., Alexandrov, M., Alvarez, R. J., Arnott, W. P., Atkinson, D. B., Baidar, S., Banta, R. M., et al.: Overview of the 2010 Carbonaceous Aerosols and Radiative Effects Study (CARES), Atmospheric Chemistry and Physics Discussions, 12(1), 1299–1400, doi:10.5194/acpd-12-1299-2012, 2012.

Zhang, Q., Jimenez, J. L., Canagaratna, M. R., Allan, J. D., Coe, H., Ulbrich, I., Alfarra, M. R., Takami, A., Middlebrook, A. M., Sun, Y. L., Dzepina, K., et al.: Ubiquity and dominance of oxygenated species in organic aerosols in anthropogenically-influenced Northern Hemisphere midlatitudes RID F-9653-2010 RID A-5294-2008 RID B-1160-

2010 RID E-4831-2011 RID F-1314-2010 RID B-2118-2008 RID B-7338-2008 RID D-2001-2010 RID A-2674-2010 RID E-3868-2010 RID D-2817-2009, Geophys. Res. Lett., 34(13), doi:10.1029/2007GL029979, 2007.

Zhong, S., Whiteman, C. D. and Bian, X.: Diurnal Evolution of Three-Dimensional Wind and Temperature Structure in California's Central Valley, Journal of Applied Meteorology, 43(11), 1679–1699, doi:10.1175/JAM2154.1, 2004.

5 Summary, Conclusions and Future Work

5.1 Summary and Conclusions

In this study, we have analyzed the multispectral aerosol optical properties from the ultraviolet (UV) to the near-infrared (IR) wavelengths by employing PA and CRD. This study also included the simultaneous aerosol light absorption and scattering measurements by a novel UV 355 nm PA of our design and manufacture. Aerosols produced by wildfire, including traffic emissions (Chapter 2), laboratory generated, including wintertime ambient urban aerosols (Chapter 3), and urban plume, including biogenic emissions (Chapter 4) are studied in detail for the spectral dependence of aerosol light absorption and scattering. These results illustrate the considerable variation of AEA values: 2.10 (405 and 870 nm) for wildfire aerosols, 1.14 (355 and 870 nm) for urban pollution, 1.60 (355 and 870 nm) for biogenic emissions and 4.53 (355-1047 nm) for incense burning aerosols. These findings are consistent with the previous study that the light absorbing organic aerosols, or brown carbon (BrC) are predominantly from biomass and wood burning (Kirchstetter and Thatcher, 2012; Chakrabarty et al., 2010; Kirchstetter et al., 2004; Sandradewi et al., 2008). In other studies, AEA of 1.21-3.46 (400-800 nm) for desert dust have been found in Bermuda from long range transport from the Sahara desert in Africa (Aryal, 2012). The spectral signature of these species indicated by the AEA is instrumental in climate models (Bergstrom et al., 2007). In the following, we provide the principle findings from this investigation in comparison to different studies.

Spectral properties of combustion-generated aerosols are highly dependent on temperature and combustion processes (Bond, 2001; Kirchstetter et al., 2004). For example, as described in Chapters 2 and 3, the aerosols resulting from the California wildfire of the summer of 2008 exhibited strong spectral variations (AEA=2.10); while the aerosols resulting from residential wood burning in Reno during the winter of 2009 and 2010 exhibited weak spectral dependence (AEA=1.14). These observations highlight the fact that the low temperature, incomplete combustion and smoldering phase burning leads to more BrC as observed in wildfires than high temperature and efficient burning processes such as residential wood burning. During these study periods, the SSA also exhibited strong spectral variation depending upon low-temperature smoldering burning versus high-temperature efficient burning. For example, SSA was consistently higher at 870 nm (0.88 - 0.96) than at 405 nm (0.88 to 0.93) during July. Contrary to this observation, in August 2008, which was unaffected by California wildfires, the SSA at 405 nm (0.71–0.97) was higher than the SSA at 870 nm (0.68–0.95).

We demonstrated that the aging of urban aerosol and biomass burning aerosol often produce quite different core shell structures that potentially affect the spectral AEA. For example, for biomass burning aerosols, BC cores (mass fraction ~1%) are heavily coated by absorbing and non-absorbing organics (mass fraction~99%) (Lewis et al., 2008). For these situations, by using the shell-core model we verified that large values of AEA are possible even when coatings do not absorb light and may increase the spectral absorption selectivity. Hence, the organic coating does not need to be intrinsically brown to observe effects commonly attributed to BrC light absorption. We referred to this absorption as "apparently light absorbing carbon" (ALAOC). Further, the measurements and the shell-core model suggested that the AEA might be less than one in the later part of the day or even become negative depending upon core and coating thickness.

The one-month-long field study, Carbonaceous Aerosols and Radiative Effects Study (CARES) conducted during June 2010 in Central Valley California, produced valuable data necessary to understanding the evolution of multispectral aerosol light absorption and scattering in a mixed urban-biogenic environment. In contrast to the regular observations of spectral features of aerosol light absorption and scattering, including the SSA and AEA in Reno, the diurnal variations of aerosol optical properties exhibited almost none of these features in the Sacramento area. The measured aerosol concentrations at both sites in Roseville and Cool, CA were highly dependent on transport from the San Francisco Bay Area and the meteorological parameters such as temperature, humidity, wind speed, and direction. In addition, the average AEA of 1.60 (for 355 and 870 nm) was observed to be associated with biogenic aerosols. This value signifies the weak spectral dependence of biogenic emission aerosols consistent with similar findings in the Amazon Basin in the absence of biomass burning (Rizzo et al., 2011).

5.2 Future Work and Scientific Recommendations

During the last decade, several studies have suggested the growing awareness of BrC due to its capability of enhanced solar radiation absorption especially in the UV spectral region (Jacobson, 1999; Andreae and Gelencser, 2006; Graber and Rudich, 2006; Moosmüller et al., 2009; Moosmüller et al., 2011), which might affect the radiation balance as well as the hydrological cycle (Ramanathan et al., 2005). One of the greatest issues of BrC research is characterizing its optical properties (Fuzzi et al., 2006; Kanakidou et al., 2005).

Future work in the study of spectral variation of BrC from biomass burning aerosols should consider analyzing the differences between the mechanisms of spectral variations of light absorption due to intrinsic absorption by organic carbon versus the effect of non-absorbing organic coatings on the amplification of aerosol light absorption. The latter one was termed ALAOC. We have discussed this phenomenon in Chapter 2, but it requires more refinement. These findings are extremely valuable for the modeling of aerosol impacts on climate.

The investigations of spectral dependence of biogenic aerosols, predominantly emissions by pine trees during the CARES projects, suggested a modest enhancement of absorption towards UV regions. However, additional field studies are required for different seasons and various forested regions to characterize a complete spectral nature of biogenic BrC.

Chamber studies are well suited to investigate the chemical pathways and optical properties of model biogenic BrC (Bones et al., 2010). These studies are often performed by ozonolysis of terpenes and α-pinene (common biogenic hydrocarbon) in the presence of acidic/non-acidic sulfate aerosol. For example, in our laboratory campaign at Pacific Northwest National Laboratory (PNNL), we found pronounced absorption at 355 and 405 nm wavelength by BrC (not included in this dissertation) formed during laboratory-simulated atmospheric conditions (Song et al., 2010) . These results should be further tested and analyzed to assess the implications of these findings.

5.3 References

Aryal, R. P., Comparison of Near Surface and Column-Integrated Atmospheric Aerosol Optical Properties, PhD dissertation, 156 pp, University of Miami, Coral gables, FL, 2012**.**

Andreae, M. O. and Gelencser, A.: Black carbon or brown carbon? The nature of light-absorbing carbonaceous aerosols RID B-1068-2008, Atmos. Chem. Phys., 6, 3131–3148, 2006.

Bergstrom, R. W., Pilewskie, P., Russell, P. B., Redemann, J., Bond, T. C., Quinn, P. K. and Sierau, B.: Spectral absorption properties of atmospheric aerosols, Atmos. Chem. Phys., 7(23), 5937–5943, 2007.

Bond, T. C.: Spectral dependence of visible light absorption by carbonaceous particles emitted from coal combustion, Geophys. Res. Lett., 28(21), PP. 4075–4078, doi:200110.1029/2001GL013652, n.d.

Bones, D. L., Henricksen, D. K., Mang, S. A., Gonsior, M., Bateman, A. P., Nguyen, T. B., Cooper, W. J. and Nizkorodov, S. A.: Appearance of strong absorbers and fluorophores in limonene-O3 secondary organic aerosol due to NH4+-mediated chemical aging over long time scales, J. Geophys. Res., 115, 14 PP., doi:201010.1029/2009JD012864, 2010.

Chakrabarty, R. K., Moosmüller, H., Chen, L.-W. A., Lewis, K., Arnott, W. P., Mazzoleni, C., Dubey, M. K., Wold, C. E., Hao, W. M. and Kreidenweis, S. M.: Brown carbon in tar balls from smoldering biomass combustion, Atmos. Chem. Phys., 10(13), 6363–6370, doi:10.5194/acp-10-6363-2010, 2010.

Fuzzi, S., Andreae, M. O., Huebert, B. J., Kulmala, M., Bond, T. C., Boy, M., Doherty, S. J., Guenther, A., Kanakidou, M., Kawamura, K., Kerminen, V.-M., et al.: Critical assessment of the current state of scientific knowledge, terminology, and research needs concerning the role of organic aerosols in the atmosphere, climate, and global change, Atmos. Chem. Phys., 6(7), 2017–2038, doi:10.5194/acp-6-2017-2006, 2006.

Graber, E. R. and Rudich, Y.: Atmospheric HULIS: How humic-like are they? A comprehensive and critical review, Atmos. Chem. Phys., 6(3), 729–753, doi:10.5194/acp-6-729-2006, 2006.

Jacobson, M.: Isolating nitrated and aromatic aerosols and nitrated aromatic gases as sources of ultraviolet light absorption, J. Geophys. Res.-Atmos., 104(D3), 3527–3542, doi:10.1029/1998JD100054, 1999.

Kanakidou, M., Seinfeld, J. H., Pandis, S. N., Barnes, I., Dentener, F. J., Facchini, M. C., Van Dingenen, R., Ervens, B., Nenes, A., Nielsen, C. J., Swietlicki, E., et al.: Organic aerosol and global climate modelling: a review, Atmos. Chem. Phys., 5(4), 1053–1123, doi:10.5194/acp-5-1053-2005, 2005.

Kirchstetter, T. W., Novakov, T. and Hobbs, P. V.: Evidence that the spectral dependence of light absorption by aerosols is affected by organic carbon, J. Geophys. Res., 109, 12 PP., doi:200410.1029/2004JD004999, 2004.

Kirchstetter, T. W. and Thatcher, T. L.: Contribution of organic carbon to wood smoke particulate matter absorption of solar radiation, Atmospheric Chemistry and Physics Discussions, 12(2), 5803–5816, doi:10.5194/acpd-12-5803-2012, 2012.

Lewis, K., Arnott, W. P., Moosmuller, H. and Wold, C. E.: Strong spectral variation of biomass smoke light absorption and single scattering albedo observed with a novel dual-wavelength photoacoustic instrument. [online] Available from: http://www.treesearch.fs.fed.us/pubs/33785 (Accessed 6 April 2012), 2008.

Moosmueller, H., Chakrabarty, R. K., Ehlers, K. M. and Arnott, W. P.: Absorption Angstrom coefficient, brown carbon, and aerosols: basic concepts, bulk matter, and spherical particles RID F-8250-2011, Atmos. Chem. Phys., 11(3), 1217–1225, doi:10.5194/acp-11-1217-2011, 2011.

Moosmüller, H., Chakrabarty, R. K. and Arnott, W. P.: Aerosol light absorption and its measurement: A review, Journal of Quantitative Spectroscopy and Radiative Transfer, 110(11), 844–878, doi:10.1016/j.jqsrt.2009.02.035, 2009.

Ramanathan, V., Chung, C., Kim, D., Bettge, T., Buja, L., Kiehl, J., Washington, W., Fu, Q., Sikka, D. and Wild, M.: Atmospheric brown clouds: Impacts on South Asian climate and hydrological cycle, Proc. Natl. Acad. Sci. U. S. A., 102(15), 5326–5333, doi:10.1073/pnas.0500656102, 2005.

Rizzo, L. V., Correia, A. L., Artaxo, P., Procópio, A. S. and Andreae, M. O.: Spectral dependence of aerosol light absorption over the Amazon Basin, Atmospheric Chemistry and Physics Discussions, 11(4), 11547–11577, doi:10.5194/acpd-11-11547-2011, 2011.

Sandradewi, J., Prévôt, A. S. H., Weingartner, E., Schmidhauser, R., Gysel, M. and Baltensperger, U.: A study of wood burning and traffic aerosols in an Alpine valley using a multi-wavelength Aethalometer, Atmospheric Environment, 42(1), 101–112, doi:10.1016/j.atmosenv.2007.09.034, 2008.

Song, C., Gyawali, M., Arnott, W. P., Zaveri, R. A.: Measurements of Optical Properties of Secondary Organic Aerosol Using Photoacoustic Instrumentation, Poster First

Atmospheric System Research (ASR) Science Team Meeting (ASR-CONF-2010, Bethesda, Maryland), 2010.